universität wien

MASTERARBEIT / MASTER'S THESIS

Titel der Masterarbeit / Title of the Master's Thesis

"Silver Nanoparticles in the Aquatic Environment - Assessing Uptake and Accumulation in the Aquatic Macrophyte *Myriophyllum spicatum* under Environmentally Relevant Conditions"

verfasst von / submitted by

Maximilian Eiser, BSc

angestrebter akademischer Grad / in partial fulfilment of the requirements for the degree of

Master of Science (MSc)

Wien, 2023 / Vienna, 2023

Studienkennzahl lt. Studienblatt / degree programme code as it appears on the student record sheet:	UA 066 862
Studienrichtung lt. Studienblatt / degree programme as it appears on the student record sheet:	Masterstudium Chemie
Betreut von / Supervisor:	Mag. Dr. Franz Jirsa, Privatdoz.

Acknowledgements

First and foremost I want to express my deepest gratitude to Franz Jirsa for supervising my master's thesis, for his patient encouragement and support during all stages of my work and his invaluable scientific guidance, without which this thesis would not have been possible.

I would also like to extend a special 'Thank you' to Jakob Windisch and Andreas Gradwohl, for the eager help they always offered me, the amusing yet valuable discussions we had and especially Jakob for introducing me to the world of specialty coffee.

Furthermore, I want to acknowledge Dr. Katy Schmidt and Dr. Norbert Cyran of the Core Facility for Cell Imaging and Ultrastructure Research for conducting the electron microscopic analyses and the assistance they provided interpreting the results.

Finally, I cannot begin to express the gratitude I owe my friends and family, who supported me throughout my time at the University of Vienna and made these years the best of my life so far. I am especially indebted to Sophia, whose empathy, passion and curiosity for all the manifold shapes and forms that life comes in, has profoundly enriched my experience of the world and reminded me that it's not about looking further, but closer.

Thank you from the bottom of my heart.

Contents

List of Figures

List of Tables

1 Introduction

1.1 Silver - Applications and Discharges to the Environment

Silver (elemental symbol Ag, atomic number 47) is a noble metal and the 68th most abundant element in the earth's crust. As a noble metal, it naturally occurs in its metallic form (Ag^0) but oxidized forms, with Ag^+ being the most stable oxidation state, also widely occur, mainly in the form of sulfides (e.g. acanthite, Ag_2S). As such, Ag is often associated with sulfidic ores of lead (up to 1 % in lead glance, PbS) and copper (e.g. chalcopyrite, CuFeS)(Wiberg, 2008a). In 2021, the global production of Ag by mines was estimated to be 24,000 metric tons by the U.S. Geological Survey (USGS), with Mexico acting as the major producer at approximately 5,600 tons (USGS, 2022).

1.1.1 Historical and Recent Applications

Archaeological evidence of Ag metallurgy and the manufacture of Ag artifacts dates back to at least the third millennium BCE, with the use of Ag containers to conserve foods and beverages reported since antiquity (Alexander, 2009; Craddock, 2014). Especially prior to the development of modern antibiotics, starting with A. Fleming's discovery of penicillin in 1929 (Fleming, 1929), preparations of Ag were used by clinicians to treat a variety of ailments, ranging from topical tinctures to treat conjunctivitis to intravenous injections of colloidal Ag for the treatment of sepsis (Kausch, 1912; Schorn, 1919). Today, Ag still retains limited medical use, for example in the treatment of ulcers of the skin and mucuous membranes as well as in wound dressings (albeit with only limited evidence for its efficacy) (Alidaee et al., 2005; Dumville et al., 2016).

In modern times, Ag has found applications in a wide variety of contexts. Everyday uses of Ag include the manufacture of dental fillings, tableware, jewelry and selected medical applications. However it is most commonly used in industrial applications, including electrical conductors and contacts, catalysts or Ag-oxide batteries. During the 20th century, the photographic industry rose to become the major consumer of Ag, owing to the success of the silver halide process (Purcell & Peters, 1998).

This process relies on the reduction of Ag in the eponymous crystals of the Ag halides AgBr, AgCl and to a lesser extent AgI encased in a photographic film. Exposure to light (or x-rays) results in the initial reduction of small amounts of Ag^+ and the formation of Ag^0 clusters, that subsequently serve

as nucleation points for further reduction by a developing agent (Hamilton, 1988). The remaining, undeveloped Ag halides are removed from the film and are released into waste water and finally the environment. Based on data published by the U.S. Environmental Protection Agency (Scow et al., 1981), Purcell & Peters (1998) reported photographic manufacture and developing to be the largest single contributor to the environmental discharge of Ag in the United States, at approximately 749 t (or 30.3 % of the total emissions of Ag). The major share of these emissions (630 t or 25.5 % of the total emissions) was reported to be discharged to the land, whereas 119 t (4.8 %) were released to water, a minor contribution compared to the 438 t (17.8 %) ascribed to weathering of mineral deposits, that were reportedly entirely discharged to water.

With the advent of digital photography at the cusp of the 21st century, the use of Ag halide films was gradually phased out and global demand for Ag from the photographic industry has steadily decreased from a peak of ca. 7,660 t in 1999 to 865 t in 2020 (Figure 1.2). New applications for Ag have been found in photovoltaics, where global demand has continually increased since the first reported data. Demand is expected to rise further in conjunction with an increasing demand for renewable energy. (The Silver Institute, 2000, 2020).

1.1.2 Silver Nanomaterials

Another new area of Ag use is in the manufacturing of nanomaterials. The European Commission (EC) has recommended to define nanomaterials as: *"... natural, incidental or manufactured material containing particles, in an unbound state or as an aggregate or as an agglomerate and where, for 50 % or more of the particles in the number size distribution, one or more external dimensions is in the size range 1 nm-100 nm"* (EC, 2011). This definition includes nanoparticles (NP) of diverse geometries (e.g. spheres, prisms or cubes), nanorods, -wires and -disks, but also nanostructured surfaces.

Nanostructured materials possess unique properties different from bulk materials or dissolved species (Burda et al., 2005). An illustrative example is the size- and shape-dependent absorption of visible light by dispersed Ag- and Au-NP (Mogensen & Kneipp, 2014; Yeshchenko et al., 2012). More important however is their high surface-to-volume ratio, resulting in more atoms being exposed to the surrounding medium compared to the same mass of bulk material. This increases the number of reactive sites on the surface, making nanomaterials promising as catalysts, but also affects other physico-chemical properties such as melting point and the release of atoms and ions from their surface (Astruc et al., 2005; Burda et al., 2005; Molleman & Hiemstra, 2017).

Due to their potent antimicrobial properties, Ag nanomaterials have found applications in areas such as medicinal wound dressings and water purification, but also in consumer products like "body

odor-free" sportswear and antimicrobial devices (Kalantari et al., 2020; Q. Li et al., 2008; Vance et al., 2015). The estimated shares of different application sectors differ dramatically between publications, as illustrated by the following examples: based on a survey of the Nanotechnology Products Database (https://product.statnano.com/), Hicks & Temizel-Sekeryan (2019) reported medical, textile and cosmetics products to make up 23.0, 18.8 and 14.7 % of the market share of Ag-NPs, respectively. In comparison, estimations used by Giese et al. (2018) for these sectors are 1.21, 31.0 and 0.42 % respectively.

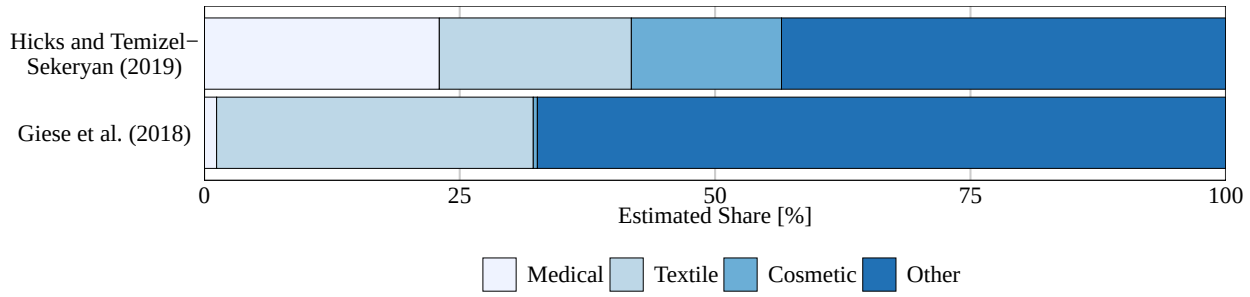

Figure 1.1: Estimations of Ag-NP market shares for the medical, textile and cosmetic sectors, illustrating uncertainties in Ag-NP use. Market shares of all remaining sectors are summarized under 'Other' and are presented for completeness.

Agricultural applications of Ag-NPs have also been explored (Deb, 2016; Heinisch & Buder, 2019), although they seem not to have found widespread use yet, with Hicks & Temizel-Sekeryan (2019) reporting an estimated market share of just 1.67 %.

Estimates for the production volumes of Ag-NPs are available from Pulit-Prociak & Banach (2016) from 2010 on, and are compared to the global demand for Ag in the photoprocessing industry in Figure 1.2. Production volumes are expected to further increase in the future and estimations for the year 2025 range between 400 and 800 t.

1.2 Silver Nanomaterials in the Environment

1.2.1 Releases into the Environment

Releases of Ag-NP into the environment may occur at all stages of a given products' lifecycle. Releases during the initial manufacturing of the particles and the products containing them depend both on the synthesis route as well as the production scale (Temizel-Sekeryan & Hicks, 2020). Releases occurring during the lifecycle of the product are also possible, as has been shown for nano-enabled textiles that leach Ag during regular washing (Geranio et al., 2009; Mitrano et al., 2014) or from facade paint during exposure to regular rain (Kaegi et al., 2010). Agricultural applications of nano-Ag such as in fertilizers, might additionally lead to direct releases into aquatic environments via runoff. Most releases are currently thought to end up into the environment during

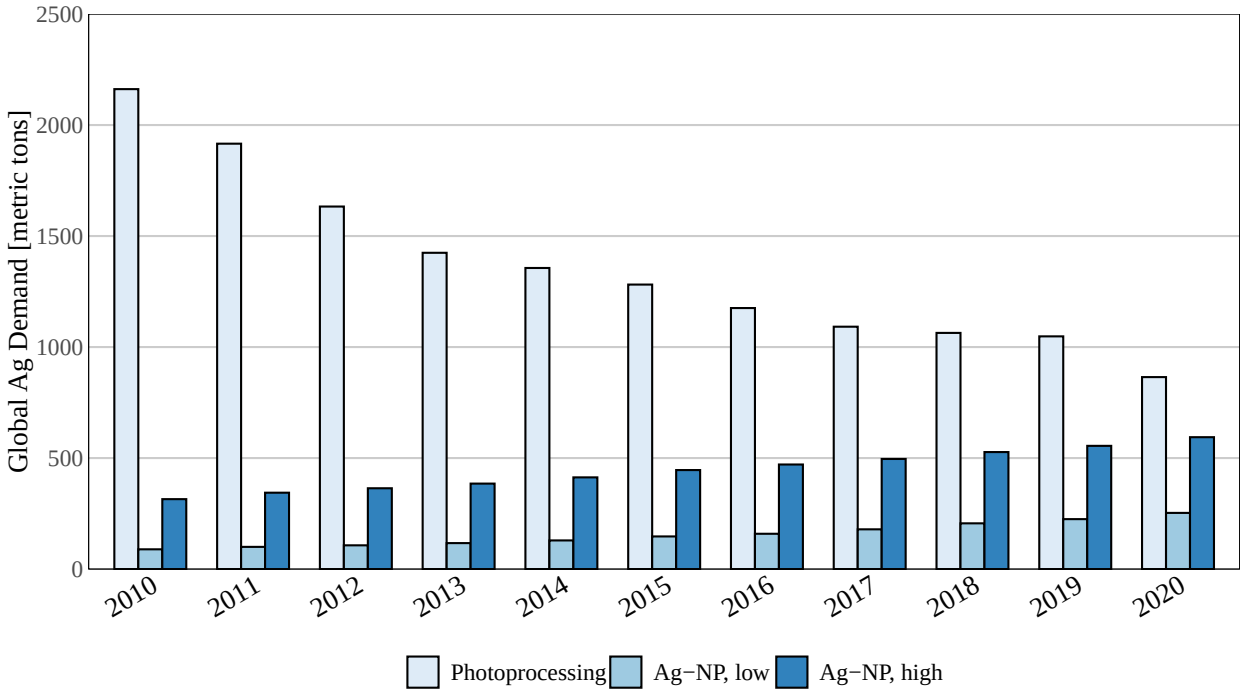

Figure 1.2: Global demand of Ag for photoprocessing compared to estimated Ag nanomaterial production volumes (low and high estimates) from 2010 to 2020. Data taken from The Silver Institute (2020) and Pulit-Prociak and Banach (2016).

the use and end-of-life phase, which includes effluents and sewage sludge from wastewater treatment plants (WWTP) and disposal in landfills (Bundschuh et al., 2018).

Releases from WWTP may discharge nanoparticles directly into aquatic systems via effluents or indirectly from sewage sludge used in agriculture or deposited in landfills. Kaegi et al. (2011) studied the behavior and transformation of Ag-NPs in a pilot-scale WWTP and calculated, that only 2.5 to 5 % of Ag-NPs were released directly via the effluents, whereas 85 to 90 % were contained in the sludge. Additionally, pristine Ag^0 particles were quickly sulfidized in the WWTP, resulting in approximately 86 % of particles in the effluent consisting of Ag_2S. Nabi et al. (2021) reported the removal of 82 to 96 % of Ag-NPs by five WWTPs in the United States. Effluent concentrations ranged between 0.008 and 0.04 µg Ag/L with practically all of the released Ag (>99 %) still present in the nanoparticulate fraction.

1.2.2 Environmental Concentrations - Analysis and Modelling

Analytical Approaches

The detection and quantification of manufactured nanoparticles in environmental matrices is highly challenging, and only very few data on the concentrations in environmental compartments exist (Azimzada et al., 2021; Peters et al., 2018; Wimmer et al., 2019). In their review, Nowack et al. (2015) described several factors that hamper these analyses: firstly, analytical methods need to be

highly sensitive to detect even low concentrations of nanoparticles, as well as selective, as particles need to be confidently discerned from dissolved species. Secondly, manufactured nanoparticles have to be distinguished from naturally formed particles and colloids such as iron oxides (Baalousha & Lead, 2007; von der Heyden et al., 2019). Element-selective techniques, such as mass spectrometry allow some degree of selectivity as long as the particles of interest differ in their elemental composition. Nano-sized particles may however also be formed from dissolved species due to environmental processes (Akaighe et al., 2011; Dong et al., 2020), and manufactured particles are additionally transformed by those very same processes, leading to indistinguishable mixtures of natural and anthropogenic particles (Lowry et al., 2012). Additionally, physical processes, such as agglomeration, homo- and heteroaggregation, sedimentation and adsorption change the form in which particles may be present in a given environmental compartment, further complicating comprehensive analyses (Lowry et al., 2012).

Thus, methods that lend themselves to the characterization of pristine nanoparticles in suspension, such as dynamic light scattering (DLS), fall short in the analysis of environmental samples. Fractionation by filtration through filters of progressively smaller pore size and analysis of the eluates is a simple approach allowing a rough estimation of the particle size distribution. Single-particle inductively-coupled plasma mass spectrometry (spICP-MS) has emerged as the method of choice for quantifying nanoparticles with high sensitivity, especially when coupled to separation techniques such as field-flow fractionation (FFF) (Mitrano et al., 2012; von der Kammer et al., 2011). The approach allows the calculation of approximate particle sizes from the obtained signal intensities. However, spICP-MS does not allow the distinction between natural and manufactured particles, and smaller particles adsorbed to larger natural ones might lead to incorrect results. Imaging techniques with element selective detection, such as electron microscopy with energy dispersive X-ray spectroscopy (EDX) or electron energy loss spectroscopy (EELS) are also a capable approach (Prasad et al., 2015). They allow the assessment of both number, shape and composition of particles present in a sample and can also confidently detect nanoparticles adsorbed to larger particles or taken up by biological specimens. However, these methods are limited by low sample throughput and relatively low sensitivity, as nanoparticles have to be present in the field of view to allow detection.

The only identified studies reporting environmental concentrations of Ag-NP in surface waters are summarized in Table 1.1. Peters et al. (2018) reported low concentrations of Ag-NPs along the rivers Meuse and Ijssel in the Netherlands with reported concentrations generally below 2.5 ng/L, except for two outlying measurements (6.0 and 6.6 ng/L), argued to have been caused by isolated large particles in the samples. Wimmer et al. (2019) investigated Ag-NPs and total Ag concentrations in the River Isar in Germany, with data on the water concentrations at several WWTP along

the river course. Ag-NP concentrations were generally elevated directly following WWTPs with up to 69.1 ng/L Ag-NP measured at a single sampling site. However, concentrations declined quickly downstream of the WWTPs due to dilution in the river and did not exceed 4.50 ng/L. Up to 36.5 % of the total Ag content were attributable to Ag-NP, highlighting that Ag emissions other than NP are still predominant. Finally, Azimzada et al. (2021) reported on Ag-NP in selected waterbodies and in precipitation on five continents, reporting up to 1.29 ng/L Ag-NPs in the Kiessee lake in Göttingen, Germany.

Table 1.1: Measured and predicted environmental concentrations of Ag nanomaterials in surface waters compiled from different sources. Where available, the predicted region, predicted year and specific type of nanomaterial considered are reported. n.d.: not detected.

Concentration [ng/L]	Year	Location	Note	Source
Measured Environmental Concentrations				
0.3 - 6.6	2018	The Netherlands	River Meuse and Ijssel	Peters et al. (2018)
0.33 - 69.08	2019	Germany	River Isar	Wimmer, Markus and Schuster (2019)
n.d. - 1.29	2021	Global	Freshwater Bodies across the World	Azimzada et al. (2021)
Probable Environmental Concentrations (PEC)				
4 - 320	2008	Germany	River Rhine	Blaser et al. (2008)
0.59 - 2.16	2009	Europe		Gottschalk et al. (2009)
0.09 - 0.43	2009	USA		
0.56 - 2.63	2009	Switzerland		
0.40 - 2.78	2014	Europe		Sun et al. (2016)
0.04 - 2.79	2017	Global		Giese et al. (2018)
0.005 - 1.35	2019	China	Hunan Province	Ding et al. (2019)
225 - 1799[a]	2020	Germany	River Rhine	Massarsky, Trudeau and Moon (2014)
0.36 - 10.70[b]	2020	Europe & USA		
0.11 - 18	2021	Europe	Pristine, dissolved and transformed particles	Hong, Adam and Nowack (2021)
0.06 - 6.26	2030	Global		Giese et al. (2018)
0.13 - 12.90	2050	Global		
Product-specific PECs				
1.09 - 15.63	2015	-	Nanotextiles	Voelker et al. (2015)
0.16 - 0.71	2015	-	Nanotextiles	Wigger et al. (2015)
0.009 - 0.014	2021	Europe	Medical Applications	Hauser and Nowack (2021)

[a] Extrapolated from Blaser et al. (2008)

[b] Extrapolated from Gottschalk et al. (2009)

Modeling Approaches - Probable Environmental Concentrations

Due to the lack of suitable analytical methods and the difficulty of distinguishing manufactured from natural nanoparticles, estimations of environmental nanomaterial concentrations have long relied on modeling approaches (Nowack et al., 2015). Material flow analysis (MFA) and its successors are among the most popular approaches and rely on the estimation of *material stocks* (e.g. production volume and products in use) that are introduced into, and *flow* through and out of the compartments of a predefined system (Figure 1.3) (Hendriks et al., 2000). Potential compartments originate from the technosphere (production, consumption, disposal) or the environment (e.g. atmosphere, surface waters, soils). MFA can be conducted using arbitrarily complex models, however, as the complexity of the model increases, so does the uncertainty of the results as well as the amount and quality of data required.

Data compiled from a variety of sources (including real world data, but also market surveys and estimates) is incorporated into the mathematical model. Thus, some studies have only focused on specific types of products, such as textiles or medical applications (Hauser & Nowack, 2021; Voelker et al., 2015; Wigger et al., 2015), while others have relied on estimated total nanomaterial production volumes (Blaser et al., 2008; Giese et al., 2018; Gottschalk et al., 2009; Sun et al., 2016). Modeling is also usually performed on large geographic scales, such as for a country or a (sub-)continent, providing only averaged results. This approach disregards potential socioeconomic differences between regions and also the spatial concentration of industrial operations, as is often seen in the chemical industry, which might lead to local hotspots of nanomaterial release into the environment.

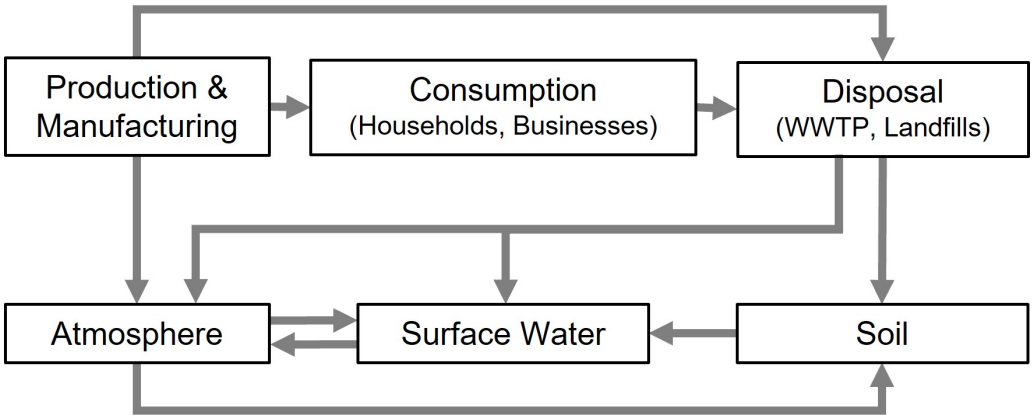

Figure 1.3: Sketch of a simple MFA model, consisting of three technosphere compartments (production & manufacturing, consumption and disposal) and three environmental compartments (atmosphere, surface waters and soils) connected by arrows that indicate the flow of material between compartments.

Probable environmental concentrations (PECs) of Ag nanomaterials in surface waters compiled from published reports are summarized in Table 1.1. It is evident that the modeled PECs vary quite widely, with a total reported range of 0.005 to 1799 ng/L. However, only Blaser et al. (2008) and

Massarsky et al. (2014) (who extrapolated Blaser et al.'s results to the year 2020) report PECs above 15.63 ng/L. These PECs lie in in the same order of magnitude as results reported from real world samples (see Section 1.2.2). Thus, it can be assumed that at the present time, the environmental burden from Ag nanomaterials is likely adequately predicted by modeling approaches, although proper validation is still lacking (Nowack et al., 2015).

1.2.3 Behavior of Nanoparticles in the Environment

Inherently, nanoparticles are thermodynamically unstable (Burda et al., 2005). Once discharged into aquatic systems, they will undergo a range of transformations that influence their properties, behavior and finally, fate in the environment. The basic transformations can be classified as physical (e.g. agglomeration, aggregation, adsorption and sedimentation) and chemical (e.g. oxidation and reduction, photochemical transformations, dissolution and precipitation) but in any real environment, these processes are interdependent and influence each other.

Physical Transformations

The agglomeration and aggregation of nanoparticles leads to the formation of larger particles with reduced surface-to-volume ratios. At a given size threshold, gravitation will overcome the suspending forces and sedimentation will commence. To prevent aggregation, nanoparticles are often coated with capping agents that stabilize the individual particles in dispersion by either electrostatic (e.g. citrate) or steric repulsion (e.g. poly-vinylpyrrolidone (PVP) or gum arabicum (GA)).

Water chemistry parameters, such as the presence of divalent cations (e.g. Ca^{2+} or Mg^{2+}) or natural organic matter (NOM) in the medium, also have a great influence on the behavior of nanoparticles. In suspension, the average size of citrate-coated Ag-NPs is highly correlated with Ca^{2+}, which neutralizes negative surface charges and thus facilitates aggregation. Sterically stabilized, PVP-coated particles on the other hand remain unaffected (Huynh & Chen, 2011; Milne et al., 2017; Topuz et al., 2015). In complex natural environments, nanoparticles are encased by a so-called *corona* of biomolecules, that may interact with, or even replace the original capping agents, significantly affecting their behavior. In their review, Docter et al. (2015) even conclude that, *"[f]rom a regulatory aspect, (bio)molecule-coated NMs may therefore be even considered as novel materials with different properties compared to pristine NMs during production"*. One of the more prominent examples is the stabilizing effect mediated by NOM, leading to less aggregation and thus longer residence times in the water column (Gao et al., 2012; Huynh & Chen, 2011; Milne et al., 2017; Topuz et al., 2015). In lotic systems for example, this will likely lead to faster transport along the river course and thus significant dilution in both water column and sediments. Conversely, in lentic environ-

ments, enhanced stability will affect the exposure (*concentration×time*) of both free-swimming and sediment-dwelling species compared to pristine particles that may sediment much quicker.

As the concentration of Ag-NP in aquatic environments (ng/L) is estimated to be much lower than that of NOM and other suspended matter (mg/L), heteroaggregation is favored over homoaggregation (H. Wang, Adeleye, et al., 2015). For example, AgNP have been shown to readily associate with clay particles often present in surface waters, forming aggregates and subsequently settling out of solution (Liu et al., 2015; H. Wang, Dong, et al., 2015; Zhou et al., 2012).

Chemical Transformations

Chemical transformations that are especially relevant for Ag-NPs are oxidation processes. These can either result in the release of toxic Ag^+ by dissolution or the formation of an insoluble "shell" (e.g. of Ag_2S or AgCl), encompassing an Ag^0 core.

Dissolution is influenced by several parameters: (I) smaller particles favor dissolution due to the increased specific surface area (Molleman & Hiemstra, 2017; Peretyazhko et al., 2014). (II) in water, dissolution is additionally dependent on the presence of dissolved O_2, as shown by both Liu & Hurt (2010) and Mulenos et al. (2020), who demonstrated significantly inhibited dissolution of nano-Ag under anoxic conditions. (III) Dissolution is further inhibited in a pH-dependent fashion, with strongly reduced Ag^+ release at increasing pH (Liu & Hurt, 2010; Molleman & Hiemstra, 2017). To complicate matters further, the type of capping agent used, or corona formed under environmental conditions, also influences dissolution: PVP-capped particles are more stable against aggregation, but release far more Ag^+ than their citrate capped equivalent (Kittler et al., 2010). Based on these results, Molleman & Hiemstra (2017) argue that high-affinity coatings like PVP might destabilize the particle surface, resulting in this phenomenon.

Oxidation and subsequent formation of insoluble Ag_2S (solubility product: $K_{sp} = 5.5 \times 10^{-51} mol^3/L^3$ at 25 °C (Wiberg, 2008b)) is the second process often observed in natural waters. Surface-sulfidized Ag-NPs are the main form of Ag-NP released from WWTP and are also formed in natural environments in the presence of sufficient quantities of S^{2-} and are much more resistant to dissolution than pristine Ag^0 particles (Kaegi et al., 2011; Levard, Hotze, et al., 2013; Lowry et al., 2012).

Two mechanisms proposed for the formation of Ag_2S from Ag-NPs are: (I) oxidation of Ag-NPs, followed by sulfidation of the released Ag^+ (Equation 1.1 and 1.2) which might lead to the formation of distinct Ag_2S-NP and -bridges between particles (Levard et al., 2011), or (II) a direct oxysulfidation of the Ag-NP surface (Equation 1.3), forming a passivating Ag_2S-shell around the remaining particle (Liu et al., 2011; Zhang et al., 2018). Both mechanisms are dependent on the

presence of dissolved O_2, which can only be present in traces under anaerobic conditions, where sulfidation occurs in the environment. In fact, in an experiment studying the long-term transformation of Ag-NPs in freshwater mesocosms (a simulated natural environment typically on the scale of a few liters to several hundred liters), only 55 % of the added Ag-NPs were found to be sulfidized after 18 months. This indicates, that sulfidation might be slow under realistic conditions, possibly due to the low concentrations of dissolved O_2 and the presence of other metals that are easily sulfidized (Lowry et al., 2012).

$$4\,Ag + O_2 + 2\,H_2O \longrightarrow 4\,Ag^+ + 4\,OH^- \tag{1.1}$$

$$4\,Ag^+ + 2\,SH^- + 2\,OH^- \longrightarrow 2\,Ag_2S + 2\,H_2O \tag{1.2}$$

$$4\,Ag + O_2 + 2\,SH^- \longrightarrow 2\,Ag_2S + 2\,OH^- \tag{1.3}$$

As chloride Cl^- is an ubiquitous anion in freshwaters, the formation of sparingly soluble AgCl (solubility product: $K_{sp} = 1.7 \times 10^{-10} mol^2/L^2$ at 25 °C (Wiberg, 2008b)) presents the third type of chemical Ag-NP transformation in aqueous systems (Zhang et al., 2018). AgCl forms by precipitation of oxidatively dissolved Ag^+ (see Equation 1.1) and is thus also dependent on the presence of dissolved O_2. X. Li et al. (2010) showed a partial dissolution and bridge-forming behavior of Ag-NP when exposed to high concentrations of Cl^-, similar to what was observed by Levard et al. (2011) in the presence of S^{2-}. Additionally, depending on the Cl^-/Ag^+ ratio in the medium, either insoluble AgCl or soluble chloro complexes ($[AgCl_2]^-$, $[AgCl_3]^{2-}$, etc.) are formed, significantly influencing the environmental behavior (Levard, Mitra, et al., 2013).

1.3 Environmental Risks posed by Silver Nanomaterials

No published guidelines for Ag-NP in aquatic ecosystems are available to date. Existing regulations on Ag in water are summarized below.

The U.S. Environmental Protection Agency (U.S. EPA) has previously published water quality guidelines for Ag in freshwater, setting acute guidance values (Criteria Maximum Concentration, CMC) for the protection of aquatic life dependent on the concentration of $CaCO_3$ dissolved in the water (Equation 1.4) (U.S. EPA, 1980). More recent guidelines are available from the Canadian Council of Ministers of the Environment (CCME), setting guidance values in freshwaters for short- and long-term exposure at 0.25 µg/L (CCME, 2015) and the World Health Organization (WHO),

setting a provisional health-based reference value of 0.1 mg/L Ag in drinking water (WHO, 2021).

$$CMC\ [\mu g\ Ag/L] = e^{1.72 \cdot ln(c(\mathrm{CaCO_3}\ [mg/L])) - 6.52} \tag{1.4}$$

1.3.1 Toxicity and Toxicity Testing in Aquatic Environments

Ag is among the elements most toxic to fish, invertebrates and microorganisms (Ratte, 1999). The concentration of free Ag ions (Ag^+) has been considered the main determinant of its toxicity in aquatic ecosystems, which is significantly influenced by water chemistry. Dissolved organic carbon as well as anions forming insoluble Ag salts and complexes (e.g. Cl^-, S^{2-}) can modulate the observed acute toxicity of Ag considerably, due to altered bioavailability (Ratte, 1999). Higher solubility does however not imply higher toxicity. The thiosulfate complex $Ag(S_2O_3)_2{}^{3-}$ for example, is the main species of Ag present in photoprocessing effluents and is highly soluble in water, but is considerably less toxic than the similarly soluble silver nitrate ($AgNO_3$), as the high stability of the complex leads to a virtual absence of free Ag^+ (Bard et al., 1976).

In recent years, the potential toxicity of nanoparticles has received increasing attention, as their unique properties (small particle size, high specific surface area, high reactivity and catalytic potential) might give rise to additional adverse effects in exposed biota - nanotoxic effects - that can not be ascribed to the properties of the bulk material or dissolved species alone (Moore, 2006).

With the known toxicity of Ag, numerous studies have been conducted to elucidate the effects of Ag-NP to a whole range of aquatic species, using standardized ecotoxicity tests as well as novel approaches to study their bioavailability and -accumulation, trophic transfer, toxicity and (sub-)cellular effects. Due to the complex behavior and transformations of nanoparticles in aqueous media (see section 1.2.3), the validity of standardized tests, designed for the assessment of "classic" pollutants that assume uniform, or static conditions over the time of exposure, has been called into question (Holden et al., 2016). This has additionally been accompanied by contradictory results from toxicity studies. Some authors report the observation of nanotoxic effects, often mediated by the induction of reactive oxygen species (ROS), whereas others report no additional or even lower toxicity compared to Ag^+ (Kalantzi et al., 2019; T. Wang & Liu, 2022). Currently, a consensus seems to be evolving that Ag-NP do bioaccumulate in exposed species, but are less toxic than their dissolved counterpart. However, open questions still remain, such as the potential of Ag-NP to biomagnify across different food chains, chronic effects of long-term exposures under environmentally realistic conditions and combinatory effects with other pollutants ("trojan horse-effect") (Dang et al., 2021; Holden et al., 2016).

Novel approaches have been proposed to better characterize the interaction of nanoparticles with

aquatic biota and to integrate their dynamic properties (surface functionalization, dissolution, particle and aggregate size, sedimentation, etc.) into ecotoxicity assessments (Bour et al., 2015). Additionally, tiered evaluation approaches have been suggested to better allocate the limited resources available for ecotoxicity testing, consisting of laboratory screening studies on the lowest tier, with higher tiers incorporating larger-scale, environmentally relevant scenarios, mechanistic investigation of effects and modeling (Holden et al., 2016).

One type of approach that has garnered increased popularity is the use of mesocosms to study the environmental effects of nanoparticles. A mesocosm is designed to represent a simplified, artificial recreation of an ecosystem, such as a river bed or an estuary on a scale of a few liters to several hundred liters. Mesocosms allow a degree of realism that is not possible in simple laboratory studies, as they (I) are large enough to accommodate multiple specimens of different test species, allowing e.g. studies of trophic transfer, species interactions and population dynamics during exposure, (II) permit control of key chemical and physical parameters, such as pH, salinity or NOM, allowing the simulation of sensitive ecosystems (such as peat bogs) that can not be studied in the field, (III) allow experiments to run for extended amounts of time (months to years) due to their self-sustaining nature, facilitating the investigation of long-term transformations and behaviors of nanoparticles and their effects, and (IV) can be conducted outdoors, where the system is exposed to the weather and seasons, adding further realism and allowing the investigation of indirect and chronic effects that may remain hidden during tightly-controlled laboratory experiments (Carboni et al., 2021).

Naturally, with increasing realism, the number of factors influencing the system also increases, complicating the interpretation and deduction of firm cause-effect relationships. The typical size of mesocosms also prohibits highly replicated studies, if not due to issues of available space, then due to prohibitively high effort required for setup and maintenance. As such, they are not appropriate for the initial screening of adverse effects and should be set up after initial risk assessments have been conducted in the laboratory (Holden et al., 2016). In such tiered approaches, they serve as invaluable tools to investigate the realistic fate and ecosystem-level effects of nanomaterials, generating valuable data for environmental risk assessments and new avenues of investigation for mechanistic studies on smaller scales (Carboni et al., 2021).

1.3.2 Aquatic Plants as Target Organisms

Next to unicellular organisms, invertebrates and vertebrate species, aquatic higher plants (or hydrophytes) are ubiquitous and essential inhabitants of aquatic ecosystems. Although they have an important role as primary producers, provide habitats to other organisms and serve as an important food source (Lodge, 1991), they remain understudied in environmental risk assessments and nanotoxicology in particular (Thwala et al., 2016). Terrestrial plants, especially food crops,

have been investigated more thoroughly, but the results obtained from these studies can not be generalized to hydrophytes due to key differences in their physiology and habitat (Chhipa, 2017; Kah et al., 2019).

Terrestrial plants take up water and nutrients from the soil through their roots as well as CO_2 through specialized openings on their leaves (called stomata) and produce glucose and oxygen through photosynthesis. Hydrophytes also depend on photosynthesis to produce glucose for their energy metabolism, however the uptake routes of nutrients differ considerably from their terrestrial counterparts. Roots constitute an important organ of many hydrophytes and are used to anchor in the sediment and extract nutrients from the sediment. However, not all aquatic plants produce true roots. Some only form reduced, so called "adventitious" roots, whose main purpose is anchorage, while the uptake of nutrients takes on a less prominent role (Arber, 2010b; Carignan & Kalff, 1980). Free-floating species acquire all required nutrients from the surrounding water, but sometimes still produce appendages that are anatomically equivalent to roots, which can serve as additional photosynthetically active surface for the assimilation of CO_2 (Arber, 2010b). Stomata are often only present in a reduced, nonfunctional state in submerged plants, as exchange of gases is mediated by the entire surface of the plant. This is often further facilitated by the absence of a waxy cuticle, typical for terrestrial plants, that prevents the evaporative loss of water but also impairs gas exchange, necessitating the presence of stomata (Arber, 2010a; Strasburger et al., 1991a).

Bioaccumulation

The close contact of the entire plant with the aquatic phase and the absence of a protective cuticle has important implications for their interaction with pollutants, such as toxic metal ions but also nanoparticles. Previous research into the interactions and especially the uptake of various heavy metals by aquatic plants has shown that bioaccumulation is commonly observed (Cardwell et al., 2002). Some plants, termed "hyperaccumulators", are able to enrich certain pollutants to unusually high levels (typically defined as $>$ 1 g/kg dw), which has been exploited in the remediation of polluted sites (Rahman & Hasegawa, 2011; Robinson et al., 2006), but might also lead to increased exposure of herbivores feeding on these plants (Lodge, 1991; Plessl et al., 2017).

Uptake mechanisms of heavy metal ions are dependent on the specific element and its speciation. For some elements, such as arsenic and cadmium, they have been elucidated in terrestrial plants, where uptake occurrs predominantly through the roots. Mechanistic evidence for the uptake of Ag^+ is still limited to a single publication investigating copper transport proteins in *Arabidopsis thaliana* and completely absent for hydrophytes (Andrés-Colás et al., 2010). In cultivated mouse cells, the overexpression of the copper transporter gene *Ctr1* increased the uptake of Ag^+, making an analogous mechanism in plants conceivable (Bertinato et al., 2010). Similarly, in plants

hyperaccumulating nickel or cadmium, the uptake is mediated by transporter proteins responsible for the uptake of zinc, which is preferentially hyperaccumulated by these plants. Hyperaccumulation additionally requires mechanisms that allow the plants to tolerate and sequester heavy metals without suffering toxic effects observed in non-accumulator plants. Thus it has been argued that this peculiarity might have evolved to deter predators (Rascio & Navari-Izzo, 2011).

With growing concerns of the potential effects of nanoparticles on the environment, their bioaccumulation has also been investigated in several plant species. The proposed uptake mechanisms are necessarily distinct from those allowing the accumulation of ionic species, save for those NP that show high dissolution potential, as is the case for Ag-NP (Thwala et al., 2016). Potential accumulation pathways in submerged aquatic plants include (Ia) sorption of particles and agglomerates to the plants' surface without penetration into tissues, (Ib) sorption and subsequent uptake of ions released from the particles, (II) uptake of particles of sufficiently small size through openings in the plant surface such as stomata or cell wall pores and into the cell by endocytosis and (IV) the uptake of ions released from particles not associated with the plants (Thwala et al., 2016).

Several studies have investigated the bioaccumulation and localization of Ag-NPs in different species of hydrophytes and are summarized in Table 1.2. Some of these studies contrasted Ag-NPs to dissolved Ag^+ (in the form of $AgNO_3$) or sulfidized Ag-NP to simulate aged particles, the results of which are also included in Table 1.2.

The reported bioaccumulation of Ag-NP in the literature is extremely variable regarding species, exposure time, concentration and types of particles used, but some common trends are observed. Most data is available for floating plant species (e.g. duckweeds: *Lemna* spp., *Landoltia* spp. and *Spirodela* spp.), while data is only available for three species of submerged plant (*Egeria densa*, *Ottelia alismoides* and *Potamogeton diversifolius*). Experiments were typically conducted for up to 28 days, but were extended up to one year in Yuan et al.'s mesocosm experiment. Concentrations were usually chosen in the high µg/L- to low mg/L-range (0.5 - 10 mg/L) and were added as a single dose, expect for Yuan et al. (2018), who conducted a pulsed experiment with weekly additions of 0.014 mg/L (total dose 0.74 mg/L).

Table 1.2: Bioaccumulation of Ag from Ag-NP in floating and submerged aquatic plants compiled from published literature. For studies reporting concentrations at multiple timepoints or over multiple concentrations, the maximally accumulated tissue concentrations are reported.

Species	Type	Size [nm]	Concentration [mg/L]	Time	Accumulated Ag [mg/kg dw]	Source
Floating Plants						
Azolla filiculoides	Ag-NP	26.7	0.1 - 100	8 d	13.4	López-Herrera et al. (2021)
Hydrilla verticillata	Ag-NP (PVP)	20	0.5	90 d	~60	Jiang et al. (2017)
	$AgNO_3$	-	0.5	90 d	~60	
Lemna gibba	Ag-NP	50	0.01 - 10	7 d	17.5	Oukarroum et al. (2013)
Lemna minor	Ag-NP	126.5	10 - 100	15 d	~110	Ding et al. (2019)
Landoltia punctata	Ag-NP	6.3	1	24 h	389	Stegemeier et al. (2017)
	Ag_2S-NP	7.8	1	24 h	372	
	$AgNO_3$	-	1	24 h	685	
Landoltia punctata	Ag-NP (GA)	12	2.5	28 d	~300	Colman et al. (2014)
	Ag-NP (PVP)	49	2.5	28 d	~300	
	$AgNO_3$	-	2.5	28 d	~300	
Landoltia punctata	Ag-NP	27.2	0.16 - 10.24	7d	48500	Lalau et al. (2020)
Nelumbo nucifera	Ag-NP	5 - 10	0.5 - 10	72 h	~90	Li et al. (2022)
Pistia stratiotes	Ag-NP	20	0.02 - 2	48 h	127	Hanks, Caruso and Zhang (2015)
	$AgNO_3$	-	0.02 - 2	48 h	101	
Salvinia minima	Ag-NP (Citrate)	8.6 & 41.5	0.6	48 h	193	Thwala, Klaine and Musee (2021)
Salvinia auriculata	Ag-NP (PVP)	36	1 - 10	64 d	58.1	Palácio et al. (2020)
Spirodela polyrhiza	Ag-NP (GA)	6	0.5 - 10	72 h	2810	Jiang et al. (2012)
	$AgNO_3$	-	0.5 - 10	72 h	11100	
Submerged Plants						
Egeria densa	Ag-NP	3.9	0.74	1 y	17.8	Yuan et al. (2018)
	Ag-NP	3.9	0.014 (per week)	1 y	19.5	
	Ag_2S-NP	24.2	0.014 (per week)	1 y	6.3	
Egeria densa	Ag-NP (GA)	12	2.5	28 d	~1600	Colman et al. (2014)
	Ag-NP (PVP)	49	2.5	28 d	~600	
	$AgNO_3$	-	2.5	28 d	~2200	
Egeria densa	Ag-NP (GA)	25	7.5	9 mo	~3400	Stegemeier, Avellan and Lowry (2017)
	Ag_2S-NP	34	7.5	9 mo	~2900	
Potamogeton diversifolius	Ag-NP (GA)	12	2.5	28 d	~1300	Colman et al. (2014)
	Ag-NP (PVP)	49	2.5	28 d	~600	
	$AgNO_3$	-	2.5	28 d	~1600	
Ottelia alismoides	Ag-NP	6.1	0.001 - 1	48 h	2940	Wang et al. (2023)

Therefore, the reported tissue concentrations also varied considerably between the experiments: in floating plants, the highest concentration was reported at an extreme 48,496 mg/kg dw in the duckweed *Landoltia punctata* after seven days of exposure to 10.24 mg/L Ag-NP (Lalau et al., 2020), whereas another species of duckweed, *Lemna gibba*, accumulated a mere 17.5 mg/kg dw after exposure to 10 mg/L for the same timespan (Oukarroum et al., 2013).

An extremely wide range of concentrations was also reported in submerged plants, with *Egeria densa* accumulating approximately 4,000 mg/kg dw within a month of exposure to Ag-NP, although this concentration declined to approx. 3,400 mg/kg dw at the conclusion of the experiment, nine months after a single Ag-NP-dose of 7.5 mg/L (Stegemeier, Avellan, et al., 2017). In contrast, Yuan et al. (2018) report finding only 17.8 mg/kg in the tissues of the same plant, nine days after exposure to a single dose of 0.74 mg/L, with tissue concentrations declining below 2.5 mg/kg after one year. Higher bioaccumulation was found by the same authors when the plants were exposed to weekly additions of 14 µg/L, with a peak concentration of 19.5 mg/kg after 54 days, declining to just below 10 mg/kg after one year.

Investigations of Ag-NP internalization have been undertaken by López-Herrera et al. (2021) in the floating fern *Azolla filiculoides*, showing that Ag-NP (29 nm) were present inside the root cells after eight days of exposure to 100 mg/L Ag-NP, although the roots were severely damaged at this concentration. They suggested the uptake of Ag^{+} released by dissolution of the Ag-NPs and subsequent intracellular precipitation as the likely mechanism. W. Wang et al. (2023) provided electron microscopic evidence of Ag-NP (6.1 nm) accumulation at the cell wall and inside the chloroplasts of *Ottelia alismoides* after 48 h of exposure to 0.1 mg/L Ag-NP. Lalau et al. (2020) also noted the accumulation of electron-dense particles in the cell wall of *Landoltia punctata*, but did not provide evidence for the identity of these particles. Likewise, Thwala et al. (2021) and Souza et al. (2021) have suggested the internalization of Ag-NP into the roots of *Salvinia minima* and *Lemna minor* but did not provide direct evidence of particles taken up into the plants' tissues.

Toxicity

Most studies of Ag-NP bioaccumulation in aquatic plants have also included some toxicological endpoints, such as growth or photosynthetic pigments, which were both affected by Ag-NP in a concentration dependent manner (Lalau et al., 2020; Oukarroum et al., 2013; W. Wang et al., 2023). Others specifically investigated the subcellular basis of the observed toxic effects. Common findings include an induction of reactive oxygen species (ROS) and a concentration-dependent increase of antioxidative enzymes, such as catalase as well as glutathione sulfotransferases [Oukarroum et al. (2013); Jiang2014; Pereira et al. (2018)]. Again, marked effects were noted regarding the nature of the used particles, with pure Ag particles produced by laser-ablation showing toxicity to *L. minor*

at concentrations as low as 5 µg/L, whereas conventionally available Ag-NPs caused toxicity only at 20-fold higher concentrations of 100 µg/L (Minogiannis et al., 2019; Oukarroum et al., 2013).

1.4 *Myriophyllum spicatum* as a Test Organism for Nanoparticle Bioaccumulation

Myriophyllum spicatum is a submerged freshwater macrophyte species native to Eurasia and North Africa and has been introduced to both North America and New Zealand, where it is considered an invasive species (Cook, 1985; Couch & Nelson, 1985). *M. spicatum*, along with *M. verticllatum*, is commonly found in the Danube floodplains, including the Lobau, a part of the Danube-Auen National Park (Rotter & Schratt-Ehrendorfer, 1999). Only the inflorescence of *M. spicatum* rises above the water surface, while all other parts of the plant remain permanently submerged. The glabrous stem is red with younger shoots still having a green color. It can reach lengths up to 7 m and frequently branches near the surface. The lush green leaves are pinnate, up to 4 cm long, with each leaflet having a round cross-section. They grow in whorls of 4 along the stem (Aiken et al., 1979). Older leaves are typically encrusted with white carbonate precipitates due to its ability to utilize HCO_3^- as a carbon source (Rotter & Schratt-Ehrendorfer, 1999). Adventitious roots are formed to anchor in the sediment but only play a limited role in nutrient acquisition (Carignan & Kalff, 1980). *M. spicatum* is tolerant to a wide range of water conditions, including acidic and akaline waters (pH 2.9 - 10.2) and tends to thrive under eutrophic conditions (Rotter & Schratt-Ehrendorfer, 1999; Warrington, 1988).

Figure 1.4: Photograph of a shoot of *M. spicatum*. Old stems appear reddish-brown with carbonate encrusted, pinnate leaves, while the young shoot appears lush green.

Due to its robustness, environmental prevalence and easy cultivation, *M. spicatum* has been employed as a test organism in two ecotoxicity tests developed by the Organisation for Economic Co-operation and Development (OECD, 2014a, 2014b). As mentioned in section 1.3.2, data on the

bioaccumulation as well as internalization of Ag-NP in submerged macrophytes is sparsely available. Furthermore, the available data was obtained in experiments with exposures much higher than current Ag-NP PECs and measured concentrations, calling into question the environmental relevance of the chosen approaches. No published data on the bioaccumulation and internalization of Ag-NP in *M. spicatum* is available so far, even though it has been investigated as a possible bioindicator for trace element contamination (Grudnik & Germ, 2010; Ustaoğlu et al., 2022).

1.5 Goal of the Thesis

Given these conditions and the fact that *M. spicatum* is an established test organism in ecotoxicology, the goal of the present thesis was a preliminary investigation of the bioaccumulation of two types of Ag-NPs and the distribution of these particles between the compartments plant, sediment and aquatic phase in a small-scale mesocosm experiment. Additionally, the bioaccumulation of Ag-NP was contrasted to dissolved Ag in the form of $AgNO_3$. To improve on existing approaches relying on environmentally unrealistic exposures, a scenario closer to current and predicted environmental concentrations was chosen. This approach allowed an enhanced degree of environmental realism while retaining sufficient analytical sensitivity to investigate the fate of Ag. Furthermore, to complete the investigation, electron microscopy was employed to elucidate whether the Ag associated with the plants was adsorbed or internalized.

2 Materials and Methods

2.1 Reagents

2.1.1 General Reagents

In the mesocosm experiments, a medium similar to water from the Danube river at Vienna (Artificial Danube Water, ADW) was used. This medium was prepared using deionized water. For all other purposes, Milli-Q water (conductivity < 0.055 µS/cm) was used.

The following salts were used either for the preparation of artificial danube water or the preparation of ion chromatography eluents: Magnesium sulfate heptahydrate ($MgSO_4 \cdot 12\,H_2O$, ACS reagent ≥ 98 %), magnesium nitrate hexahydrate ($Mg(NO_3)_2 \cdot 6\,H_2O$, ACS reagent 98.0-102.0 %), calcium chloride dihydrate ($CaCl_2 \cdot 2\,H_2O$, p.a. 99-103 %), sodium bicarbonate ($NaHCO_3$, SigmaUltra $\geq$ 99.5 %), potassium bicarbonate ($KHCO_3$, p.a. ≥ 99 %), calcium carbonate ($CaCO_3$, ACS reagent ≥ 99.0 %), magnesium carbonate ($MgCO_3$, purum ≥ 40 % Mg (as MgO)) and humic acid sodium salt (technical grade) were purchased from Sigma-Aldrich (Vienna, Austria). Anhydrous sodium carbonate (Na_2CO_3, Analytical reagent grade) was purchased from Fisher Scientific (Vienna, Austria). Quartz Sand (grain size: 0.4 - 0.8 mm) was purchased locally and thoroughly washed with tap water until the water was free of turbidity.

Pressurized carbon dioxide (CO_2, N4.5), argon (Ar, N5.0) acetylene (C_2H_2, N2.6) and synthetic air (N5.0, 79.5 % N_2, 20.5 % O_2) were purchased from Messer Austria GmbH (Vienna, Austria).

Hydrochloric acid (≥ 30 %, TraceSELECT™, for trace analysis) was purchased from Honeywell International (Vienna, Austria). Phosphoric acid (puriss. p.a. ≥ 85 %) was purchased from Merck KGaA (Vienna, Austria). Nitric acid (> 68 %, PrimarPlus-Trace analysis grade) was purchased from Fisher Scientific and hydrogen peroxide (≥ 30 %, for trace analysis) from Sigma-Aldrich.

A silver standard solution (1,000 mg/L, Ag in 2 % HNO_3, AVS Titrinorm®) was purchased from VWR International GmbH (Vienna, Austria) and stored at room temperature. Working solutions for the preparation of calibration standards were prepared by diluting this standard to 10 mg/L and 100 µg/L using 2 % HNO_3 in 100 mL volumetric flasks. The working solutions were stored away from light to prolong stability.

2.1.2 Silver Nanoparticles

Ag Nanopowder (< 100 nm particle size, 99.5 %, dispersed with PVP) was purchased from Sigma Aldrich and stored at room temperature under an Ar atmosphere. A stock dispersion containing 57.8 mg/L was prepared by suspending 14.46 mg of the nanopowder in 250 mL of Milli-Q water and sonicating the suspension in an ultrasonic bath for 90 min.

Ag Nanospheres (50 nm diameter, 5 mg/mL in water, functionalized with PVP 40 kDa) were purchased from nanoComposix (San Diego, US) and stored at 4 °C.

2.2 Nanoparticle Characterization

At 50 mg/L, the Ag-NP suspensions were visually distinct (Figure 2.1 A): the freshly sonicated nanopowder suspension was almost opaque with a brownish-grey color. Sedimentation of black agglomerates was already apparent 30 minutes after sonication (Figure 2.1 C). In contrast, the PVP-coated nanospheres formed a highly stable, deeply orange-yellow, under direct light opaque, yellowish-grey appearing, suspension (see Figure 2.1 D). No sedimentation of the nanospheres was apparent at any point during the entire course of the experiments.

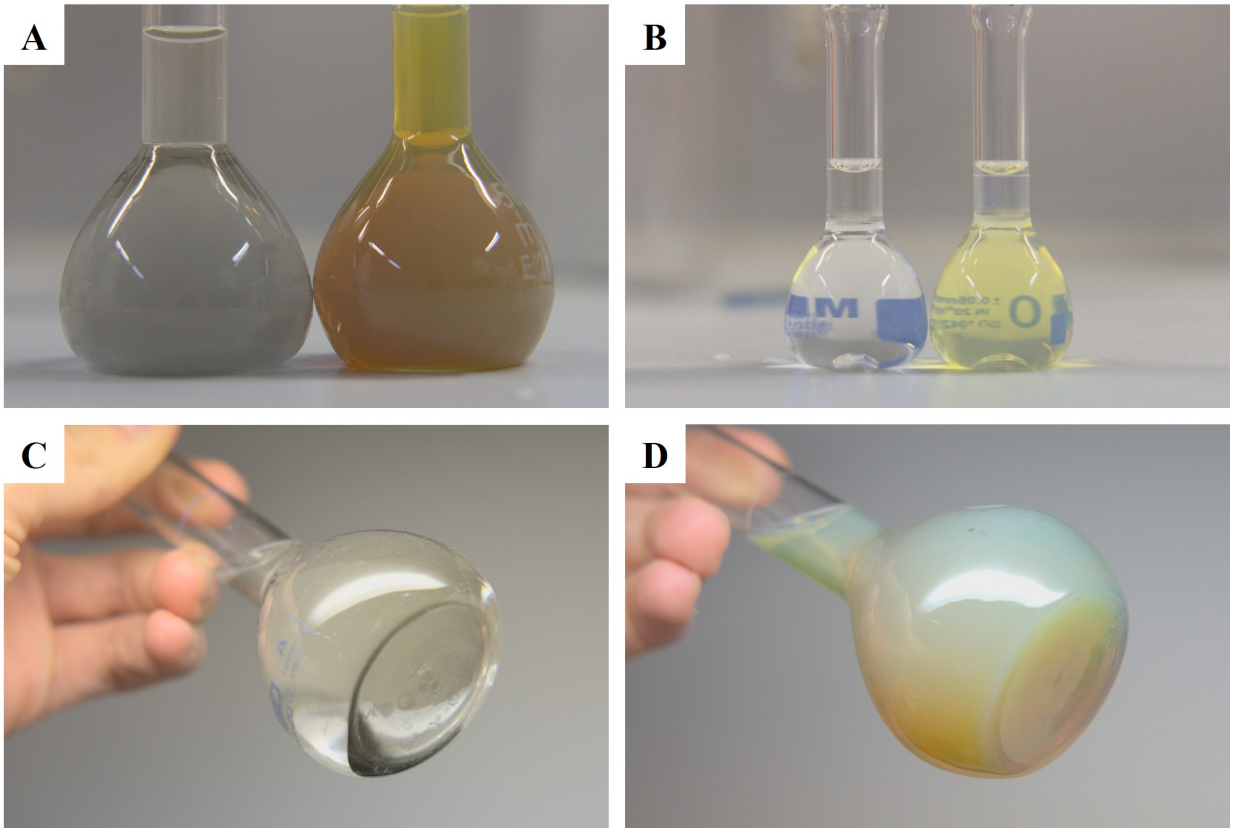

Figure 2.1: Photos of the Ag-NP suspensions at A: 50 mg/L. and B: 5 mg/L (left: Nanopowder, right: Nanospheres). C: Sedimented Nanopowder at the bottom of the volumetric flask. D: The Nanospheres under direct light, showing a pale yellowish-grey color.

2.2.1 Preliminary Digestion Experiments

To accurately quantify the content of Ag-NPs in aqueous solution, different digestion protocols were evaluated using a suspension of the Ag nanopowder. Principally, 5 mL of an Ag-NP stock solution was diluted with 5 mL of concentrated HNO_3 and digested: a) for one hour at room temperature, b) in an oven at 70 °C or c) at 130 °C in glass digestion tubes in a digestion oven (Liebisch Labortechnik). At room temperature and 70 °C, 10 ml glass volumetric flasks were used for the digestion. After digestion and cooling to room temperature, the samples were diluted to 10 mL with Milli-Q water. The samples were then measured either unfiltered or after filtering through 0.22 µm PTFE syringe filters to remove agglomerated undigested particles.

Digestion for one hour at room temperature proved to be sufficient to fully digest the Ag-NPs in aqueous solution and was thus used to characterize the dosing stocks (see section 2.3.4) and the contaminated mesocosm water.

2.2.2 Hydrodynamic Diameter

Dynamic light scattering (DLS) of the Ag-NPs was kindly assessed by the Environmental Geosciences Research Group at the Centre for Microbiology and Environmental Systems Science of the University of Vienna.

An Anton Paar Litesizer 500 Particle Analyzer was used to determine the hydrodynamic diameter (HDD) in the stock suspensions. The instrument was operated in backscatter mode (23° and 175° measuring angle) and the samples were equilibrated for 60 s before measurements.

2.2.3 Transmission Electron Microscopy

Transmission electron microscopy (TEM) of the Ag-NPs was kindly performed by the Core Facility of Cell Imaging and Ultrastructure Research (CIUS) of the University of Vienna.

A drop of the respective stock suspension, diluted to 5 mg/L was placed onto a film-coated copper grid, left to evaporate and then imaged on a Zeiss Libra 120 transmission electron microscope at a magnification of up to 31,500×. Electron energy loss spectroscopy (EELS) was additionally performed for the element-selective detection of Ag.

The obtained images were evaluated semi-automatically at a magnification of 4,000×. Particle area, circularity (see equation 2.1) and the Feret diameter (caliper diameter) were calculated using the image processing software Fiji (Schindelin et al. (2012), version 1.53t).

The circularity of a particle describes how closely a particles' shape matches that of a circle, with a value of 1 indicating a perfect circle. When the perimeter of the particle increases, while the area

stays constant (for example if the spherical particle was elongated), the circularity of the particle decreases. An illustrative example showing the circularities of three different shapes is given in Figure 2.2.

$$Circularity = 4\pi \frac{Area}{Perimeter^2} \tag{2.1}$$

Circularity: 1.00 0.78 0.24

Figure 2.2: Circularity values of three different shapes.

Semi-automated Analysis of TEM-micrographs

The analysis was carried out on micrographs at 4,000× magnification, as this allowed the detection of a sufficient number of particles while still allowing accurate quantification of their sizes. The resolution of the analyzed pictures was 3.7 nm/px. A minimum particle area of 20 px^2 (approximately the area of a circular particle with a diameter of 18.5 nm) was additionally set for the analysis, to prevent the erroneous identification of ambiguous signal (noise) as particles.

For both types of Ag-NP, the contrast in the micrographs was initially insufficient to accurately detect the individual particles using intensity thresholding with Fiji (Figure 2.3 A). To increase contrast, a Gaussian blur with a standard deviation of 25 px was applied to the original image and subsequently subtracted from the original image to reduce the intensity of background noise in the micrographs (Figure 2.3 B). Thresholding was then performed to accurately detect the particles and agglomerates (Figure 2.3 C). Individual particles that were insufficiently resolved were manually separated after the initial automatic detection.

2.3 Experimental Setup

2.3.1 Plant collection and maintenance

Shoots of the common aquatic macrophyte *Myriophyllum spicatum* were collected on June 30th, 2022 from Danube wetland waterbodies in Vienna. The plants and about 10 L of water from each of the respective waterbodies were transferred to sealed plastic containers for transport. After transport, the plants and water were promptly transferred to an aquarium filled with about 100 L of tap water (Figure 2.4 A). The aquarium was maintained on a 12:12 h light:dark-cycle. To prevent

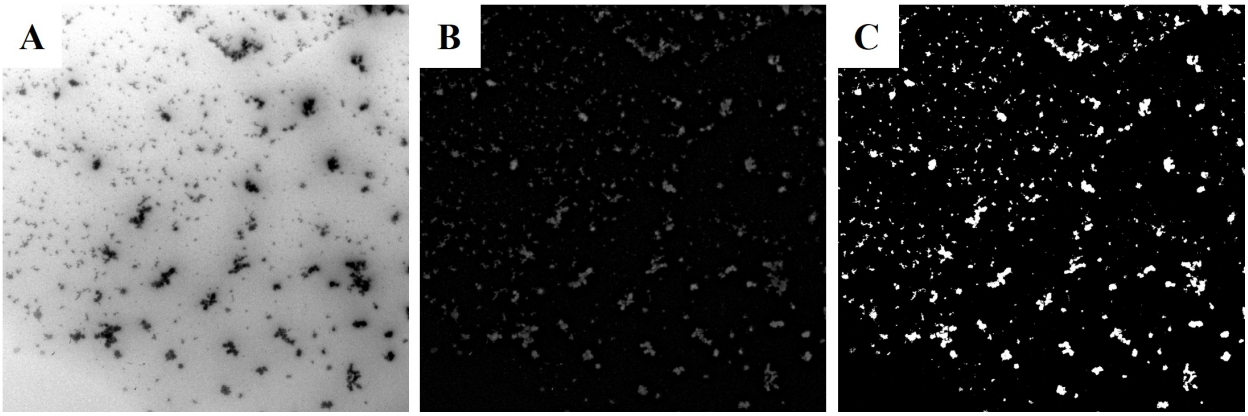

Figure 2.3: Illustration of the image processing workflow to semiautomatically detect particles in TEM micrographs. A: The original micrograph. B: The micrograph after background subtraction, showing enhanced contrast between background and particles. C: The detected particles after applying a brightness threshold.

the formation of an anoxic layer at the bottom of the aquarium, ambient air was constantly bubbled into the aquarium through an airstone to create a gentle current.

The plants adapted well to the culture conditions, exemplified by continuous growth of new shoots and rhizomes from the stems. After 5 weeks of floating cultivation, the young, bright green shoots of the remaining *M.spicatum* plants were separated from the old plant tissue. They were subsequently planted into submerged beakers filled with pre-washed quartz sand and further cultivated.

The excursion flora for Austria, Liechtenstein and South Tyrol (Fischer & Gottschlich, 2005) was used to identify the collected plants. *M. spicatum* was distinguished from *M. verticillatum*, a closely related and often co-occurring plant (Rotter & Schratt-Ehrendorfer, 1999), by the presence of carbonate encrusted leaves, typical for *M. spicatum* (Figure 2.4 B).

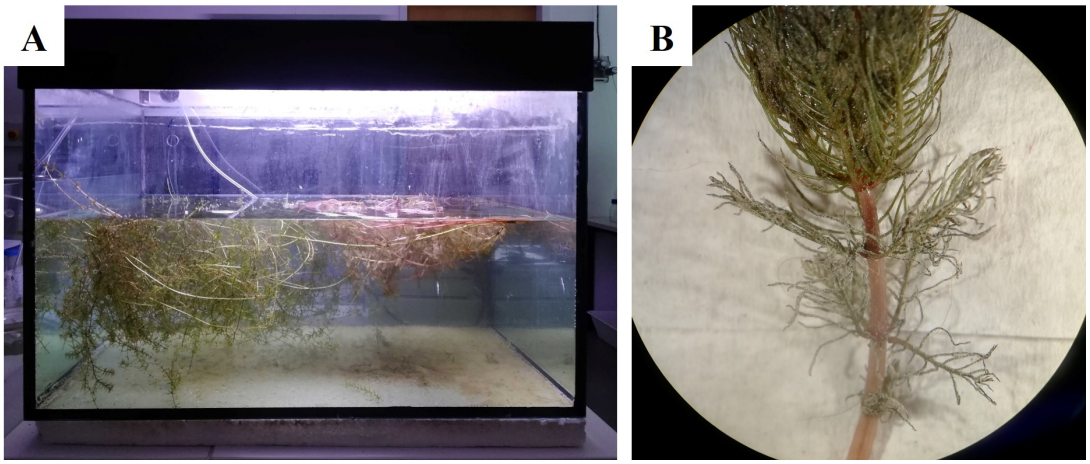

Figure 2.4: A: The storage tank used to maintain the collected plants. B: Carbonate encrustations on the leaves of *M. spicatum* seen under a Nikon SMZ 645 stereo microscope.

2.3.2 Preparation of Artificial Danube Water

To provide controlled conditions for the experiments, water with a composition similar to that of the Danube at Vienna (Artificial Danube Water, ADW) was prepared according to the protocol published by Smith et al. (2002). The chosen ionic composition of the ADW was based on results of water analyses at Lobau waterworks, provided by the Municipal Department 31 of the city of Vienna (Hellmeier, 2022) and is given in Table 2.1. The concentrations measured in the batch of ADW used in the experiments are also reported in this table.

Table 2.1: Concentration range of ions at Lobau Waterworks as well as chosen and measured composition of the prepared ADW. HA: Humic Acids.

	Na^+ [mg/L]	K^+ [mg/L]	Mg^{2+} [mg/L]	Ca^{2+} [mg/L]	Cl^- [mg/L]	SO_4^{2-} [mg/L]	NO_3^- [mg/L]	F^- [mg/L]	HA [mg/L]
Lobau[a]	7.7 - 11.0	1.5 - 3.9	15 - 22	65 - 83	11 - 18	26 - 39	1 - 5	< 0.2	-[b]
Measured	8.95	2.53	14.9	64.8	13.1	30.7	0.78	$<$ LOD	1.39

[a] According to the Municipal Department 31 of the city of Vienna

[b] not reported

Briefly, ADW was prepared by diluting 250× concentrated stock solutions of $MgSO_4$ and $Mg(NO_3)_2$ (S1), $CaCl_2$ (S2), $NaHCO_3$ and $KHCO_3$ (S3) and humic acid sodium salt (S4) in a 1.1× concentrated solution of $Ca(HCO_3)_2$ and $Mg(HCO_3)_2$ (S5) and subsequently diluting to the appropriate volume with Milli-Q water (see Table 2.3). S1-4 were prepared by dissolving the calculated amounts of the respective salts in Milli-Q water (for the concentrations of stocks, see Table 2.2). As the bicarbonate salts of Ca and Mg are unstable as solids and not commercially available, S5 was prepared by dissolving the appropriate amounts of $CaCO_3$ and $MgCO_3$ in Milli-Q water. The solubility of these salts in water is well below the required concentrations in S5 and dependent of the presence of dissolved CO_2 to form the more soluble bicarbonates. Thus, CO_2 was vigorously bubbled into the water through a ceramic gas frit for 10 min prior to the addition of the salts and during the entire dissolution process (approximately 2 h). To aid in the dissolution and prevent sedimentation of the undissolved salts during the process, S4 was continuously stirred (Figure 2.5).

To remove excess dissolved CO_2 and equilibrate the final ADW with the ambient atmosphere, air was vigorously bubbled through the final ADW through a gas frit, until a stable pH was achieved ($\Delta pH \leq 0.04/h$).

The ionic composition of the ADW was analyzed for the given ions by F-AAS (Na^+, K^+, Mg^{2+}, Ca^{2+}), IC (Cl^-, NO_3^-, SO_4^{2-}) and acidimetric titration against 0.1 M HCl (CO_3^{2-} and HCO_3^-). The plausibility of these analyses was checked by calculation of the charge balance error (CBE, equation 2.2).

Table 2.2: Preparation of the stocks used for the ADW.

Stock	1	2	3	4	5
			[g/L]		
$MgSO_4 \cdot 7\,H_2O$	21.17	-	-	-	-
$Mg(NO_3)_2 \cdot 6\,H_2O$	0.52	-	-	-	-
$CaCl_2 \cdot 2\,H_2O$	-	7.78	-	-	-
$NaHCO_3$	-	-	8.9	-	-
$KHCO_3$	-	-	1.79	-	-
Humic acids	-	-	-	1.25	-
$CaCO_3$	-	-	-	-	0.18
$MgCO_3$	-	-	-	-	0.038

Table 2.3: Preparation of ADW from the stocks.

Step	Final Volume [l]	1	5	100
		[mL]	[L]	
1	Stock 5 (1.1x)	909	4.55	91.0
2	Stock 1 - 4 (250x)	4	0.02	0.4
3	Water	75	0.37	7.4

$$CBE\ [\%] = \frac{\sum cations - |\sum anions|}{\sum cations + |\sum anions|} \cdot 100 \tag{2.2}$$

Additionally, total and dissolved organic carbon (TOC/DOC) were determined to assess the concentration of the added humic acids (see section 2.5.3).

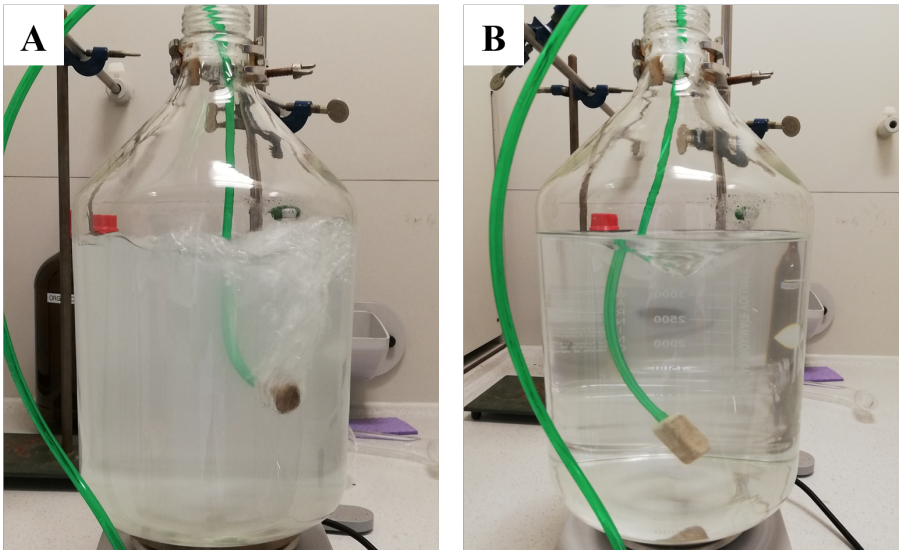

Figure 2.5: The carbonates stock (Stock 5) of a 5 L test batch during the dissolution process. A: At the beginning. B: After approximately 30 min, most of the added carbonates had dissolved.

2.3.3 Mesocosms

The mesocosms were constructed from acrylic glass tubes (h = 300 mm, $\varnothing_{outer}$ = 150 mm, wall thickness = 3 mm). The top of the mesocosms was left open to the atmosphere and a 15 cm pasteur pipette, connected via PVC tubing to an air pump, was affixed to the inner wall of each mesocosm with a suction cup.

1000 ± 1 g prewashed and dried quartz sand were filled into each mesocosm, creating a sediment layer of approximately 3.5 cm height. Each mesocosm was then filled with 4 l of ADW. To prevent the formation of a stagnant water layer, ambient air was constantly bubbled into the mesocosms through the pasteur pipette at a rate of approximately 1 bubble per second (ca. 3.8 mL/min), 10 cm below the water surface.

The mesocosms were arranged in a 2 × 6 grid and a 36 W fluorescent lamp was installed on each side of the arrangement (Figure 2.6 and 2.7). The lamps were affixed approximately 10 cm above the water level at a distance of 1.5 cm from the mesocosms and programmed to a 12:12 h light:dark-cycle. They each provided an average photosynthetic photon flux density (PPFD) of 36 $\mu mol \cdot m^{-2} \cdot s^{-1}$ (Measured using a Hansatech Quantitherm PAR sensor).

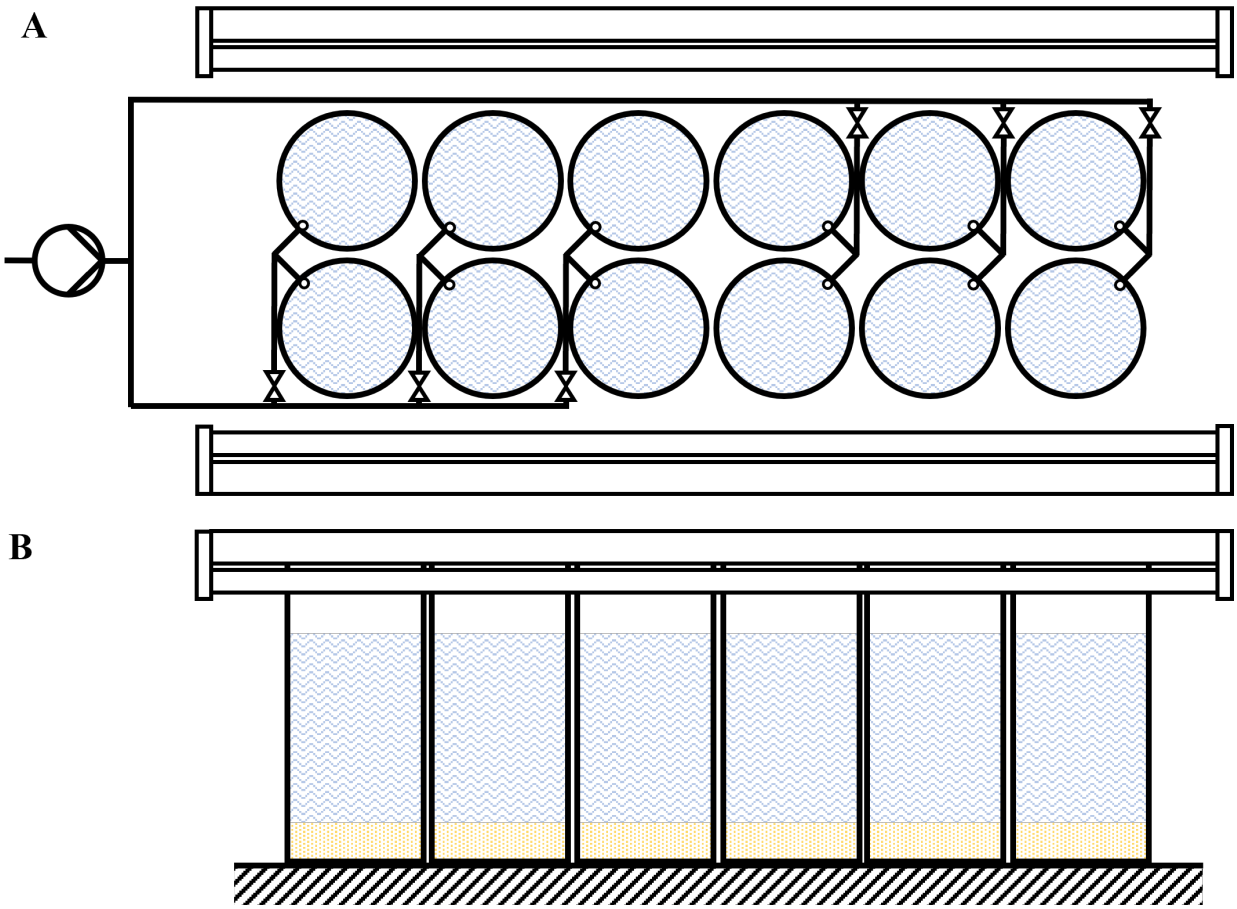

Figure 2.6: An illustration of the mesocosm setup, shown from (A) the top and (B) the front.

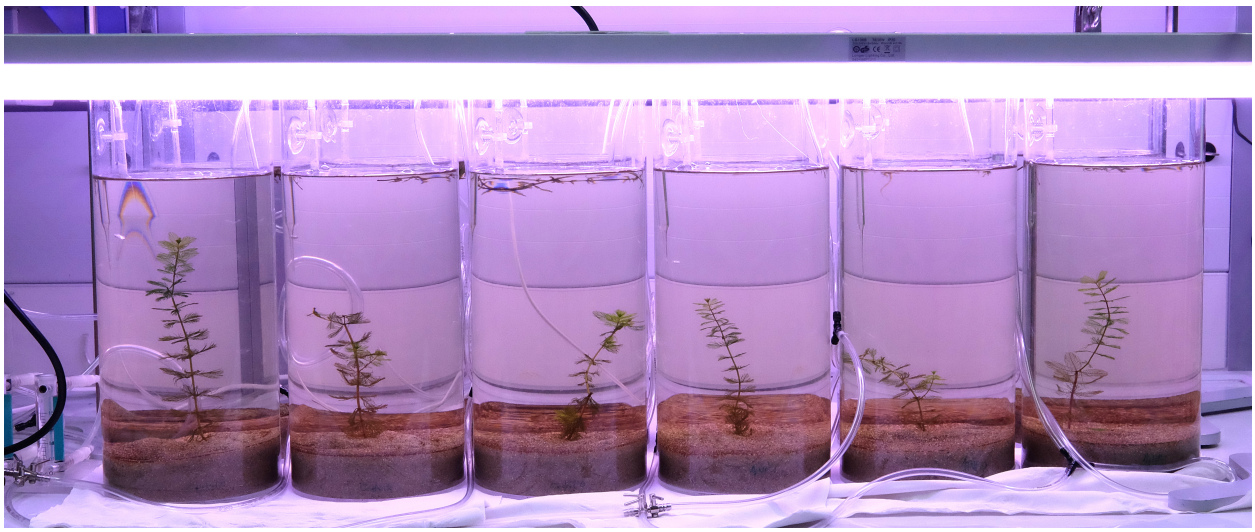

Figure 2.7: The final Mesocosm setup shown from the front.

2.3.4 Experiments

A series of experiments were conducted, assessing the distribution of two different Ag-NPs as well as ionic Ag ($AgNO_3$) in aquatic freshwater mesocosms within aquatic plants, sediment and the water column. Additionally, a reference experiment was conducted where no addition of Ag was performed. All experiments were performed in triplicate.

Initially, two different species of plants were planned to be exposed to two different experimental conditions in parallel, followed by a second round of experiments with exposure to the second pair of conditions. However, only one of the three collected species of plants (*M. spicatum*) successfully acclimatized to the experimental conditions. Thus, during each round of experiments, only six mesocosms (one plant, two conditions) were actually used.

One week before the first addition of Ag (Day of Experiment: -7), one shoot of *M. spicatum* was planted into each mesocosm and acclimatized until the start of the experiment. During this time, the shoots were monitored regularly for continued growth.

A repeated dosing scheme compromising three additions of Ag at day 0, 7 and 14 was chosen (Figure 2.8). At each addition, 40 µg of the respective form of Ag (equaling 10 µg/L) was added to each mesocosm, resulting in a nominal exposure concentration of 30 µg/L after the third addition. Following the additions, the mesocosms were maintained for 21 days before the final sampling of plant material and sediments. The experiments were thus performed for a total of 42 days (seven days of acclimatization followed by 35 days of exposure).

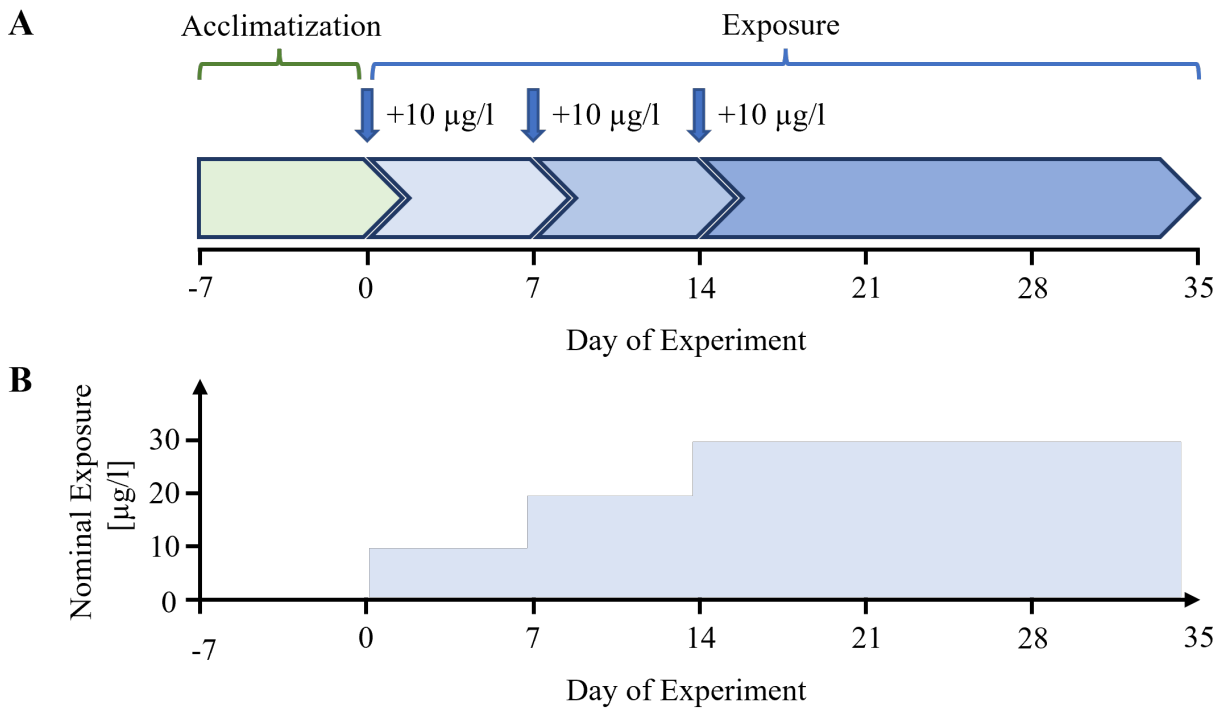

Figure 2.8: Setup of the mesocosm experiment. A: Timecourse of the experiment. Plants were placed into the mesocosms at the start of the acclimatization period and exposed to repeated additions of Ag-NPs or $AgNO_3$. The blue arrows mark the addition events. B: Nominal exposure concentrations during the experiment. After the third addition, no further Ag was added.

Dosing stocks

Dosing stocks were prepared at 5 mg/L for both types of Ag-NP (Nanopowder and Nanospheres) and ionic Ag. Prior to each addition of Ag, a 5 mL aliquot of the respective stock solutions was digested and the Ag content determined. The appropriate volume of the stock was then calculated and added to each mesocosm.

Stock A, containing Ag Nanopowder, was prepared by diluting 43.2 mL of the concentrated stock (see section 2.2) to 500 mL with Milli-Q water. Stock A was then used after redispersing the suspension in an ultrasonic bath for 90 min and cooling to room temperature.

The stably-dispersed Ag Nanospheres were diluted to a final concentration of 5 mg/L (Stock B). For this, 250 µl of the concentrated dispersion were diluted to 250 mL with Milli-Q water and homogenized by shaking.

A third stock solution (Stock C), containing ionic Ag, was freshly prepared at 5 mg/L from a 1000 mg/L Ag standard solution prior to every addition. For this, 250 µl of the standard solution were diluted to 50 mL and homogenized by shaking.

Sampling

Over the course of the experiment, a number of physico-chemical parameters were assessed twice weekly (see section 2.5.3). These were either measured *in-situ* using handheld devices or in samples of mesocosm water taken at an approximate depth of 10 cm below the surface.

To assess the total concentration of Ag in the mesocosms, water samples were taken directly before and one hour after each addition of Ag. One week after the last addition until the end of the experiment, samples were taken twice weekly, together with the aforementioned physico-chemical parameters.

After the conclusion of the experiment, a final sampling was undertaken. Here, all physico-chemical parameters were determined for a last time. An unfiltered as well as a filtered aliquot of the mesocosm water was taken for the determination of total and dissolved Ag. In limnological research, the dissolved fraction of a water body is operationally defined as those constituents able to pass through filters with a pore size of typically 0.45 µm (Danielsson, 1982). In the present work, 0.22 µm PTFE filters were used to obtain the dissolved fraction of Ag, as they functionally yield a very similar, if not indistinguishable filtrate.

Subsequently, the plant shoots were carefully removed from the mesocosms by grabbing the base of the shoot with a pair of stainless steel tweezers and slowly pulling the shoot and its rhizomes out of the sediment. The plants were then rinsed with Milli-Q water, the shoots separated from the rhizomes and the length measured using a ruler. For electron microscopy analysis (see section 2.4.4), three leaves of *M. spicatum* were separated from the rest of the plant using a razor blade, placed into 50 mL PP tubes filled with Ag-free ADW and stored in the dark over night. The remaining shoots and rhizomes were placed into separate 50 mL PP tubes and frozen at -20 °C before freeze-drying.

The majority of the mesocosm water was then discarded until the sediment layer was only barely covered by the water. The sediment was thoroughly mixed using a glass rod and three samples were taken in 50 mL PP tubes.

2.4 Sample Preparation

2.4.1 Acid Leaching of Sediment Samples

All sediment samples were oven dried at 85 °C for at least 48 h before digestion. Then, 500 ± 10 mg of dry sediment were weighed on an analytical balance and transferred to clean glass digestion tubes. Subsequently, 4.5 mL of Milli-Q water, 4.5 mL of concentrated HNO_3 and 1 mL of concentrated

hydrogen peroxide solution were added. The tubes were then fitted with air coolers and placed into a digestion block at 130 °C for 1 h. After digestion, the tubes were removed and cooled to room temperature in a beaker filled with cold tap water. The air coolers were then carefully rinsed with a small volume of Milli-Q water and removed from the digestion tubes. The contents of the digestion tubes were transferred to 20 mL volumetric flasks, rinsed twice with a small volume of Milli-Q water and the contents of the volumetric flasks made up to 20 mL. The digested samples were filtered through 0.22 µm PTFE syringe filters into 15 mL PP tubes and stored until analysis.

2.4.2 Acid Digestion of Water Samples

To determine the total concentration of Ag in water samples from the mesocosms, 5 mL aliquots were transferred unfiltered into 15 mL PP tubes. 5 mL of concentrated HNO_3 were added, the mixtures homogenized by shaking and left to digest at room temperature for 1 h. After digestion, 440 µl of Milli-Q water were added to account for volume contraction and make up the volume to 10 mL. The digested solutions were then filtered through 0.22 µm PTFE syringe filters into 15 mL PP tubes and stored until analysis.

2.4.3 Acid Digestion of Plant Material Samples

All plant material samples were freeze dried and ground into a coarse powder using a clean mortar and pestle prior to digestion. Then, 200 ± 10 mg, or all available material of a sample, in case less than 200 mg of dry matter were obtained, were transferred to PTFE digestion tubes. Subsequently, 4.5 mL of Milli-Q water, 4.5 mL of concentrated HNO_3 and 1 mL of concentrated hydrogen peroxide solution were added. The tubes were then sealed and the samples digested in a microwave digestion oven (CEM Mars Xpress) at 180 °C for 30 min. After digestion, the samples were allowed to cool down and the screw caps were carefully removed. The contents were transferred to 15 mL volumetric flasks and the tubes were then rinsed twice with a small volume of Milli-Q water. Following dilution to 15 mL, The digested samples were filtered through 0.22 µm PTFE syringe filters into 15 mL PP tubes and stored until analysis.

2.4.4 Preparation of Plant Material for Electron Microscopy

The sample preparation for electron microscopic analyses was performed by the Core Facility of Cell Imaging and Ultrastructure Research (CIUS) of the University of Vienna. The general procedures are described below.

The samples from the first round of experiments (plants treated with PVP-dispersed nanopowder) were pre-fixed for TEM analysis at the Institute of Inorganic Chemistry and subsequently trans-

ported to the CIUS where they were prepared further. For TEM analysis, the samples were prepared according to a protocol for hydrophytic plants (Fedorenko et al., 2018) with minor modifications (Schmidt B., personal communication, August 23, 2022).

Pre-fixation of the plants exposed to PVP-dispersed nanopowder was performed as follows: the sampled leaves were first placed into degassed tap water at 4 °C over night, to allow the gentle removal of gas trapped inside the plant organs. Subsequently, individual segments of the leaves were placed in a drop of primary fixative containing 2.5 % glutaraldehyde dissolved in 0.1 M potassium phosphate buffer (PB, pH = 7.4) on a glass microscope slide and cut into small sections using a razor blade. The sections were then transferred to 1 mL microcentrifuge tubes containing the same fixative. They were fixed for 2 h in a vacuum desiccator, after which the samples were returned to ambient pressure and fixed for another 2 h. After removal of the primary fixative, the samples were washed three times with 0.1 M PB for 10 min. Dehydration in a graded Ethanol (EtOH) series up to 70 % EtOH was then performed before storage in 70 % EtOH at 4 °C. After transport to the CIUS, these samples were post-fixed and further treated as described below.

Sample preparation of the leaves collected from plants exposed to the PVP-coated nanospheres and $AgNO_3$ was performed by the CIUS. Briefly, instead of 2.5 % glutaraldehyde, a primary fixative containing 3.8 % paraformaldehyde and 0.5 % glutaraldehyde in 0.1 M PB was used. The sections were then fixed and washed as described above. Post-fixation was performed in a solution consisting of 1 % OsO_4 in Milli-Q water for one hour. The fixative was again removed and the samples washed three times with PB.

Dehydration was performed in a graded EtOH series up to 100 %, followed by infiltration with propylene oxide (PO) and a graded series of epoxy resin - PO mixtures. After infiltration with pure resin, the samples were polymerized and the hardened resin blocks stored at room temperature.

Sectioning of the embedded samples was performed on a Leica UC6 ultramicrotome. The sections were collected on copper grids and stained with 4 % neodymium(III) acetate hydrate ($(CH_3CO_2)_3Nd \cdot x\,H_2O$) followed by post-staining with 3 % lead citrate ($(C_6H_5O_7)_2Pb_3$).

2.5 Analyses

2.5.1 Atomic Absorption Spectroscopy (AAS)

Flame AAS

A PerkinElmer AAnalyst 200 flame AAS system, equipped with PerkinElmer Single Element Lumina™ Hollow Cathode Lamps was used for the determination of Ag during the preliminary diges-

tion experiments and in the dosing stocks (sections 2.2.1 and 2.3.4) as well as for the determination of Na^+, K^+, Mg^{2+} and Ca^{2+} in the ADW (section 2.3.2).

Calibration was performed on five levels at the beginning of each analysis and evaluated using polynomial regression through zero. Blank measurements were performed for background correction using 2 % HNO_3 prior to calibration. The calibration standard solutions were freshly prepared prior to each analysis in 2 % HNO_3 from stock solutions containing 10 mg/L (Ag^+) or 20 mg/L (Na^+,K^+, Mg^{2+}, Ca^{2+}) of the respective element in 2 % HNO_3. Each sample was measured in triplicate and the mean value was reported. A correlation coefficient R^2 of at least 0.9995 was used as the acceptance criterion for a successful calibration. A summary of the operation parameters for each element is summarized in Table 2.4.

Table 2.4: Flame AAS operation parameters.

	Wavelength [nm]	Slit Width [mm]	Calibration Levels [mg/L]
Ag^+	328.07	2.7/0.8	0 - 0.25 - 0.5 - 1.0 - 2.0
Na^+	589.00	2.7/0.6	0 - 0.25 - 0.5 - 1.0 - 2.0
K^+	766.49	2.7/1.05	0 - 0.25 - 0.5 - 1.0 - 2.0
Mg^{2+}	285.21	2.7/0.45	0.0 - 0.0625 - 0.125 - 0.25 - 0.5
Ca^{2+}	422.67	1.8/0.6	0 - 2.5 - 5.0 - 10 - 20

Graphite-Furnace AAS

A PerkinElmer PinAAcle 900Z GF-AAS system equipped with a PerkinElmer AS900 Furnace Autosampler was used for all analyses. For the determination of Ag, a PerkinElmer Single Element Lumina™ Hollow Cathode Lamp for the detection of elemental Ag was installed in the instrument and warmed up for at least two hours before the start an analysis. Ar gas (N5.0) was used to flush the graphite furnace at 250 mL/min during the analysis. The atomic absorption was measured at a wavelength of 328.07 nm (slit width 0.7 nm) and background corrected peak areas were used for quantification.

Samples and calibration standards were measured in triplicate and the average was used to report the final sample concentration. For each replicate, 20 µl were automatically dispensed into the furnace and the following temperature program was performed: first, the sample was evaporated and dried at 110 °C for 30 s, followed by a 15 s ramp to 130 °C, which was then held for 30 s. Pyrolysis of the sample was performed by heating to 800 °C within 10 s and holding for 20 s, followed by an atomization step at 1700 °C for 5 s. During this step, the argon flow was stopped and the absorption measured during an interval of 4.6 s. The argon flow was then resumed, and within 1 s, the furnace was heated to 2550 °C and held for 3 s to clean the furnace from any remaining sample constituents. Finally the furnace was allowed to cool down for 20 s before the

next analysis. This resulted in a replicate measurement time of 135 s.

Calibration was performed at the beginning of each analysis on five levels (0, 0.5, 1.0, 5.0 and 10 µg/L) and evaluated by linear regression of the peak areas. The calibration standard solutions were freshly prepared prior to each analysis in 2 % HNO_3 from a 100 µg/L Ag stock solution in 2 % HNO_3. A correlation coefficient R^2 of at least 0.999 was used as the acceptance criterion for a successful calibration. The method LOD for Ag was 0.03 µg/L, resulting in a sample LOD of 0.06 µg/L in water samples.

To assess changes in the recorded signal intensities, the highest standard (10 µg/L) was remeasured at regular intervals, at least every ten samples. The concentrations thus obtained were used to correct the concentrations of samples measured between two respective standards by linear interpolation.

2.5.2 Electron Microscopy

All electron microscopic analyses were performed by the CIUS.

SEM was performed on a JEOL IT300 scanning electron microscope equipped with a lanthanum hexaboride LaB_6 filament and operated at a voltage of 1 - 30 kV. Additionally, EDX was performed to visualize possible depositions of Ag on the leaf surface. TEM of ultrathin sections was performed on a Zeiss Libra 120 transmission electron microscope equipped with a LaB_6 filament and an Olympus Sharp:eye TRS (2×2 k) bottom mount camera. The electron beam was was operated at energies between 80 and 120 kV. The presence of Ag was assessed in regions of interest (ROI) of the TEM samples by EELS.

2.5.3 Other Physico-Chemical Parameters

The physico-chemical parameters conductivity, temperature, dissolved oxygen, pH, total organic carbon, dissolved organic carbon and anion concentrations (Cl^-, ${SO_4}^{2-}$ and ${NO_3}^-$) were monitored twice a week in the mesocosms.

The following parameters were measured *in-situ* in the mesocosms with handheld instruments: conductivity using a Mettler Toledo FiveGo™conductometer with an LE703 IP67 conductivity sensor, dissolved oxygen and temperature using a WTW Oxi330 handheld oxygen meter with a WTW CellOx 325 sensor and pH using an SI Analytics Lab 850 pH-meter with an SI Analytics BlueLine 14 pH pH electrode.

For the determination of TOC, DOC and anions, a 20 mL aliquot was taken from each mesocosm at a depth of about 10 cm. From these samples, 5 mL were directly diluted with 5 mL of Milli-

Q water for TOC determination. The remaining sample volume was filtered through pre-rinsed 0.22 µm syringe filters and another aliquot of 5 mL was diluted with 5 mL of Milli-Q water for DOC determination. The remaining aliquot was used undiluted for anion chromatography.

Total and Dissolved Organic Carbon

TOC and DOC were measured as non-purgeable organic carbon (NPOC) on a Shimadzu TOC-V CPH Total Organic Carbon Analyzer equipped with an ASI-V autosampler. The samples were acidified to a pH < 2 by the addition of HCl and sparged for 3 min using synthetic air. 50 µl were subsequently injected onto the combustion column at 720 °C.

Calibration was performed periodically on five levels using a potassium hydrogen phthalate standard solution and evaluated by linear regression of the peak areas. A correlation coefficient $R^2 > 0.9995$ was used as the acceptance criterion for successful calibration.

Blanks of Milli-Q water were measured in between each sample and the average of all blank measurements was used to correct the sample concentrations.

Shimadzu TOC-Control V 2.10 was used to control the instrument and to evaluate the results.

Chloride, Sulfate, Nitrate and minor anions

The major anions Cl^-, $SO_4{}^{2-}$ and $NO_3{}^-$, as well as F^-, Br^-, $NO_2{}^-$, and $PO_4{}^{3-}$, were determined in the undiluted, filtered samples using a Metrohm 930 Compact IC Flex ion chromatography system equipped with a Metrohm Metrosep A Supp 5 column for anion chromatography ($\varnothing_{particle} = 5$ µm, length = 250 mm, $\varnothing_{inner} = 4.0$ mm) and an Metrohm IC conductivity detector. The instrument was operated at a flow rate of 0.700 mL/min. The eluent was composed of 3.2 mM Na_2CO_3 and 1.0 mM $NaHCO_3$. The column oven was set to 25 °C and the column operated up to a maximum pressure of 15 MPa. 0.1 M H_3PO_4 was used to suppress the eluent signal in the detection cell. 20 µl of sample were injected onto the column for each analysis.

Before the start of each analysis run, the instrument was equilibrated for at least 30 min under the analysis conditions until a stable pressure (12.0 - 12.6 MPa), temperature (25.0 °C) and conductivity (0.9 - 1.1 µS/cm) were reached.

Calibration was performed periodically on ten levels using standard solutions of the respective anions and evaluated by linear or polynomial regression of the peak areas. Additionally, solutions containing a known amount of Cl^- and $SO_4{}^{2-}$ were analyzed with each analysis run for quality control. The calibration ranges, limits of detection and limits of quantitation of the respective anions are given in Table 2.5.

Metrohm MagIC Net 3.2 was used to control the instrument and to evaluate the results.

Table 2.5: Method Performance Parameters for anion chromatography: Regression types, calibration ranges, LOD, LOQ and R^2.

	Cl^- [mg/L]	SO_4^{2-} [mg/L]	NO_3^- [mg/L]	F^- [mg/L]	Br^- [mg/L]	NO_2^- [mg/L]	PO_4^{3-} [mg/L]
Type	linear	linear	quadratic	quadratic	quadratic	quadratic	quadratic
Range	0.625 - 200	0.625 - 200	0.125 - 40	0.0625 - 20	0.0625 - 20	0.0625 - 20	0.0625 - 20
LOD	0.01	0.05	0.1	0.05	0.05	0.05	0.05
LOQ[a]	0.03	0.15	0.3	0.15	0.15	0.15	0.15
R^2	0.99996	0.99986	0.99986	0.9999	0.99984	0.9998	0.99981

[a] LOQ = LOD * 3

Loss on Ignition

The loss on ignition (LOI) of the sediment was measured in the washed, dry quartz sand before the mesocom experiments (five determinations) and in the mesocosm sediments after the experiments (in triplicate for every mesocosm). For this 500 ±10 mg of dried sediment were weighed into porcelain crucibles on an analytical balance and subsequently incinerated in a muffle furnace at 550 °C for two hours. After cooling to room temperature, the crucibles were weighed again and the LOI determined using Equation 2.3.

$$LOI[\%] = \frac{m_{Sediment,before} - m_{Sediment,after}}{m_{Sediment,before}} \cdot 100 \tag{2.3}$$

Bioconcentration Factor

The bioconcentration factor (BCF, Equation 2.4) of the exposed plants was calculated in contrast to the mesocosm water as well as the sediments. For the water, the BCF was calculated for the chosen nominal exposure (30 µg/L) and the measured peak Ag concentrations. For the sediments, the measured concentrations at the end of the experiment were used.

$$BCF = \frac{c_{Ag,Plant}}{c_{Ag,Compartment}} \tag{2.4}$$

2.5.4 Data Analysis and Visualization

Statistical evaluation of the data and data visualization was performed in R (R Core Team (2022), version 4.2.2). Data visualization was performed using the package "ggplot2" (Wickham, 2016). In all cases, the null hypothesis H_0 was rejected at $P < 0.05$.

A flowchart of the statistical analysis process is depicted in Figure 2.9.

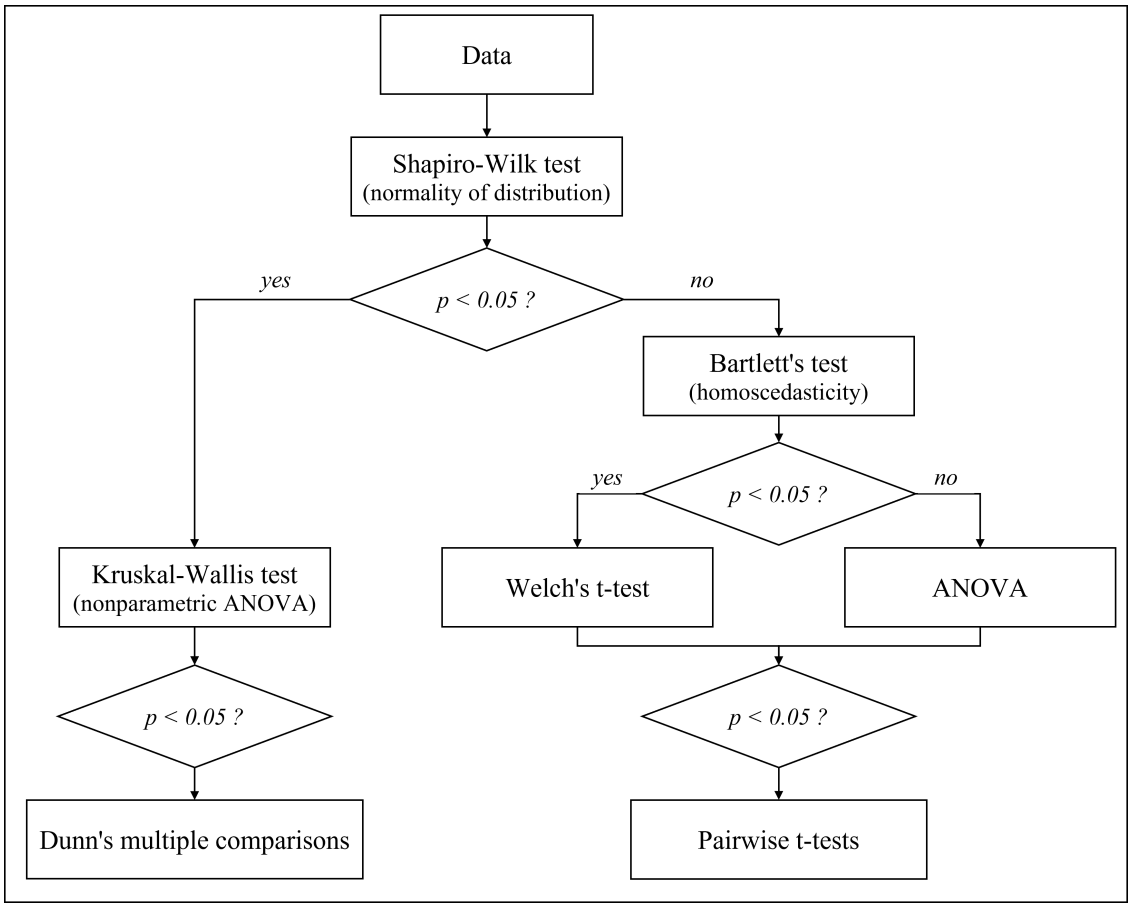

Figure 2.9: Flowchart of the statistical analyses. These tests were performed to assess statistical differences of selected parameters between the treatment groups of plants, sediments and mesocosm water

Statistical differences between treatment groups were assessed as follows: All groups were first tested for normality of distribution using the Shapiro-Wilk test and homoscedasticity using Bartlett's test. If both criteria were met, Analysis of variance (ANOVA) was performed. If the criterion of homoscedasticity was not met, Welch's unequal variances t-test, generalized for the comparison of multiple means (Welch's ANOVA (Welch, 1951)) was performed instead of ANOVA.

If ANOVA or Welch's ANOVA met the significance criterion, *post-hoc* testing was carried out by pairwise comparison of all groups by two-sample Student's t-tests.

In case normality of distribution was rejected in at least one group, nonparametric tests were employed. As alternative to ANOVA and Welch's ANOVA, the Kruskal-Wallis test was performed. If significance was met, *post-hoc* testing was performed using Dunn's test (Dunn, 1964).

3 Results

3.1 Nanoparticle Characterization

3.1.1 Particle Size

The size distribution of both types of nanomaterials was characterized using DLS and TEM. As DLS assumes spherical particles for the calculation of particle sizes from the scattered light beam (Stetefeld et al., 2016), particle shape was only assessed using TEM.

The measured size distributions are summarized in Table 3.1 and Figure 3.1.

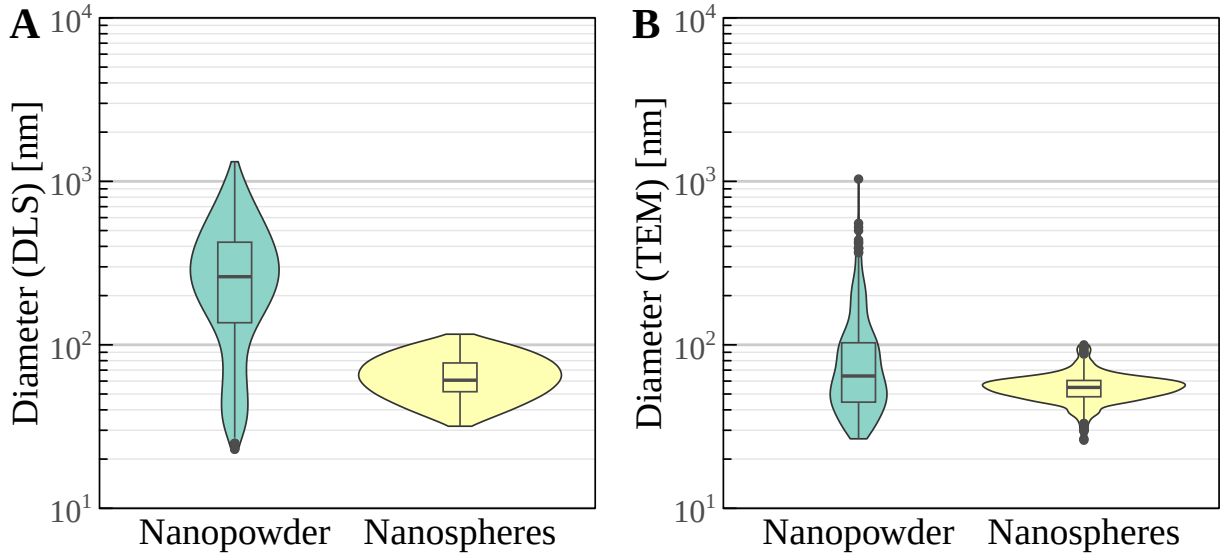

Figure 3.1: Size Distributions of the Ag-NP as combined density and boxplots. A: Hydrodynamic diameters determined by DLS, given as intensity weighted relative frequency. B: Maximum caliper diameters determined by image analysis of TEM micrographs at 4,000× magnification.

As the output format of the DLS data is comprised of relative frequencies (in percent of the entire population) at specific hydrodynamic diameters, only summary and no comparative statistics were calculated. From these measurements, the HDDs of the Nanopowder show a rather wide, bimodal distribution (Range 23 - 1319 nm) with two relative frequency maxima at 36 and 612 nm. The median hydrodynamic diameter was determined at 261 nm. In comparison, the Nanospheres appear monodisperse with a much narrower distribution (range 32 - 116 nm). The highest relative frequency was measured at a hydrodynamic diameter of 64 nm, close to the median of 61 nm (3.1 A).

In comparison, the maximum caliper diameters obtained by TEM appear quite different. While the size distribution of the Nanopowder is still significantly wider than that of the Nanospheres

Table 3.1: Summary of particle sizes and circularity of the Ag-NP as determined by DLS and TEM. Statistical significance was assumed at $P < 0.05$ and assessed by Wilcoxon rank-sum test.

		Range	1st Quartile	Median	3rd Quartile	P^a
Dynamic Light Scattering						
Diameter [nm]	Nanopowder	23 - 1319	137	261	424	n.d.
	Nanospheres	32 - 116	52	61	77	
Transmission Electron Microscopy						
Diameter [nm]	Nanopowder	27 - 1033	45	64	93	5.02×10^{-8}
	Nanospheres	26 - 100	48	55	61	
Circularity	Nanopowder	0.04 - 0.95	0.35	0.49	0.62	$< 2.2 \times 10^{-16}$
	Nanospheres	0.48 - 1.00	0.9	0.93	0.96	

[a] Wilcoxon rank-sum test

(27 - 1033 nm vs. 26 - 100 nm), the measured median diameters are much more similar, albeit still significantly different (64 vs. 55 nm, Wilcoxon rank-sum test *P = 5.02×10^{-8})

3.1.2 Particle Shape

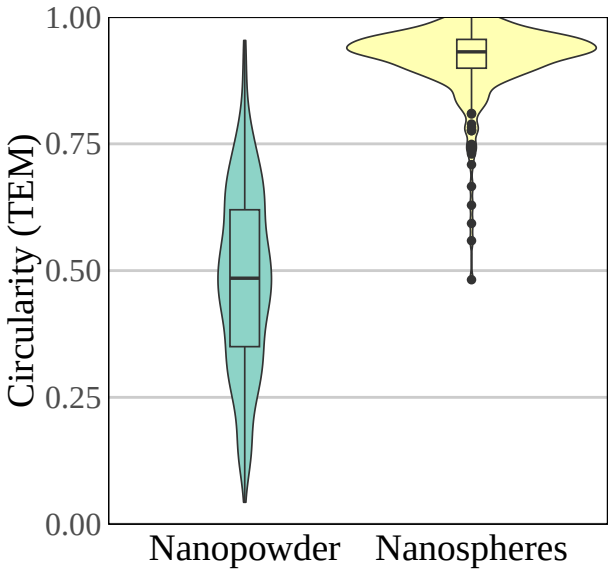

Figure 3.2: Combined density and boxplots of the circularity of both types of Ag-NP .

Figure 3.3 shows the electron micrographs obtained from the Nanopowder and Nanospheres at magnifications of 4,000× and 31,500×. As can be seen, the Nanopowder mostly consists of irregularly shaped, likely agglomerated particles with varying dimensions and often low contrast (Figure 3.3 A, B). In comparison, the Nanospheres clearly stand out from the background, showing a well-defined, circular shape with only minor variation in particle diameter (Figure 3.3 C, D).

Using image analysis, not only size, but also the circularity was determined, giving an indication of the uniformity and shape of the particles. The results of the evaluation are summarized in Table 3.1 and plotted in Figure 3.2. As expected, the Nanopowder particles are on average significantly

less circular than the Nanospheres (Median 0.49 vs. 0.93, Wilcoxon rank-sum test $P < 2.2 \times 10^{-16}$) with a much wider range of values. This is in good agreement with the initial visual comparison of the micrographs.

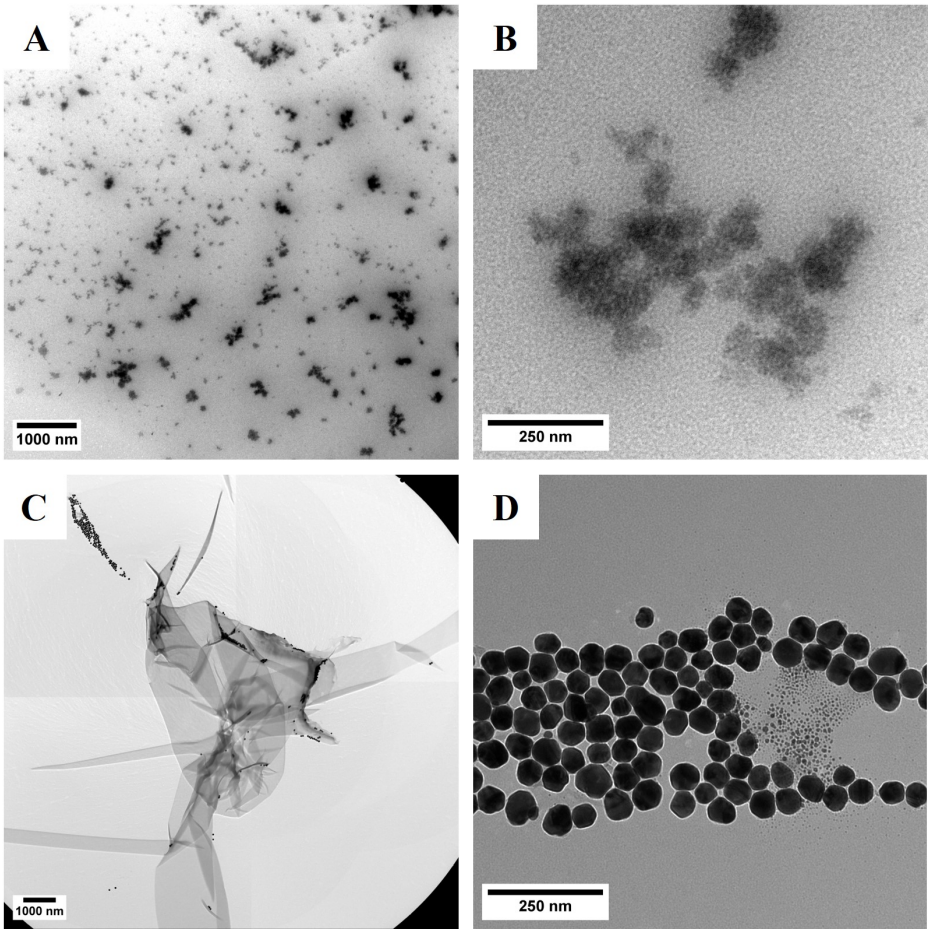

Figure 3.3: TEM micrographs of the Ag Nanopowder and Nanospheres. A: The Nanopowder at 4,000× magnification. The irregularly shaped agglomerates and wide distribution of particle sizes are evident. B: Detail view of a Nanopowder agglomerate at 31,500× magnification. C: The Nanospheres at 4,000× magnification. The particles are recognizable as small black spheres. D: Detail view of the Nanospheres at 31,500× magnification. The particles are of circular shape and very similar size.

3.1.3 Electron Energy Loss Spectroscopy

The pure Ag-NPs were additionally subjected to analysis by EELS, yielding the spectra in Figure 3.4. Interestingly, the characteristic M4,5-edge of Ag, with its maximum at approximately 440 eV was not observed for both types of Ag-NP, even though the presence of Ag was confirmed by GF-AAS (for comparison, see the high-loss EELS spectrum of a Ag thin film given in Figure 3.5. Only a small, sharp peak at approximately 425 eV is shared by both spectra. However, no evidence of a peak indicative of Ag at this position and shape was found in the literature. Additionally, a previous publication characterizing Ag-NPs by EELS reported the presence of the M4,5-edge (Römer et al., 2016). No further interpretation of this signal was attempted.

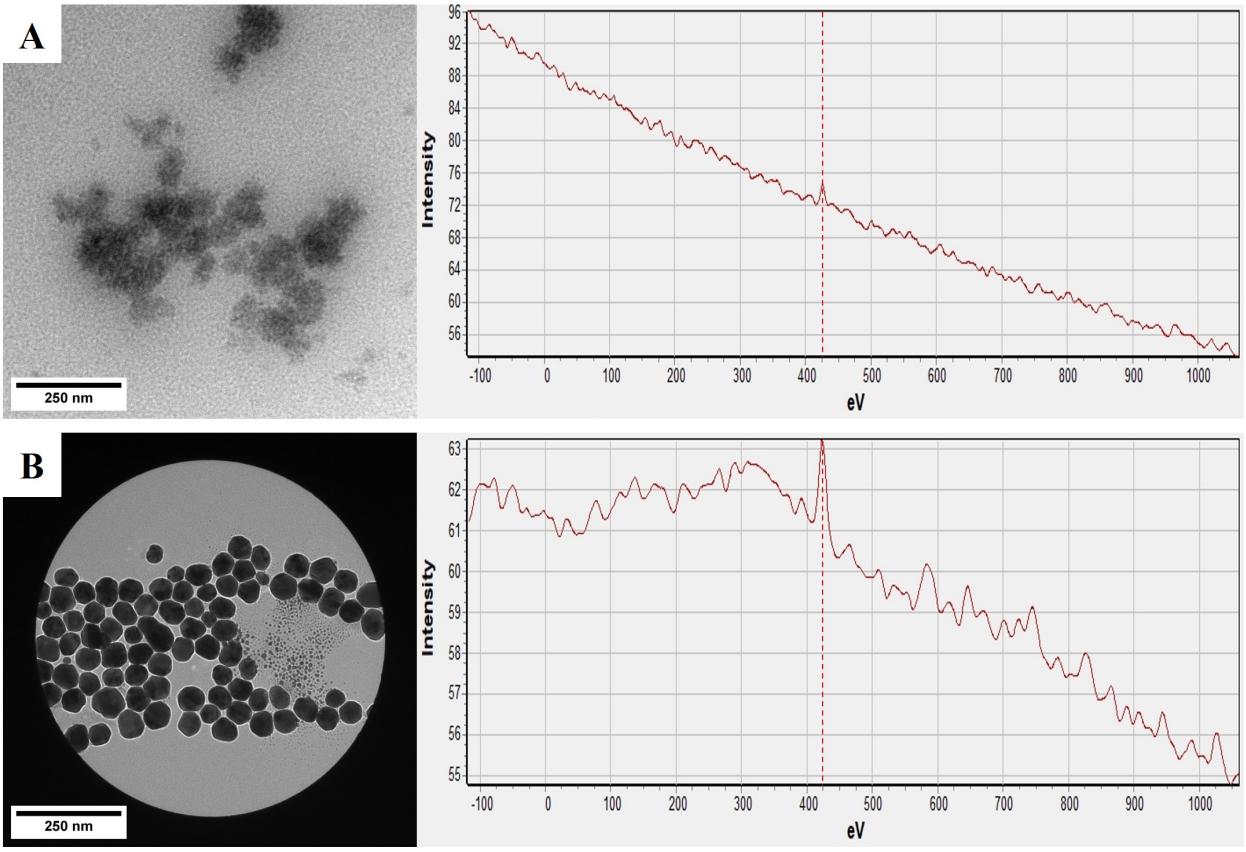

Figure 3.4: EELS spectra of the Ag Nanopowder (A) and Nanospheres (B). Both spectra contain a small peak at approximately 425 eV (dotted red line), but do not display the characteristic M4,5-edge of Ag.

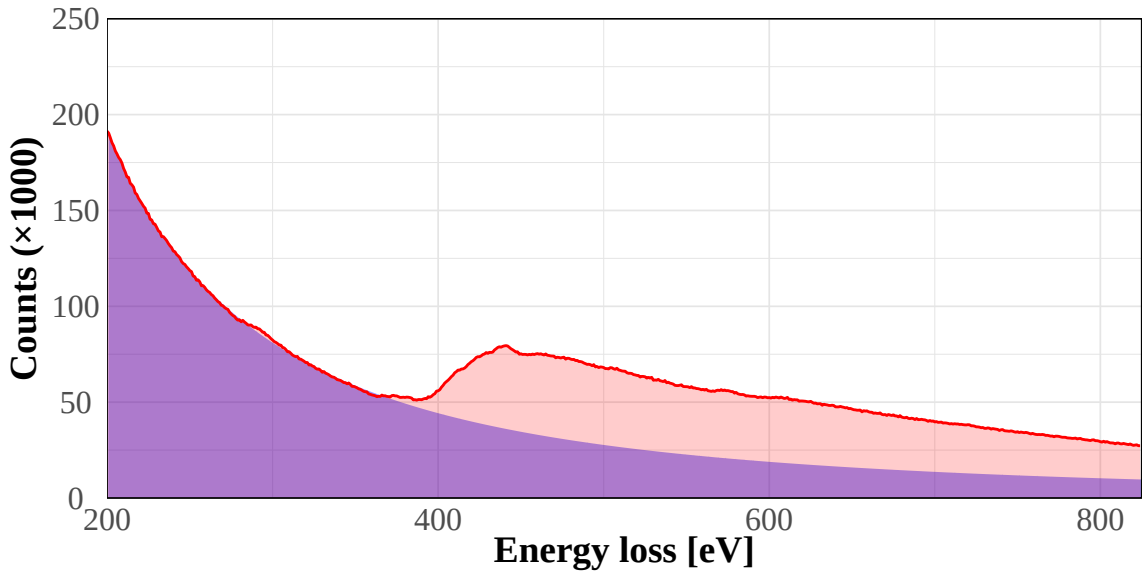

Figure 3.5: High-loss EELS spectrum of an Ag thin film (in red) versus the simulated background signal (in blue, simulated by fitting a power law function of the form $y = a * x^b$ to the data in the interval of 250 - 350 eV). Data from Gatan Ametek (2022)).

3.2 Mesocosm Experiments

3.2.1 Course of the Experiment

Physico-chemical Parameters

During the experiment, a number of physico-chemical parameters were measured at regular intervals. Only minor changes were observed, except for the concentrations of NO_3^-, which had sunken below the LOD of 0.1 mg/L in all groups by the end of the experiment. As the stocks of ionic Ag were prepared from a standard solution containing 2 % HNO_3, the additions resulted in measurable increases in NO_3^- concentrations shortly after dosing, which by the final sampling had also decreased below the LOD.

A summary of the measured parameters is given in the Appendix (Table A.1).

Loss on Ignition

After the experiments, the LOI of the sediments was determined and compared among the different groups (Table 3.2 and Figure 3.6). No trend was discernible from the obtained results: all groups showed significant overlap. From a visual inspection of the means (Figure 3.6), differences seemed to exist and especially the reference group and the Nanospheres group had a mean LOI lower than the background (0.11 and 0.13 % compared to 0.15 %). To understand if these perceived differences were statistically significant, a one-way ANOVA of all groups (including the background) was performed. This analysis yielded an insignificant result ($P = 0.089$).

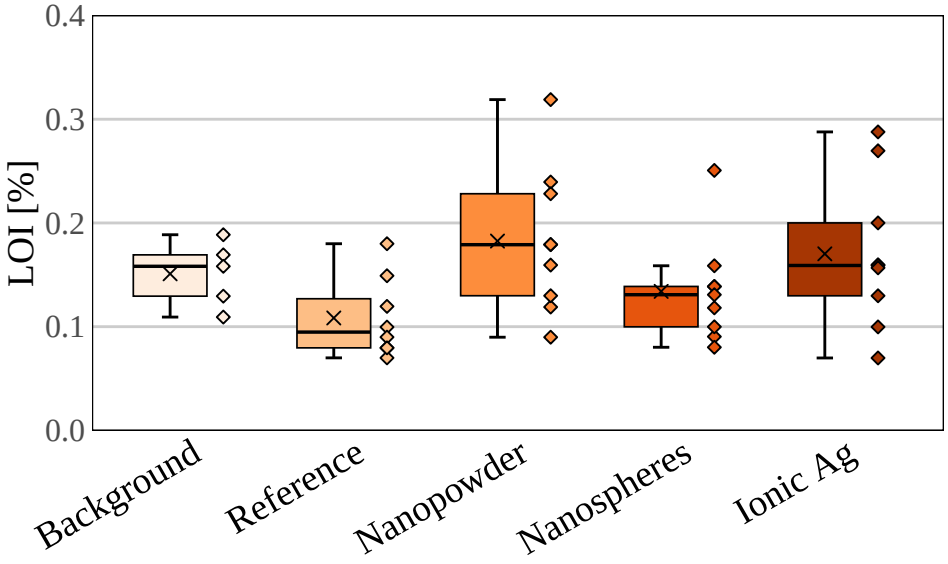

Figure 3.6: LOI of the unexposed sediment (Background) and of the mesocosm sediments after the experiments. Boxes and Whiskers represent quartiles, group means are indicated as black crosses. Individual data points are displayed as colored diamond symbols.

Table 3.2: LOI (mean ± SD) of the unexposed sediment (Background) and of the mesocosm sediments after the experiments. No statistically significant difference was detected between groups by one-way ANOVA.

Group	n	Time [days]	LOI [%]
Background	5	0	0.15 ± 0.03
Reference	8[a]	35	0.11 ± 0.04
Nanopowder	9	35	0.18 ± 0.07
Nanospheres	9	35	0.13 ± 0.05
Ionic Silver	9	35	0.17 ± 0.07
P			0.089[b]

[a] One value was removed due to a LOI <0 %.
[b] one-way ANOVA

Silver Additions and Monitoring during the Experiment

The measured concentrations of Ag in the mesocosm water are given in Table 3.3 and are graphically summarized in Figure 3.7. On the addition days, the total Ag concentration in the mesocosms was measured before and 1 h after the addition. The difference of these values (the added concentration of Ag) ranged between 8.39 and 10.78 µg/L per addition. In all groups, there was a gradual increase of the total Ag concentration over the course of the additions, as the added Ag did not fully precipitate during the days in between additions. After the final addition, on average 16.32, 16.26 and 14.03 µg/L Ag were present in the mesocosms exposed to the Nanopowder, the Nanospheres and ionic Ag, respectively (Figure 3.7 A,C,E). No further Ag was added after that, while the concentrations were monitored regularly until the end of the experiment (Figure 3.7 B,D,F).

Following the final addition, the Ag content in the water column declined rapidly in all groups, especially in the Nanopowder group, where one week after the final addition, on average only 15.4 % (2.52 µg/L) of the peak concentration remained in the water column, whereas the Nanospheres and the ionic Ag proved to be much more stable (50.1 and 43.4 % of the peak, on average). Until the end of the experiment, the concentrations declined further, reaching final values of 0.76, 1.34 and 0.93 µg/L, respectively. These correspond to 4.6, 8.2 and 6.7 % of the peak concentrations in the respective group. This quick sedimentation behavior of the Nanopowder was previously noticed in the concentrated stocks (see Figure 2.1 C).

3.2.2 Accumulated Silver in Plants, Sediments and the Aquatic Phase

At the end of the experiment, plants, sediments and the aquatic phase were sampled and analyzed for their total Ag content. The aquatic phase was additionally analyzed for it's content of dissolved Ag, the fraction of Ag remaining in the sample after filtration through a 0.22 µm PTFE syringe filter. The results are summarized in Table 3.4.

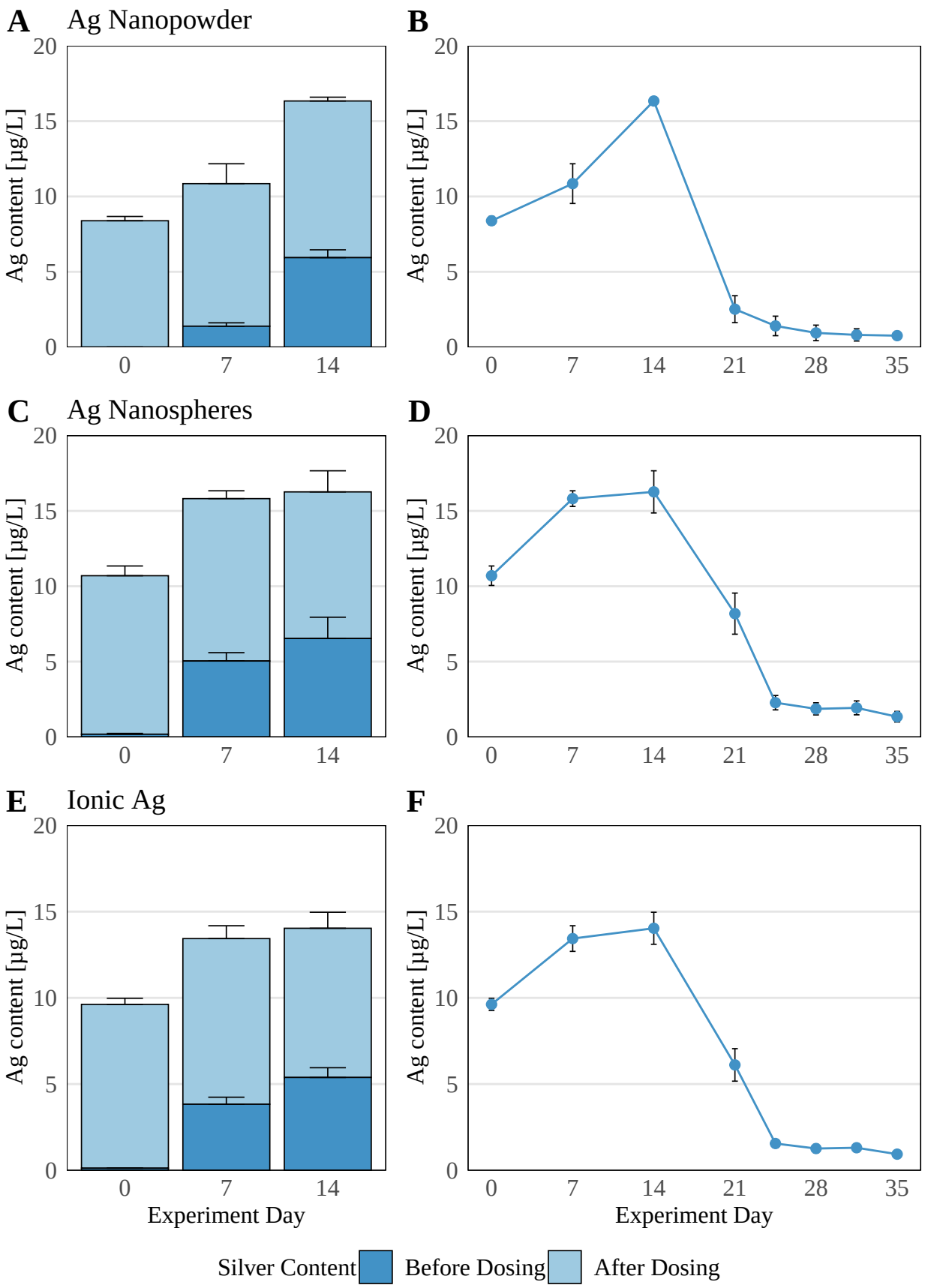

Figure 3.7: On the left: Total Ag content (mean ± SD) in the mesocosm water on the days of addition. Dark blue: before the addition, light blue: 1 h after addition of 10 µg/L Ag. On the right: Total Ag content (mean ± SD) in the mesocosm water over the entire experiment.

Table 3.3: Measured concentrations of total Ag (mean ± SD) in the mesocosm water during the experiments. Ag concentrations after additions are given in parentheses. (n = 3).

Day	Nanopowder [µg/L]	Nanospheres [µg/L]	Ionic Silver [µg/L]
0	<LOD[a]	0.18 ± 0.06	0.12 ± 0.01
	(8.39 ± 0.29)	(10.70 ± 0.65)	(9.62 ± 0.35)
7	1.39 ± 0.22	5.04 ± 0.55	3.83 ± 0.41
	(10.85 ± 1.32)	(15.82 ± 0.52)	(13.44 ± 0.74)
14	5.94 ± 0.52	6.53 ± 1.41	5.38 ± 0.56
	(16.32 ± 0.25)	(16.26 ± 1.40)	(14.03 ± 0.93)
21	2.52 ± 0.89	8.18 ± 1.36	6.11 ± 0.94
24	1.41 ± 0.65	2.27 ± 0.48	1.55 ± 0.23
28	0.94 ± 0.52	1.86 ± 0.40	1.26 ± 0.24
31	0.81 ± 0.41	1.92 ± 0.46	1.30 ± 0.23
35	0.76 ± 0.28	1.34 ± 0.35	0.93 ± 0.15

[a] LOD = 0.06 µg/L

Table 3.4: Total Ag content (mean ± SD) accumulated in the shoots of *M. spicatum*, sediments and the aquatic phase. The dissolved Ag content in the aquatic phase is also reported.

Group	Time [days]	Exposure [µg]	Shoots (n = 3) [mg/kg dw]	Sediment (n = 9) [mg/kg dw]	Water, tot. (n = 3) [µg/L]	Water, diss. (n = 3) [µg/L]
Background	0	0	0.044 ± 0.015	0.015 ± 0.005	< LOD	< LOD
Reference	35	0	0.035 ± 0.002	0.022 ± 0.025	< LOD	< LOD
Nanopowder	35	120	10.6 ± 4.8	0.096 ± 0.020	0.76 ± 0.28	0.53 ± 0.34
Nanospheres	35	120	12.0 ± 7.5	0.063 ± 0.019	1.34 ± 0.35	0.98 ± 0.19
Ionic Silver	35	120	41.6 ± 46.2	0.073 ± 0.039	0.93 ± 0.15	0.73 ± 0.20
P			0.078[a]	0.00012[b]	0.0023[a]	0.0034[a]

[a] Welch's ANOVA for unequal variances

[b] Kruskal-Wallis test

Plants

Bulk analysis of the exposed plant material showed high accumulation of Ag in all test groups exposed to nanoparticulate Ag with mean values of 10.6 and 12.0 mg/kg dw for the PVP-dispersed Nanopowder and PVP-coated Nanospheres, respectively (Figure 3.8). The highest Ag concentrations were however measured in the plants exposed to ionic Ag (Ag^+), with a mean value of 41.6 mg/kg dw. The range of measured concentrations was rather wide in all exposed groups, however in the plants exposed to ionic Ag, a single specimen contained 95.0 mg/kg dw Ag, accounting for the high mean and standard deviation in that group. In comparison, the highest measured values in the Nanopowder and Nanosphere-exposed plants were 16.0 and 20.6 mg/kg dw, respectively. The concentrations in the unexposed reference group was slightly lower than, but comparable to the Ag content in the freshly collected shoots (background values) at 0.035 compared to 0.044 mg/kg

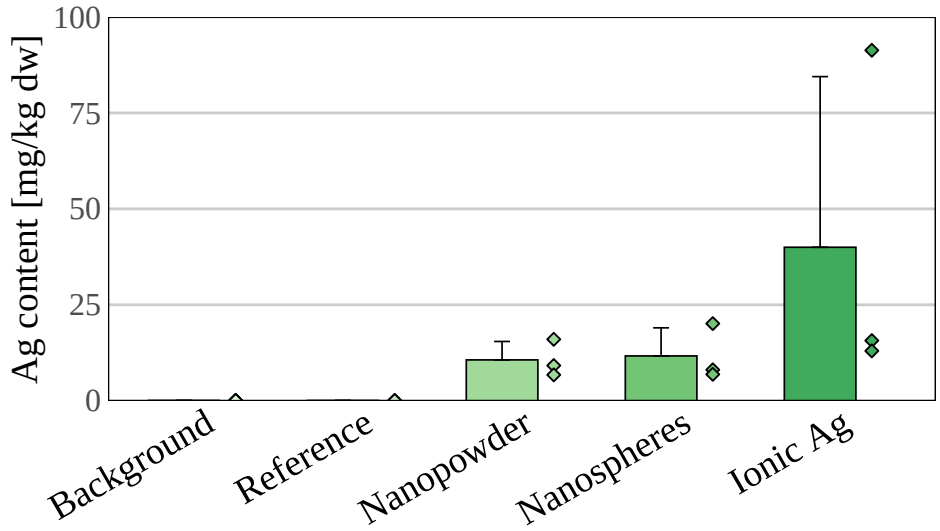

Figure 3.8: Total Ag content (mean ± SD) in the shoots of *M. spicatum*. Individual data points are displayed as colored diamond symbols.

dw.

For the assessment of significant differences between the experimental groups, all four groups were tested for normally distributed values (Shapiro-Wilk test, all $P > 0.05$). For the treatment groups, equality of variances was not met (Bartlett's test, $P = 5.1 \times 10^{-8}$), thus, significant differences between the treatment groups were assessed by Welch's ANOVA. No significant difference was detected between the treatment groups ($P = 0.078$). This is most likely due to the small number of observations per group (n = 3) and the outlier value in the ionic Ag group (95.0 µg/kg dw), which led to a standard deviation reaching into (physically impossible) negative concentrations (lower bound: -4.6 mg/kg dw).

Assuming a less stringent significance threshold of $P = 0.1$ and performing pairwise comparisons between all groups by unadjusted t-tests, only the mean difference between the Nanopowder-treated and Reference group achieved significance at a P-value of 0.062, while all other pairs of groups did not reach significance ($P > 0.1$).

Significant differences were separately assessed between the background values and the reference group by one-way ANOVA after assessing equality of variances (Bartlett's test, $P = 0.39$). As expected, no significant difference was thereby detected ($P = 0.37$).

Sediments

Similarly, high Ag concentrations were also detected in the sediments of the exposed mesocosms (Figure 3.9). Mean values of 0.096, 0.063 and 0.073 mg/kg dw were measured in the Nanopowder-, Nanospheres- and ionic Ag-exposed mesocosms, compared to 0.022 and 0.015 mg/kg dw in the

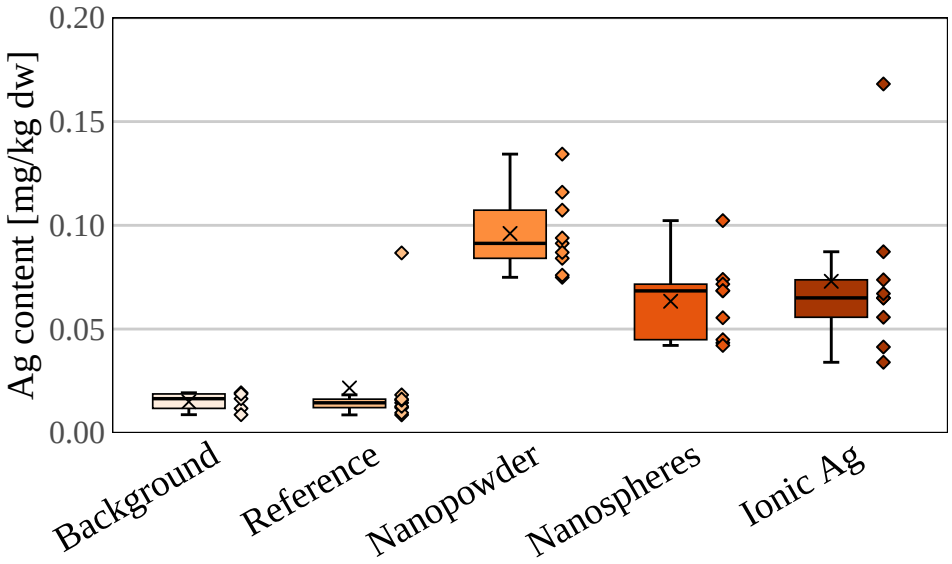

Figure 3.9: Total Ag content in the mesocosm sediments. Box and Whiskers represent quartiles, group means are indicated as black crosses. Individual data points are displayed as colored diamond symbols.

reference group and the unexposed sediment. The relative differences between the exposed and unexposed sediment were not as striking as in the shoots (minimum relative difference in the sediment: 2.86 (Reference vs. Nanospheres), compared to shoots: 303 (Reference vs. Nanopowder)). However, the highest percentage of added Ag was recovered in the sediments, at 67.6 ± 16.7 % (Nanopowder), 40.3 ± 0.5 % (Nanospheres) and 48.3 ± 13.6 % (Ionic Ag). The absolute recovery in the shoots could not be calculated, as the total dry weight was not recorded for those plants exceeding the required 200 mg for GF-AAS analysis. However, in those plants where the entirety of the dry shoot was analyzed (all except two plants from the Nanopowder group), not more than 2.5 % of the total dose was recovered, indicating that only a minor amount was taken up by the plants.

As not all groups were found to follow a normal distribution, statistical analysis was carried out by nonparametric Kruskal-Wallis test, which revealed statistically significant differences between the experimental groups ($P = 0.00012$) and was thus followed by pairwise comparison via the unadjusted Dunn's test. As expected, all Ag-exposed groups were found to be significantly different from the reference group (all $P < 0.05$). Additionally, the Ag content in the Nanopowder-exposed sediments was found to be significantly higher than in the other treated groups, whereas the Nanospheres- and Ionic Ag-exposed mesoscosms did not differ ($P = 0.87$).

Again, statistical differences between the background values and the reference group were separately assessed. As expected, the Kruskal-Wallis test did not return significant results between these groups ($P = 0.64$).

These results, in conjunction with the highest absolute recovery of Ag in the sediments of the Nanopowder-treated mesocosms and the quick decline in water column concentrations (see above),

fall nicely in line with the observed behavior of the Nanopowder stock (see Figure 2.1 C), where sedimentation occurred within hours for the PVP-dispersed Nanopowder.

Water column

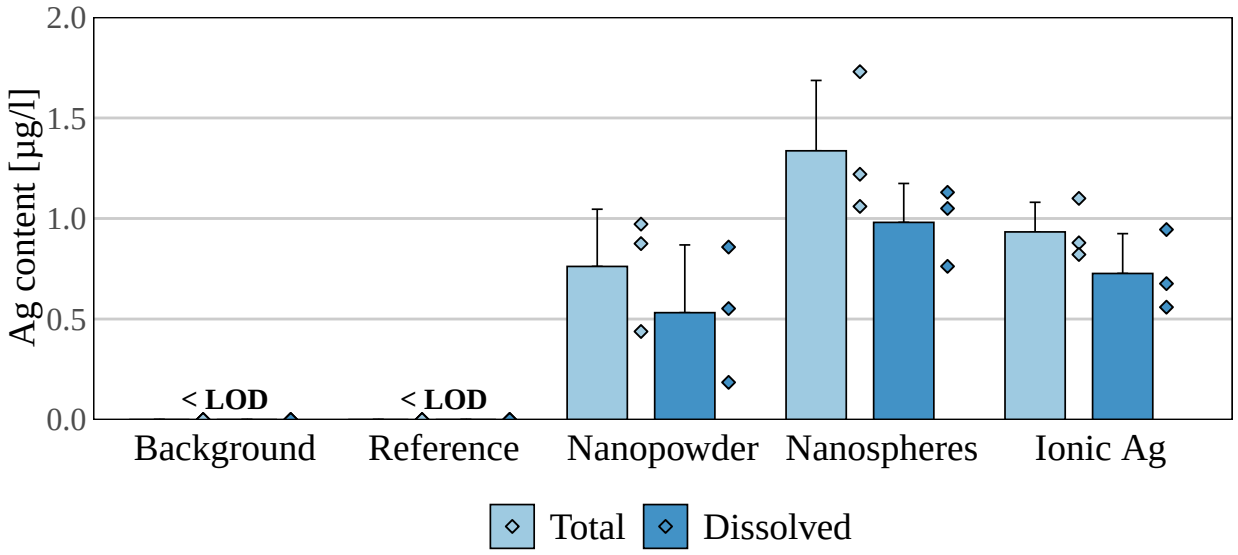

Figure 3.10: Total and dissolved Ag content (mean ± SD) in the ADW (Background) and mesocosm water at the end of the experiment. Individual data points are displayed as colored diamond symbols.

Regarding the concentrations of Ag remaining in the water column at the end of the experiment, 64.6, 74.4 and 77.2 % of the total concentrations were recovered in the dissolved fractions of the Nanopowder-, Nanosphere- and ionic Ag-treated mesocosms, respectively. As expected, the Nanopowder-treated group contained the smallest dissolved fraction of all groups, as already during the characterization of the Ag-NPs, the Nanopowder was shown to contain a large fraction of particles larger than the filter pore size of 0.22 µm (see Section 3.1). Interestingly however, the mesocosms exposed to ionic Ag also contained a sizable fraction (22.8 %) of Ag retained in the filter. The measured total concentrations accounted for 2.5 ± 0.9, 4.5 ± 1.2 and 3.11 ± 0.5 % of the nominal 120 µg of Ag added to each mesocosm.

To assess whether statistically significant differences existed, Welch's ANOVA was performed on the experimental groups after assessment of normality (Shapiro-Wilk test, all $P > 0.05$) and homogeneity of variances (Bartlett's test, $P_{tot.} = 0.0015$, $P_{diss.} = 0.0037$). As the Ag content in the reference mesocosms was below the LOD of 0.3 µg/L, synthetic values had to be imputed to allow statistical calculations. For this, normally distributed random values with a mean of 0.03 µg/L (LOD/2) and a standard deviation of 0.01 µg/L were generated.

Significant differences were found for both total and dissolved Ag ($P_{tot.} = 0.0039$ and $P_{diss.} = 0.0076$) and were thus followed by pairwise comparisons via t-tests. For total Ag, all exposed groups were significantly different from the reference group (all $P < 0.05$) but did not differ between each other.

Likewise for dissolved Ag, significant differences were not found between the exposed groups, but between the reference group and the Nanosphere- as well as the ionic Ag-treated groups ($P = 0.013$ and 0.026, respectively). No significant difference was found between the reference and Nanopowder group ($P = 0.122$).

Bioconcentration Factors

Table 3.5: Calculated bioconcentration factors (mean ± SD) of Ag in the shoots of *M. spicatum* compared to the nominal exposure in the water column, the peak concentrations in the water column and the Ag content accumulated in the sediment. (n = 3).

Group	Bioconcentration Factor		
	Shoot-Water,nominal [L_{Water}/kg dw_{Plant}]	Shoot-Water,peak [L_{Water}/kg dw_{Plant}]	Shoot-Sediment [kg $dw_{Sediment}$/kg dw_{Plant}]
Nanopowder	355 ± 160	650 ± 287	116 ± 66
Nanospheres	399 ± 249	716 ± 387	189 ± 119
Ionic Silver	1386 ± 1544	2890 ± 3150	583 ± 638

[a] Welch's ANOVA for unequal variances

[b] Kruskal-Wallis test

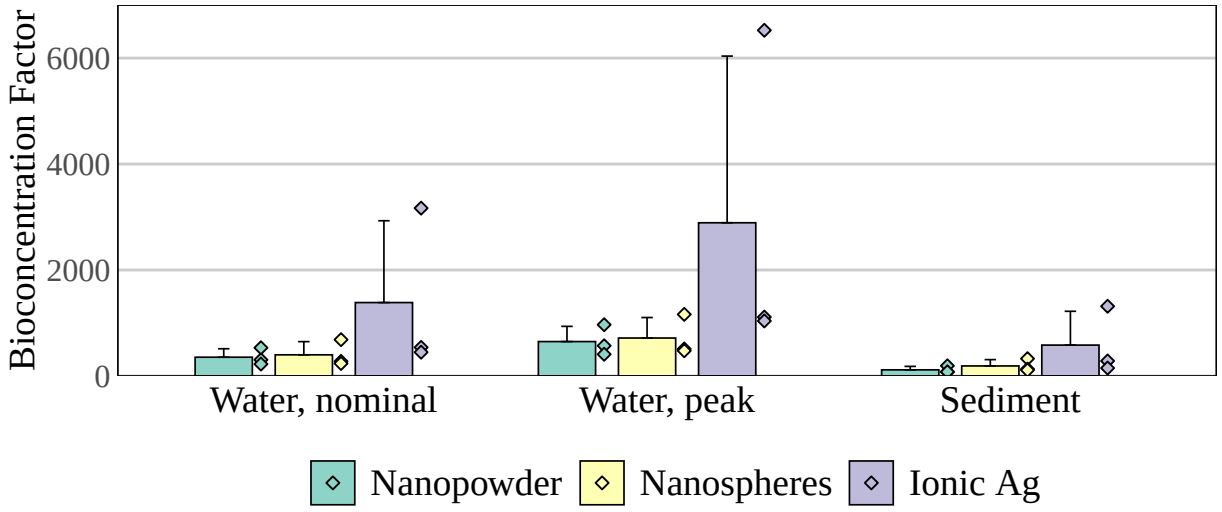

Figure 3.11: Calculated bioconcentration factors (mean ± SD) of Ag in *M. spicatum*. Individual data points are displayed as colored diamond symbols.

The calculated bioconcentration factors (BCF, see Equation 2.4) are summarized in Table 3.5. In general, the BCFs were characterized by very high variability in all groups, but especially in the ionic Ag group due to one outlying value (see section 3.2.2 above). Here, for all groups, the standard deviation was larger than the calculated mean.

Due to the identical nominal exposure concentration and the similar peak concentrations in the water column, the BCFs of both types of Ag-NP were of comparable sizes, with the Nanosphere-BCFs generally slightly larger than the Nanopowder-BCF. This difference was more pronounced in

the Sediments, as here, the Nanopowder accumulated to significantly higher concentrations, while the Ag content in the shoots was similar between both groups, resulting in a lower Nanopowder-BCF.

Compared to the BCFs of all nanoparticulate forms, ionic Ag, due to one outlying value, showed the highest mean BCFs, which were found to be at least a factor of 2.7 higher than for any Ag-NP. Even when this value is removed from the calculation, the mean BCFs remain higher than those of the Ag-NP exposed groups. Statistical testing did not reveal any differences between the BCFs of the treated groups, again likely due to the high variability and small sample size.

3.3 Effects on the Aquatic Plant *Myriophyllum spicatum*

Following the harvest of the shoots, the length was measured before freeze drying and acid digestion. The growth parameters of the plants are summarized in Table 3.6.

Table 3.6: Experimental parameters and growth characteristics (mean ± SD) of *M. spicatum*. P-values obtained from testing for differences between treatment groups are reported for relative growth only.

Group	n	Time [days]	Exposure [µg]	Init. Length [cm]	Fin. Length [cm]	Growth [%]
Reference	3	35	0	15.0 ± 0	27.7 ± 6.1	84.4 ± 40.7
Nanopowder	3	35	120	12.3 ± 0.8	24.7 ± 5.9	99.1 ± 38.6
Nanospheres	3	35	120	14.4 ± 0.2	22.5 ± 2.2	56.2 ± 14.1
Ionic Silver	3	35	120	13.4 ± 2.9	18.9 ± 3.0	43.3 ± 22.4
P						0.2479[a]

[a] Kruskal-Wallis test

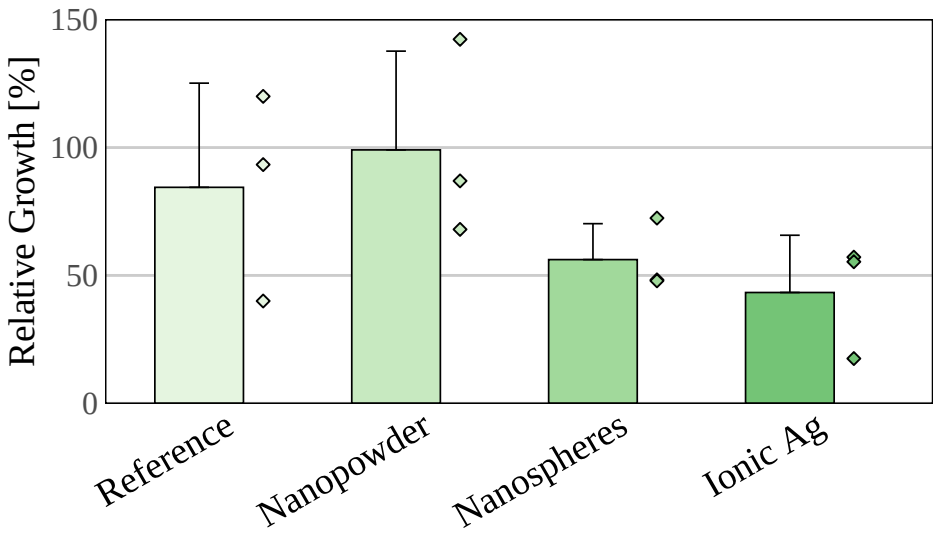

Figure 3.12: Relative growth (mean ± SD) during the experiment, expressed as percentage of the initial length. Individual data points are displayed as colored diamond symbols.

Regarding the growth of *M. spicatum*, Figure 3.12 shows the relative growth (in percent of the initial shoot length) of the plants in every treatment group. During the experiment, the unexposed reference plants, on average, grew by 84.4 %, while the plants exposed to ionic Ag and the PVP-coated Ag Nanospheres grew the least, at 43.3 and 56.2 %, respectively. The plants exposed to the Ag Nanopowder grew even more than the reference plants, averaging at a growth of 99.1 %.

Generally, less growth was observed in the shoots of the second experiment (Nanospheres and ionic Ag). The effect of ionic Ag on the plants was visually apparent (see Figure 3.13), as these showed considerable browning of the leaves in addition to stunted growth. In contrast, the reference and Ag-NP-treated groups, appeared quite healthy throughout the experiment, with the shoots continually

showing healthy green leaves fresh growth.

For the assessment of significant differences, all groups were tested for normally distributed values. One group did not meet the assumption of normal distribution (Nanospheres, $P = 0.0272$), thus, the nonparametric Kruskal-Wallis test was applied. However, no significant differences in relative growth were thereby detected ($P = 0.2479$).

Some algal growth was apparent on the plants in all treatment groups, with growth in the ionic Ag exposed mesocosms appearing to be most pronounced. No attempts were made to quantify algal biomass and upon harvest, the algae were removed from the plants by rinsing with Milli-Q water.

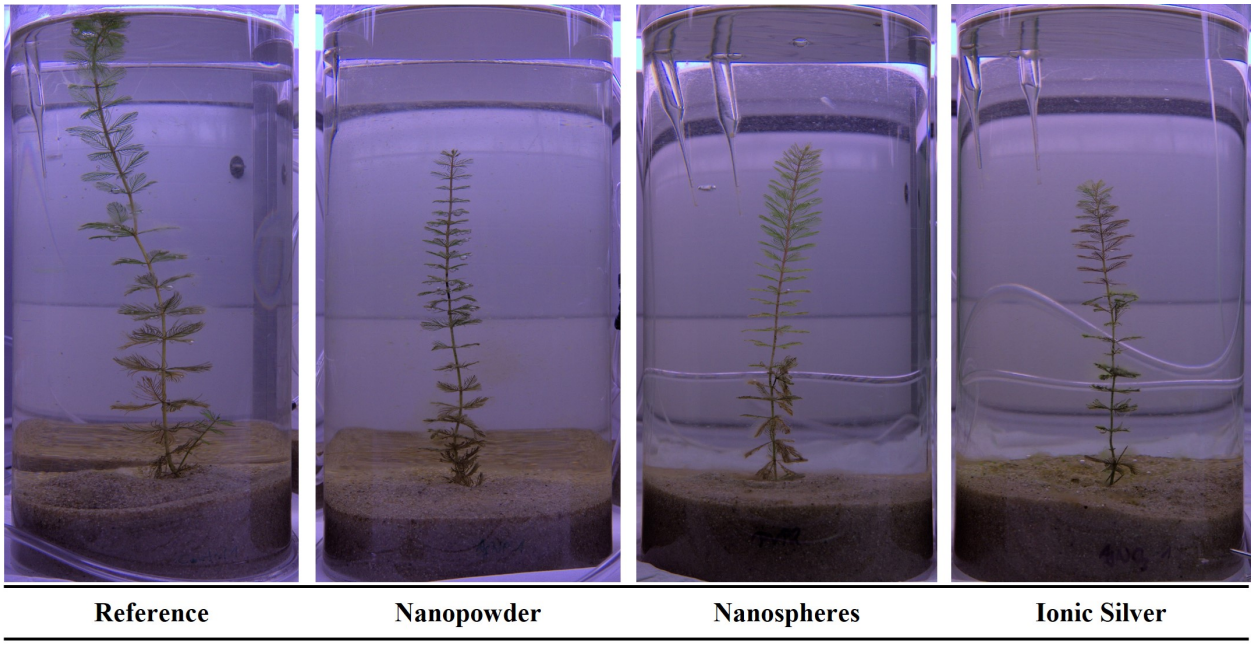

Figure 3.13: Side-by-side view of one mesocosm from each treatment group at the end of the experiment.

3.3.1 Uptake of Silver and Silver Nanomaterials

To assess, whether Ag was adsorbed onto the plants' surface or taken up, leaves of the exposed plants were collected and the surface analyzed by SEM and EDX. Additionally, ultrathin slices of resin-embedded leaves were imaged by TEM and EELS for the element-selective detection of internalized Ag.

3.3.2 Electron Microscopy of the Exposed Plant Material

SEM-EDX Imaging

SEM measurements were performed on leaves exposed to PVP-coated Ag Nanospheres and ionic Ag. No SEM measurements of the PVP-dispersed Nanopowder exposed plants were conducted, as the entire collected plant material was used for TEM analysis.

Deposited Ag was only detected on the leaves of the ionic Ag treated plants, where a faint layer, as well as local precipitates were detected by EDX (Figure 3.14 B, D). The corresponding EDX spectra are given in Figure 3.15. In both spectra, a peak at approximately 3 keV is evident, corresponding to the characteristic X-ray of the Lα_1 spectral line of Ag at 2.983 keV.

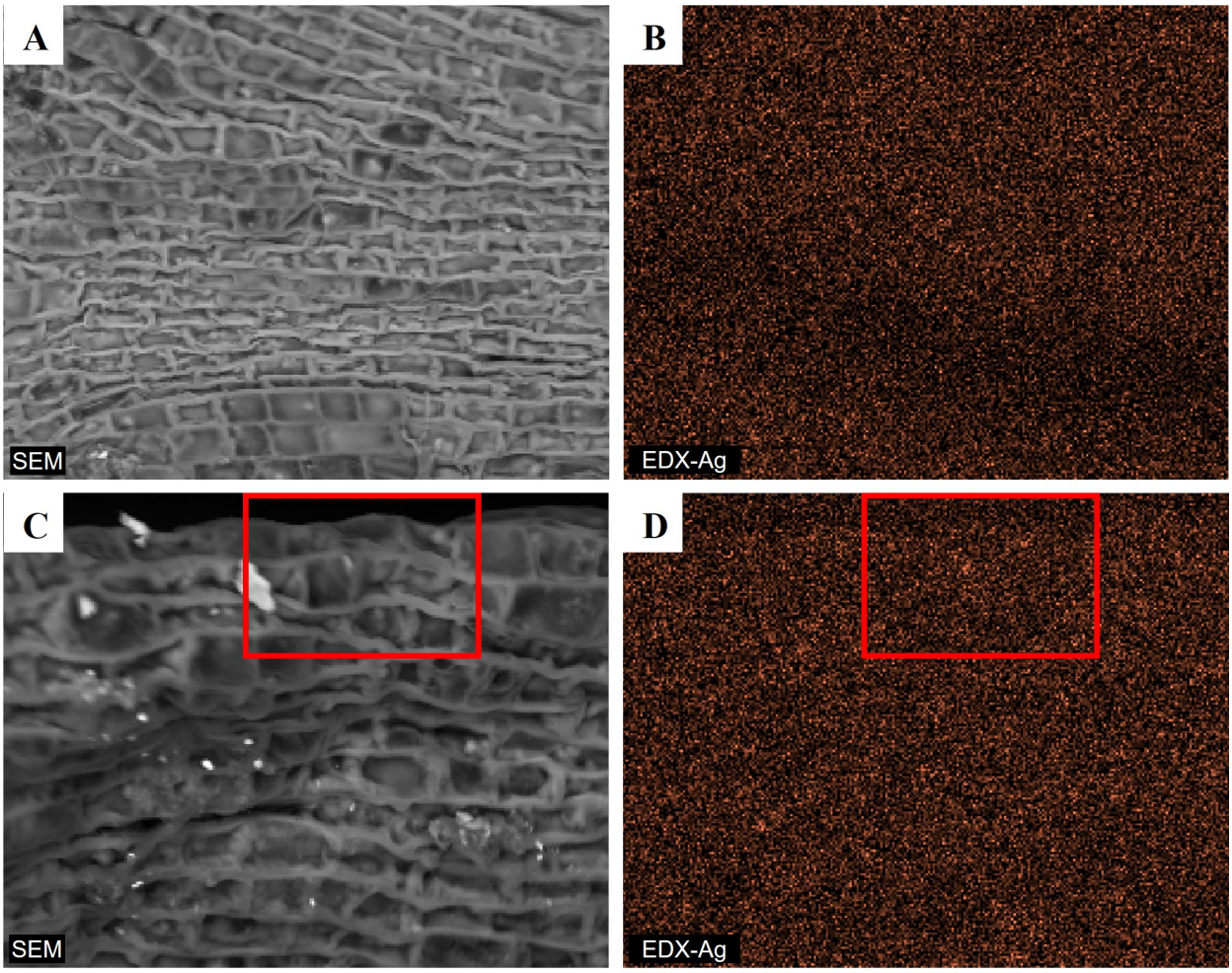

Figure 3.14: SEM micrographs (A, C) and EDX-maps of Ag (B, D) on the surface of a leaf of *M. spicatum* exposed to $AgNO_3$. C, D: Local accumulates of Ag are identifiable as brighter spots inside the highlighted box in both the EDX and SEM image. A detailed view is presented in Figure 3.16.

A detailed view of the highlighted area in Figure 3.14 C and D is presented in Figure 3.16. Two local clusters are discernible in the EDX-map of Ag and are also visible in the SEM micrograph (red arrows). Interestingly, colocalized with Ag, elevated levels of S were detected, indicating the association of the precipitated Ag with sulfur-containing groups, possibly as poorly soluble silver sulfide (Ag_2S). Due to the limited sample material, no further investigation of the speciation was carried out to characterize the precipitates.

Cluster 1 was additionally submitted to a detailed EDX-analysis, the result of which is shown in Figure 3.17. Compared to the EDX spectrum of the entire detail area (depicted as the red line), the cluster shows considerably higher Ag and S peaks (sulfur Kα_1 = 2.309 keV), confirming the association seen in Figure 3.16.

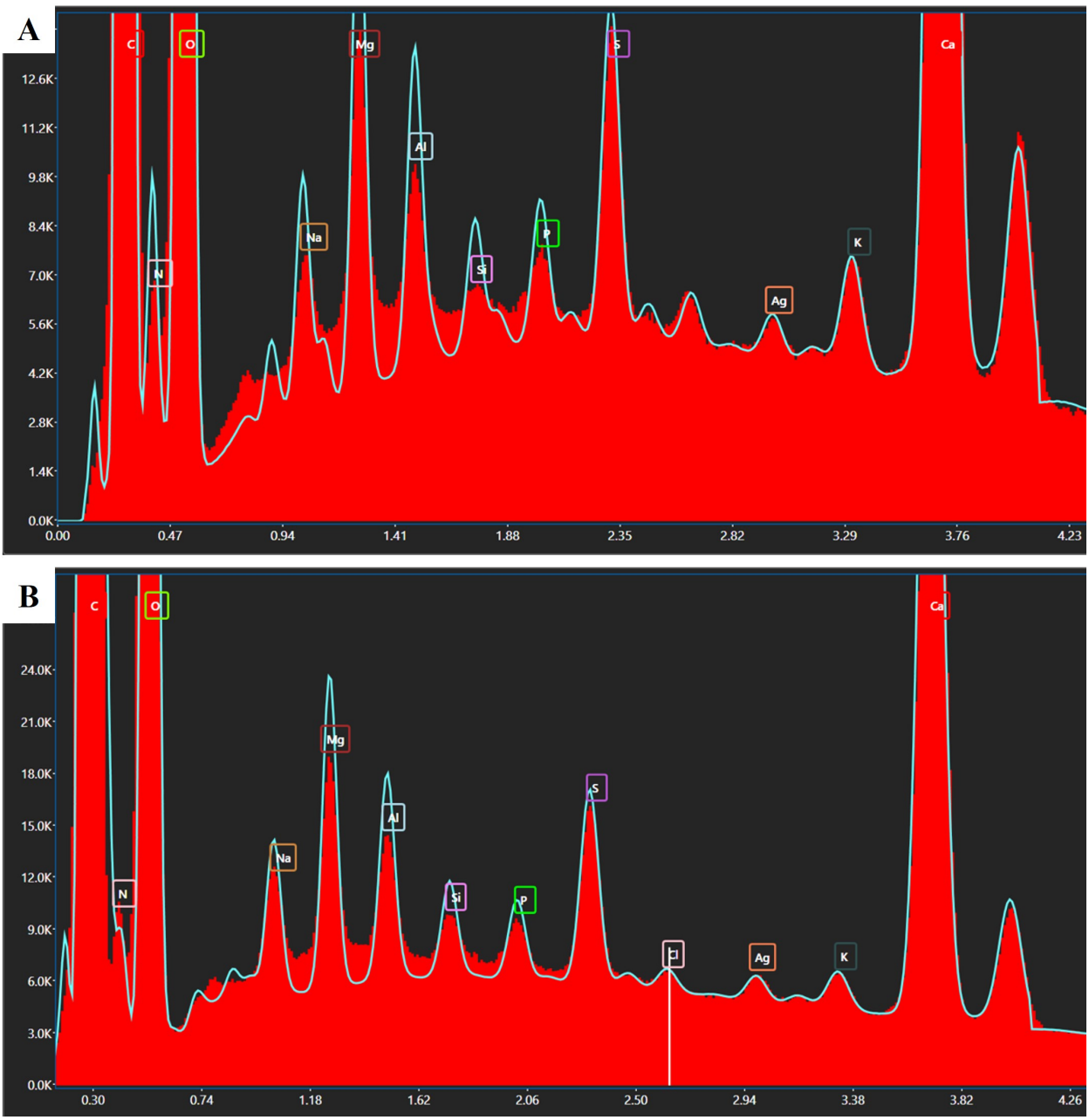

Figure 3.15: EDX spectra of the sample areas in Figure 3.14. A peak at approximately 3 keV, correspoding to the $L\alpha_1$ X-ray of Ag is present in both spectra. A: EDX spectrum of 3.14 A. B: EDX spectrum of 3.14 C.

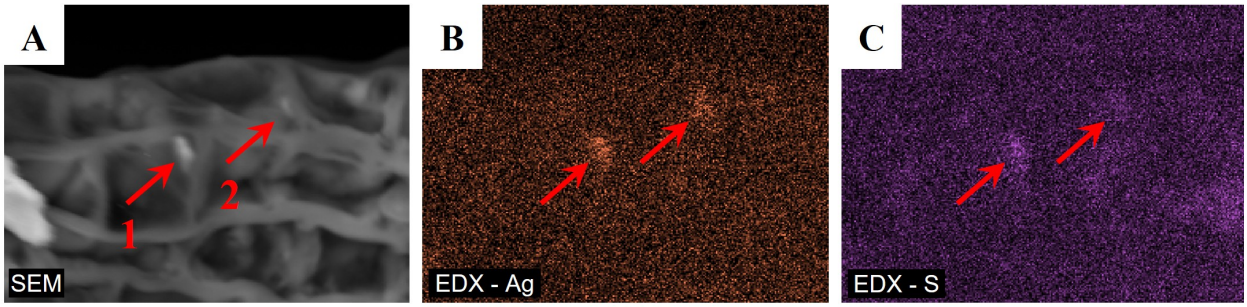

Figure 3.16: Detail SEM micrograph (A) and EDX-maps of Ag and S (B and C) of the highlighted area in Figure 3.14. Areas rich in Ag are also characterized by elevated levels of S.

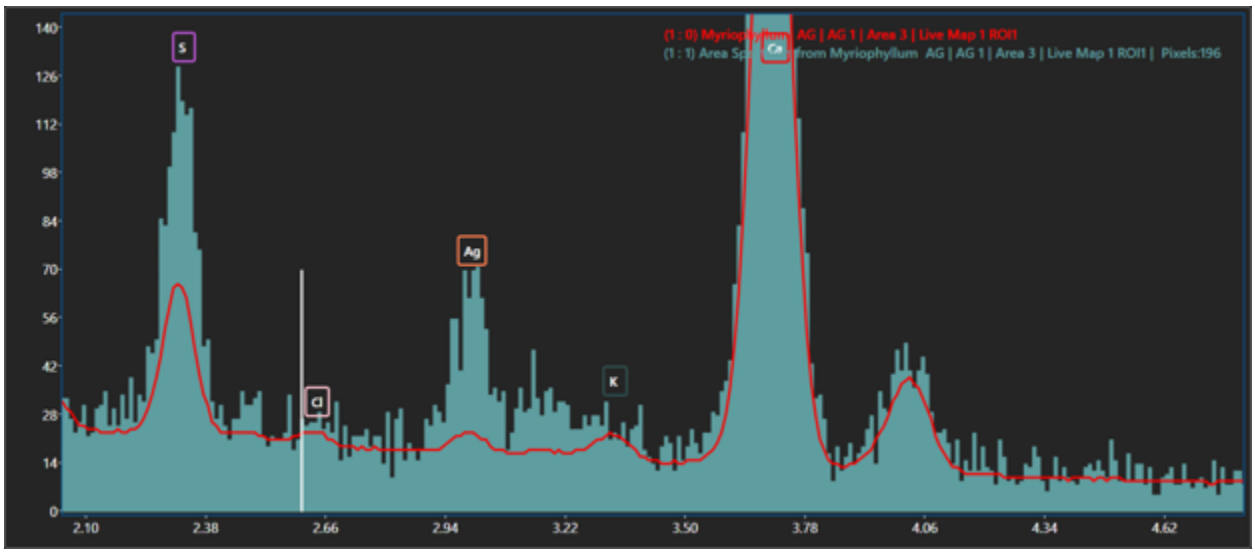

Figure 3.17: Detail view of the EDX spectrum of cluster 1 (light blue histogram) compared to the average EDX spectrum of Figure 3.16 (red line). Both Ag and S are considerably enriched in cluster 1.

In comparison, no Ag was detected by EDX on the leaves of the plants exposed to Ag Nanospheres (Figure 3.18). In the EDX spectrum (Figure 3.18 C), no clear peak corresponding to Ag can be discerned. However, there is an almost indiscernible deviation from the baseline at approximately 3.0 keV, close to the theoretical position of the Ag $L\alpha_1$ spectral line. This might have been caused by Ag present in amounts below the LOD of EDX, but can not be ascertained.

As no Ag was detected on the surface of these samples, they were not subjected to analysis by TEM and EELS.

TEM-EELS Imaging

TEM micrographs were obtained from longitudinal sections of leaves exposed to the PVP-dispersed Nanopowder and those exposed to ionic Ag. For comparison, the leaves of unexposed plants were also imaged. No imaging of the plants exposed to PVP-coated Nanospheres was performed, as no Ag could be detected on the surface of these leaves and uptake of detectable amounts was thus deemed unlikely. Regions of interest (ROI) on the imaged samples were additionally subjected to EELS analysis to identify the possible intracellular uptake of Ag by the plants.

Figure 3.19 shows representative TEM micrographs of unexposed plant samples, showing intact cells and the morphology of different organelles, including mitochondria, chloroplasts and starch grains. The micrographs obtained from the leaves exposed to the Nanopowder are summarized in Figure 3.20. While the cells were intact and organelles such as starch grains are clearly discernible, the prolonged storage of the samples in 70 % EtOH and the subsequent wash steps during post-fixation likely extracted any remaining incorporated Ag-NPs. No ROIs with suspected Ag accumulates were detected in these samples and thus no analysis by EELS was performed.

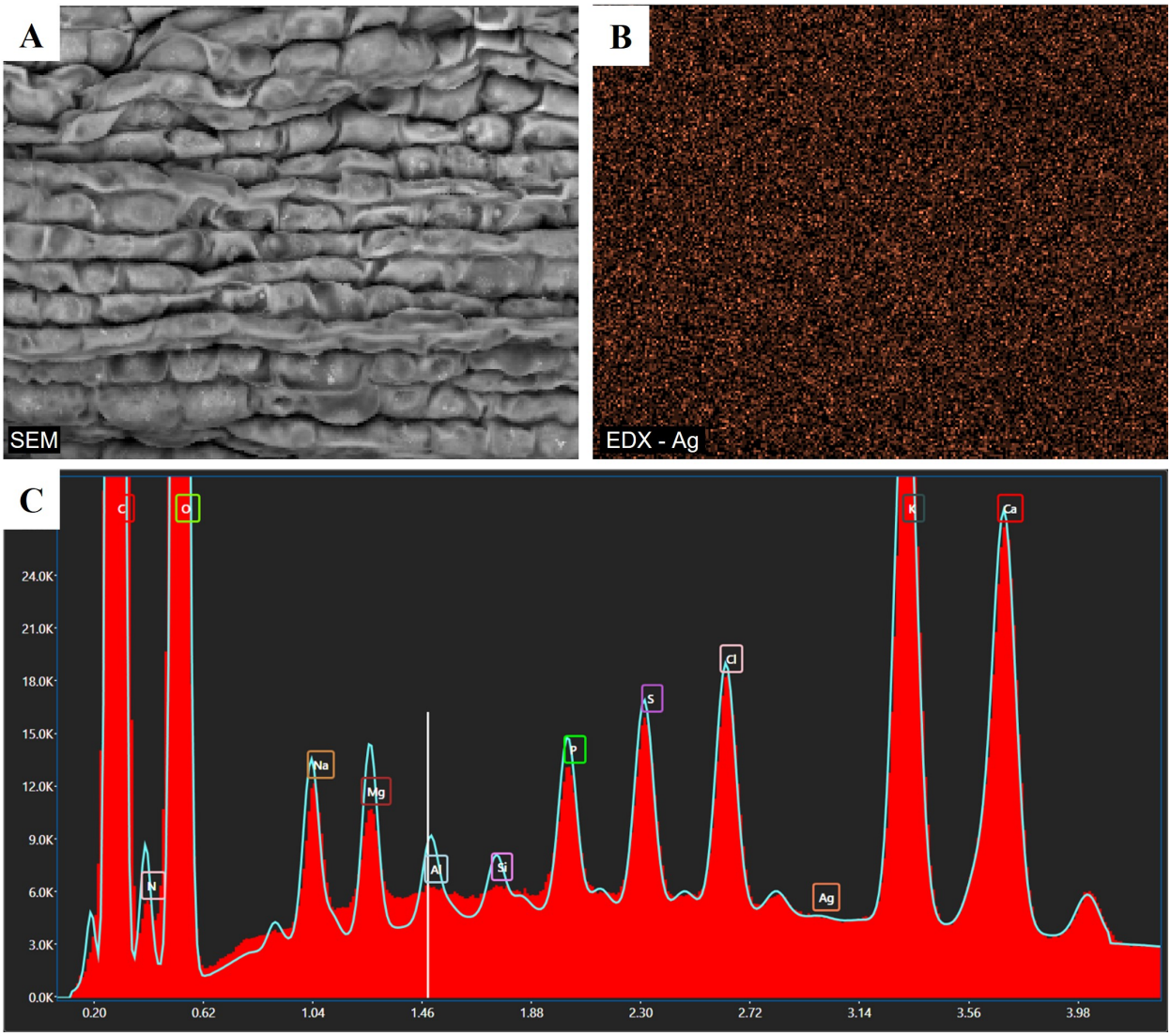

Figure 3.18: SEM-EDX measurements of *M. spicatum* leaves exposed to PVP-coated Ag Nanospheres: A: SEM micrograph, B: EDX map of Ag and C: EDX spectrum of the imaged area. No peak corresponding to Ag was detected by EDX, however a miniscule deviation from the baseline near the energy corresponding to Ag is present, indicating the possible presence of Ag.

As EDX analysis revealed the presence Ag on the surface of the leaves exposed to $AgNO_3$, TEM micrographs were captured of ultrathin sections of these leaves and ROIs subjected to EELS. Figure 3.21 shows a selection of composite micrographs at low magnification. Clearly, the intracellular structure of the samples was severely compromised, with no intact cells and only fragments of cellular content present. The only intact structures on these micrographs appear to be the individual cell walls as well as some chloroplasts (Figure 3.21 B). As described previously (see Figure 3.13 D), browning of the leaves was observed during the experiment and these leaves were also sampled for imaging.

EELS analysis was carried out on several ROIs of the samples (red rectangles in Figure 3.21). The detail micrographs and EELS spectra are given in Figures 3.23, 3.22 and 3.24.

As is immediately evident, in none of the acquired EELS spectra signals similar to the Ag M4,5-edge

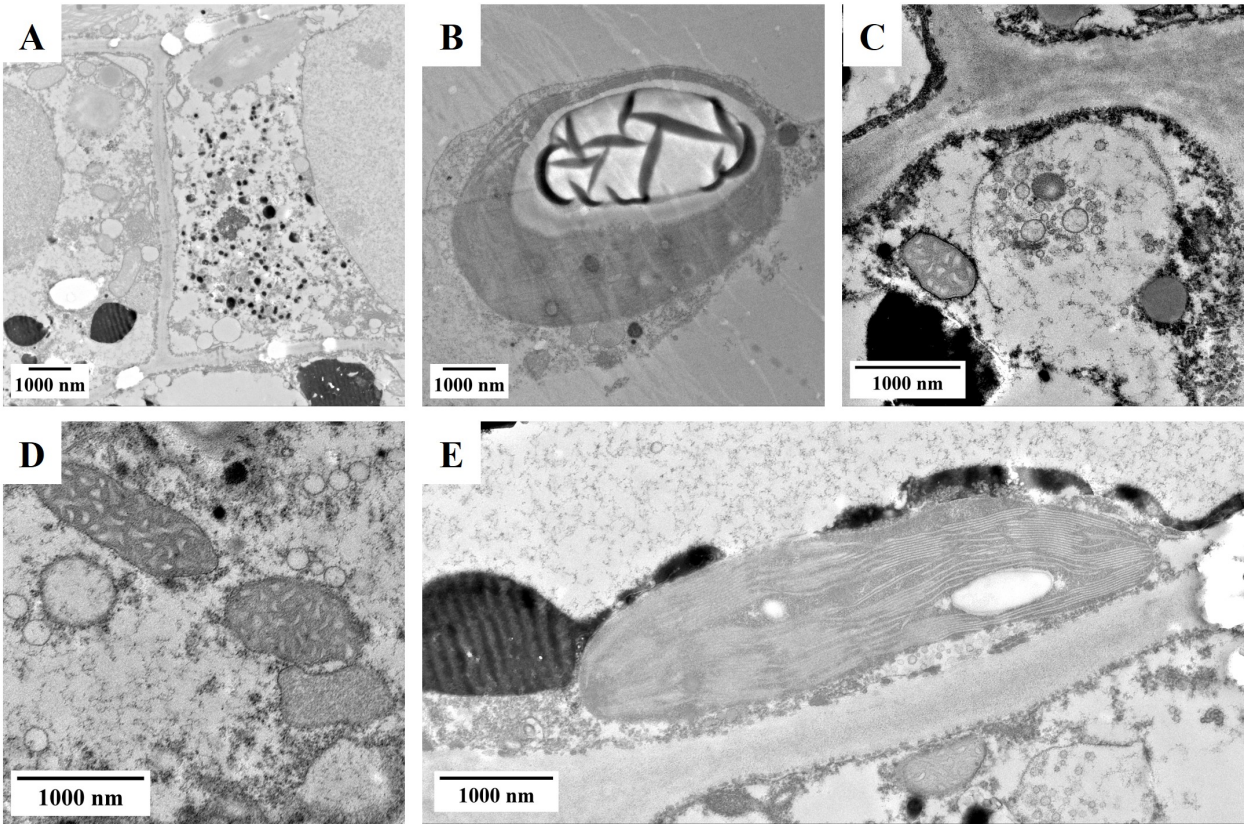

Figure 3.19: TEM micrographs of unexposed *M. spicatum* leaves, showing the morphology of different cell organelles. A: Overview of two neighboring cells at medium magnification. Nuclei are visible as large organelles on the left and right border of the image. B: A cut through a starch grain. The crystalline contents are visible. C: Intensely black stained cell membranes in contrast with the almost translucent cell wall and several vesicles. D: Mitochondria. E: A chloroplast, thylakoids are clearly visible inside the chloroplast.

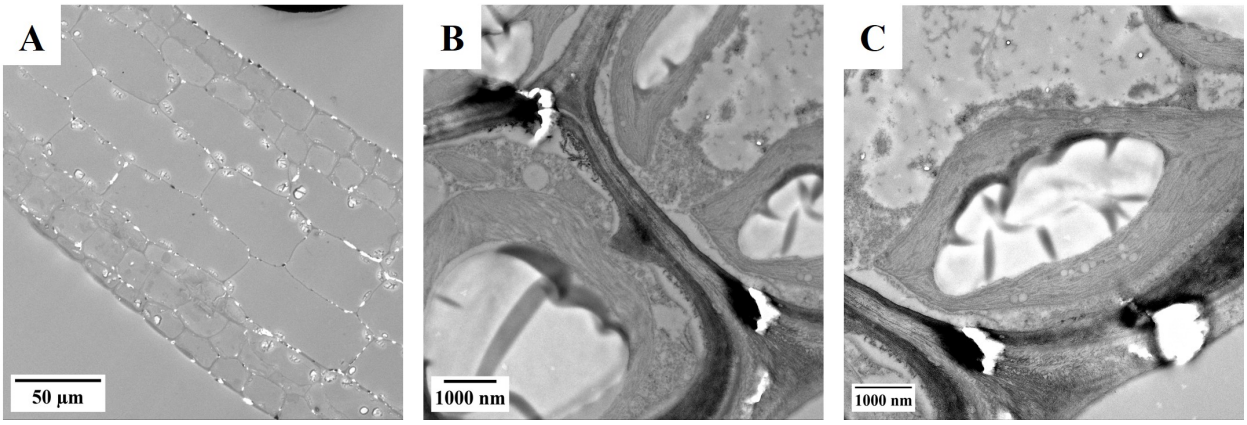

Figure 3.20: TEM micrographs of *M. spicatum* leaves exposed to PVP-dispersed Ag Nanopowder. No regions of interest containing Ag were identified. A: Overview of the sample at low magnification, showing the spatial organization of the leaf tissue. B and C: High magnification micrographs showing starch grains engulfed by chloroplasts and sections of cell wall. Black, electron dense sections in the cell wall arose from sample preparation.

(see Figure 3.5) are present, indicating that none of the ROIs contained Ag in detectable quantities. Only the spectrum in Figure 3.24 C contains a small, rather sharp peak at approximately 425 eV that was previously also observed in the EELS spectra of the pure Ag-NPs (see Figure 3.4).

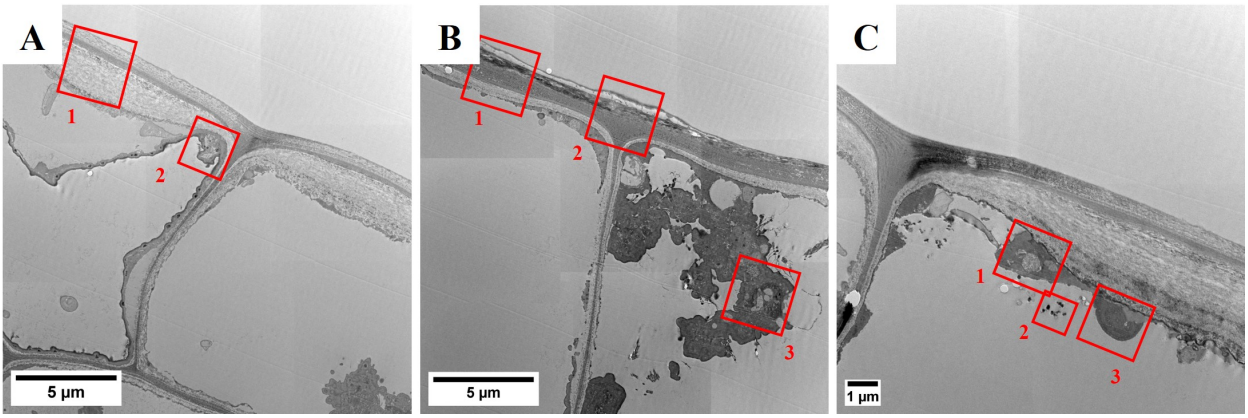

Figure 3.21: Composite TEM micrographs of *M. spicatum* leaves exposed to ionic Ag at low magnification illustrating the impaired intracellular morphology of the sample. The cytoplasm of all observed cells appears to be ruptured and only fragments of the cytoplasmatic content are visible. The red rectangles represent regions or interest that were subjected to EELS analysis for the presence of Ag.

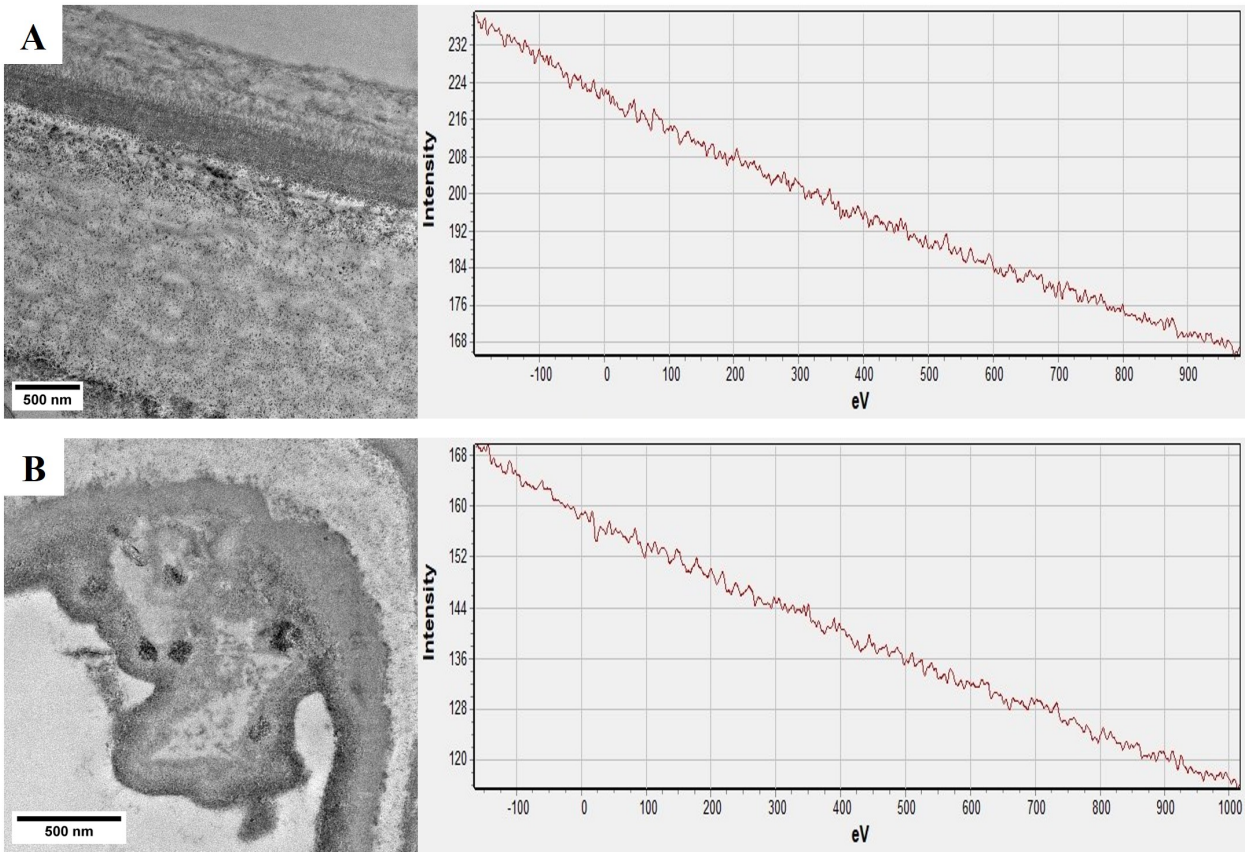

Figure 3.22: TEM micrographs and EELS spectra of the ROIs in Figure 3.21 A.

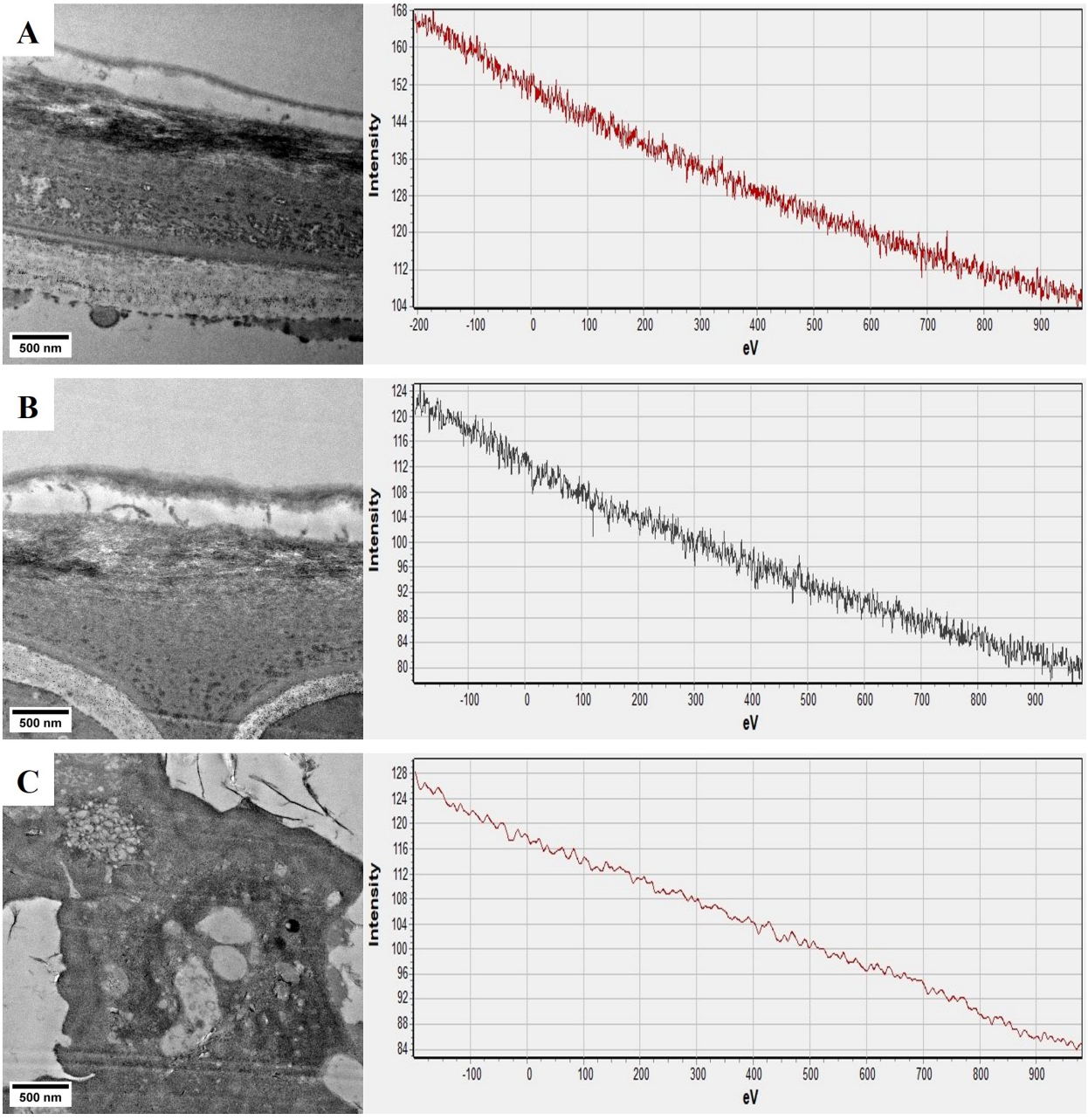

Figure 3.23: TEM micrographs and EELS spectra of the ROIs in Figure 3.21 B.

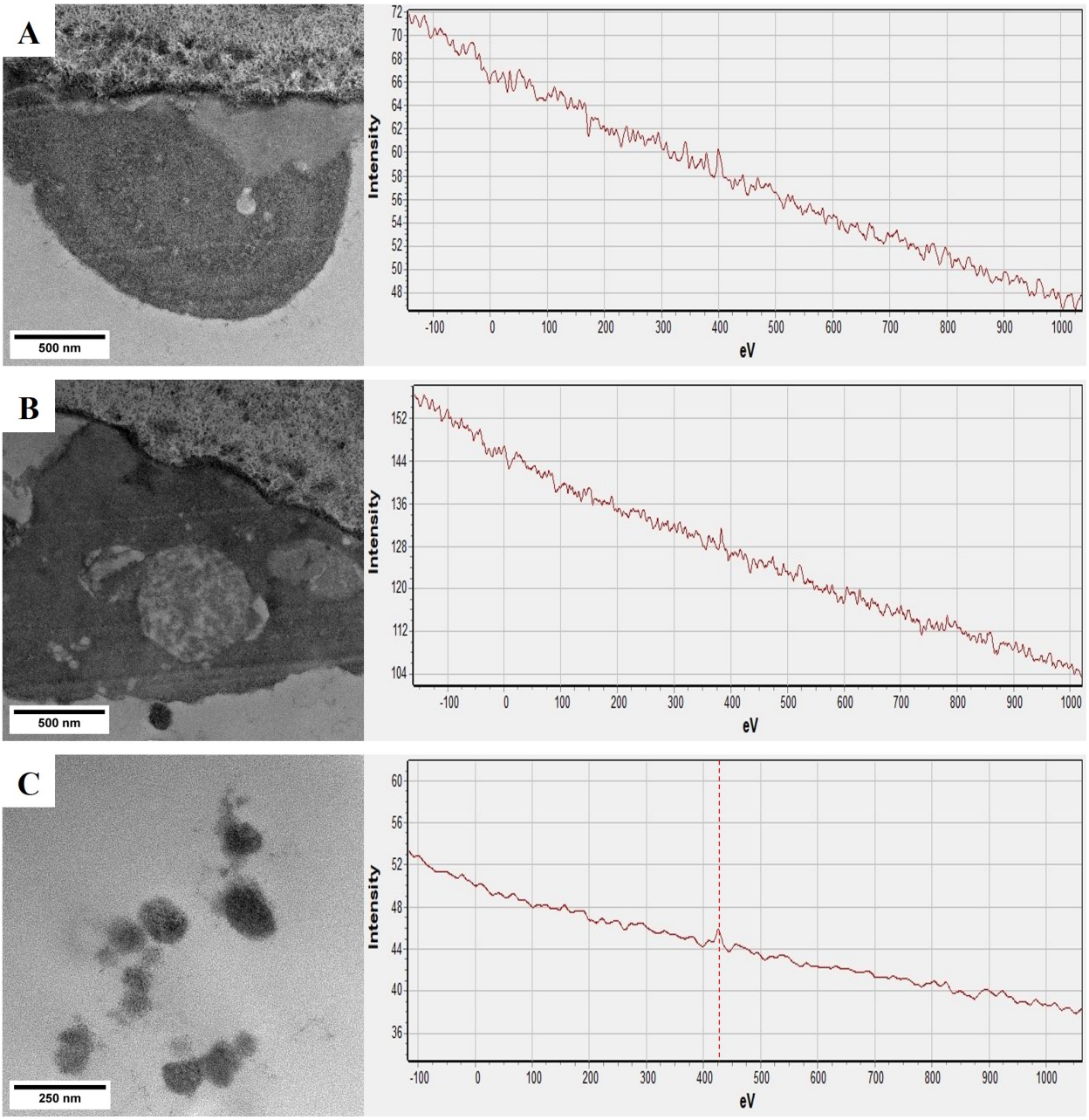

Figure 3.24: TEM micrographs and EELS spectra of the ROIs in Figure 3.21 C.

4 Discussion

4.1 Silver in the Aquatic Phase and the Sediments

As was described in section 3.2.2, the distribution of the added Ag between the analyzed compartments (aquatic phase, sediments and plant shoots) was qualitatively similar for all types of Ag, with the sediments serving as the main sink. However, much of the added Ag was not recovered in any of the analyzed compartments, in case of the Nanospheres accounting for over 50 % of the total amount.

4.1.1 Aquatic Phase

The general dynamics in the aquatic phase were similar between all applied forms of Ag. During the initial phase of dosing, the concentrations in the aquatic phase progressively increased after each addition due to incomplete sedimentation in the intervening time, followed by a decline in concentrations after cessation of dosing.

The declines in water Ag concentrations were quicker for the PVP-dispersed Nanopowder and considerably slower in the remaining groups, but arrived at similarly low levels by the end of the experiment. Compared to the coated Nanospheres, which were of highly uniform size and shape, the Nanopowder formed much larger aggregates (see Figure 4.1 A, B), which likely led to reduced suspension stability, also observed in the stock solutions (Figure 4.1 C). Even though this resulted in differences in the absolute exposure of the plants via the aquatic phase (in terms of Ag available to the plants over time), this behavior would also be expected in a natural environment and thus did not impair further interpretation.

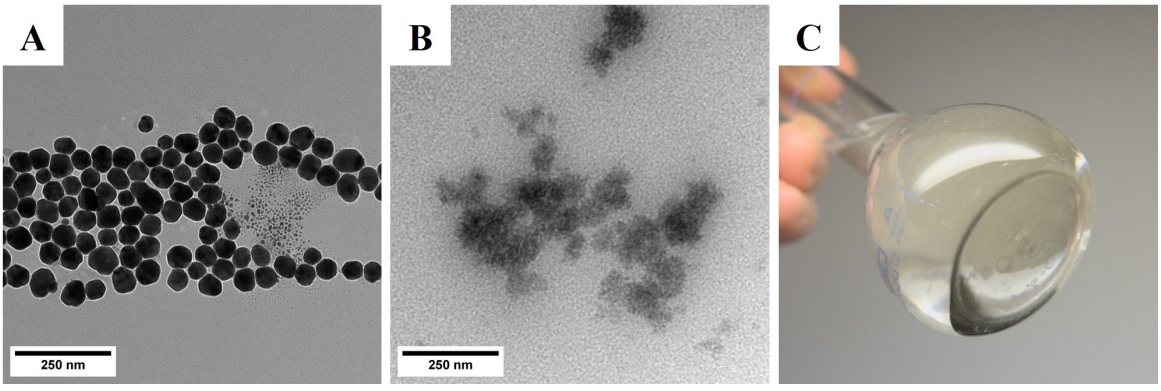

Figure 4.1: A, B: The Ag-Nanospheres and Nanopowder at 31 500x magnification. C: Sedimented Ag-Nanopowder in the stock suspension.

Ag from $AgNO_3$ was found to be rather stable in the water column, but followed a similar sedimentation behavior as its nanoparticulate counterparts, although more similar to the Nanospheres. Given the concentrations of Cl^- in the water at approximately 367 µM, compared to the added Ag (approximately 93 nM), the formation and precipitation of insoluble AgCl, seems likely. However, depending on the molar ratio of Ag^+/Cl^-, the predominant form of Ag changes between free Ag^+, insoluble AgCl and soluble chloro complexes (e.g. $[AgCl_2]^-$). At molar ratios comparable to the present experiment, Ag^+ still constitutes the major species in water, with only a minor contribution of AgCl (Lee et al., 2004). At the end of the experiment, a sizable fraction of the originally ionic Ag (approximately 23 %) was found in the particulate fraction (> 0.22 µm). No investigation of the speciation of this retained fraction was pursued, however it was likely compromised of suspended AgCl as well as Ag complexed with aggregates of humic substances, which have additionally been shown to mediate the reduction of Ag^+ to form "natural" Ag^0-(nano)particles (Akaighe et al., 2011; Chen et al., 2012; Dong et al., 2020).

4.1.2 Sediments

The largest percentage of the added Ag was recovered in the sediments. Here again, the Nanopowder accumulated to significantly higher levels than the other forms of Ag, in line with its observed sedimentation behavior.

Similar results have previously been reported in experiments featuring higher exposures. For example, Jiang et al. (2017) reported the accumulation of 12 mg/kg dw PVP-coated Ag-NPs in the top 5 mm of the sediment 90 days after a single exposure event at 500 µg/L Ag. Sediments below that depth did not differ from the reference group. A direct comparison of these results to the present study is not possible, as only the average concentration of Ag in the sediments was assessed. However in both studies, there was no significant difference between Ag accumulated from PVP-coated Ag-NPs and $AgNO_3$.

Sediments have also been shown to serve as the major environmental sink for Ag-NPs in a number of experiments conducted in larger-scale mesocosms, irrespective of the surface functionalization (e.g. citrate, gum arabicum, PVP or sulfidation to simulate aged particles) (Colman et al., 2014; Lowry et al., 2012; Metreveli et al., 2021).

In the long term, even low releases of NPs into aquatic environments may lead to a slow buildup of sediment concentrations. Thus, apart from acute exposure events, the chronic effects of Ag-NPs in aquatic environments might be most severe in benthic organisms, which have been shown to readily accumulate Ag-NP (T. Wang & Liu, 2022), and in microbial communities residing within the sediment (Jiang et al., 2017).

4.2 Effects on *Myriophyllum spicatum*

4.2.1 Effects on Growth

All forms of Ag had statistically insignificant effects on the growth of *M. spicatum*. Growth seemed to be inhibited in the plants exposed to $AgNO_3$ and PVP-coated Nanospheres, however. Visually perceptible toxicity was only observed after exposure to $AgNO_3$, resulting in the degradation (browning) of established leaves. These leaves were also subjected to TEM analysis, where severe deterioration of the subcellular structure was observed, whereas the structure of the reference and Ag-NP exposed leaves remained unaffected. Browning is a sign of chlorophyll degradation and part of the natural process of leaf senescence, but can also be induced by environmental stressors, such as heavy metals (Strasburger et al. (1991b), Maksymiec (2007)). On the cellular level, this process culminates in the disruption of the cell wall and thus cell death (Lim et al. (2007)), possibly leading to the observed compromised morphology.

All plants continued to produce fresh growth after the exposure events and seemed to tolerate the highest achieved concentrations in the time frame of the experiment.

Similarly, recovery of *E. densa* has been demonstrated after an initial exposure to much higher concentrations of Ag^+ and Ag-NPs (2.5 mg/L) (Colman et al., 2018). While the toxic effects of Ag initially led to a dramatic deterioration of the plants, as the concentrations in the water column declined due to sedimentation, the toxic effects also subsided and sustained new growth was noted 16 days after the initial exposure.

4.2.2 Silver Bioaccumulation

While *M. spicatum* accumulated quite high concentrations of Ag from each respective form, only a minor percentage of the total Ag added was recovered in its tissues, due to only a single shoot being present in each mesocosm. Larger scale experiments with more plant biomass have reported up to 50 % of the added Ag recovered in aquatic plants, demonstrating the potentially substantial effect of plants on Ag-NP removal (Stegemeier, Avellan, et al., 2017).

With exception of a single plant exposed to Ag^+ that accumulated 95.0 mg/kg dw, the accumulated concentrations ranged between 6.7 and 20.5 mg/kg dw and were comparable between the groups. Due to the low number of plants per group (n = 3) and the high variance in the plants exposed to Ag^+, no statistically significant differences were apparent between any of the groups, including the unexposed reference mesocosms. A higher number of replicates per group or a higher number of shoots per mesocosm would likely have allowed to discern at least differences between the exposed and reference groups, if not even between the different types of Ag.

At the time of the experiment, no published reports on the interaction of *M. spicatum* with Ag-NP were identified in the literature, even though *M. spicatum* is considered an established test organism in OECD-ecotoxicity tests (OECD, 2014a, 2014b). Data on the interaction of other aquatic plants with Ag-NP is available, although cross-species comparisons are difficult, especially when differing life-forms (e.g. floating and submerged) and habit are involved. However, in both floating as well as submerged plants, bioaccumulation of Ag-NP was generally observed (see Table 1.2). Especially the submerged plant *Egeria densa* qualifies as a hyperaccumulator, with reported tissue Ag concentrations well beyond 1000 mg/kg dw (Colman et al., 2018; Stegemeier, Avellan, et al., 2017).

Accumulation to concentrations comparable to the present experiment was reported by W. Wang et al. (2023) in the submerged plant *Ottelia alismoides*: exposure to 10 µg/L PVP-coated Ag-NP for just 48 h resulted in tissue concentrations of approximately 20 mg/kg dw, however the BCFs (calculated in comparison to the water concentration) were below 200 for all Ag-NP concentrations. In the present study, the mean BCFs (in relation to the peak water concentrations of Ag) were significantly higher at 650 and 716 for both types of Ag-NP. These higher BCFs might be attributable to the longer exposure duration (35 d compared to 48 h) and repeated addition of Ag-NP, resulting in a higher exposure. This was also shown in *E. densa*, exposed to weekly additions of Ag-NP: tissue Ag concentrations slowly increased over time, resulting in approximately 4-fold higher Ag content 54 d after the initial addition, compared to those after just 36 h (Yuan et al., 2018). Additionally, W. Wang et al. (2023) exposed *O. alismoides* to 50 µg/L $AgNO_3$, which resulted in a BCF of 329, significantly higher than all Ag-NP BCFs, similarly reflected in the present study, with a mean $AgNO_3$-BCF of 2890.

As Ag-NP undergo a variety of physical and chemical transformations in the water column, no static exposure can be assumed, thus hampering the interpretation of BCFs. The additional variability due the differing sedimentation rates of the Ag-NPs and $AgNO_3$ adds further complexity. However, from the present results, a general trend towards lower accumulation of Ag-NPs compared to ionic Ag was observed even though statistical significance was not reached in any case.

The interpretation of the BCF calculated in comparison to the sediments is problematic, as the main route of exposure was the aquatic phase, with sedimented Ag at most presenting a secondary route of exposure via the rhizomes of the plants growing inside the sediment. This however assumes at least a certain amount of vertical mobility of the Ag in the sediment, which was not assessed in the present study but seems unlikely to be of much significance given the rather short timescale of the experiments and results of previous studies, showing no enrichment of Ag-NP below the top 0.5 cm of sediment after 90 d of exposure (Jiang et al., 2017).

4.2.3 Localization of Accumulated Silver

As the bulk analysis of the plant material confirmed the accumulation of Ag in all exposed plants, the localization was investigated by electron microscopy. Possible scenarios included the simple deposition of Ag onto the plants during sedimentation, the adsorption onto the plant tissue from the surrounding water or the uptake of ionic Ag as well as particles of sufficiently small size into the plants (Thwala et al., 2016).

Ionic species are hypothesized to be more bioavailable to aquatic plants than particulates, as the cell wall pore size likely limits the uptake of NPs (Thwala et al., 2016). Pore sizes have been determined in some species of terrestrial plants, with reported diameters below 6 nm (Carpita et al., 1979; Fleischer et al., 1999). However data on pore sizes is scarce and might differ considerably in aquatic species, for which no published data was identified. Uptake might also occur through open stomata. However in submerged plants, stomata are often functionless or completely absent (Arber, 2010a). No evidence supporting the presence or absence of stomata on the leaves of *M. spicatum* was identified in the literature. However, a microscopic investigation of young leaves did not result in the identification of stomata. Additionally, the closely related *M. alternifolium* does not produce stomata on its leaves when grown submerged (Arber, 2010a), giving further credibility to the absence of stomata on *M. spicatum*.

Size dependent intracellular uptake of Au-NP has previously been shown in the related species *M. simulans* by Glenn et al. (2012): 4 nm Au-NP were detected inside the rhizomes, whereas particles with a mean diameter of 18 nm were only found adsorbed onto the surface. Au-NP are less prone to dissolution than Ag-NP (Hedberg et al., 2019) and thus internalization pathways are likely confined to processes relevant for particulate matter, such as endocytosis. Ag-NP dissolve more readily, depending on the environmental conditions (see section 1.2.3), and released Ag^+ might then be absorbed via hijacking of copper ion transporters (Andrés-Colás et al., 2010) and subsequently precipitated inside the cell. This has been suggested by Roubeau Dumont et al. (2022), who reported the internalization of Cu from 65 nm CuO-NP and ionic Cu^{2+} in *M. spicatum* after 10 days at 70 mg/L CuO-NP. While on the epidermis, CuO-NP accumulated to much higher levels than Cu^{2+}, the internalized concentrations were not significantly different for both forms of Cu, giving plausibility to uptake being mainly mediated via Cu ions. López-Herrera et al. (2021) also suggested this route for Ag-NP, showing intracellular Ag in the roots of the floating aquatic fern *Azolla filiculoides* after exposure to 100 mg/L 26.7 nm Ag-NP for 8 days. Although the authors noted severe deterioration of the internal structure of the root at this concentration, they hypothesized that the detected particles were formed by the precipitation of Ag^+ released from the NPs. This hypothesis was based on the slightly larger diameter of the intracellular Ag-NP (approx. 29 vs. 26.7 nm), although conceivably, the damage to the roots alone might have already allowed

the penetration of Ag-NPs.

The investigation of samples from the present study by SEM-EDX however only allowed the detection of Ag on the surface of the leaves exposed to ionic Ag, whereas none of the used Ag-NPs were detectable. SEM-EDX was previously successfully employed by Thwala et al. (2021) to detect Ag on the roots of the floating aquatic plant *Salvinia minima* exposed to 600 µg/L Ag-NP for 48 h. No further investigation of internalization by TEM was performed, as they argued that the probability of detecting internalized particles would have been very low, in light of only low amounts of Ag detectable on the plants' surface. In comparison to the present study, *S. minima* accumulated ca. 100 mg/kg dw Ag on average, comparable to the 95.0 mg/kg dw measured in the only specimen of *M. spicatum* that allowed Ag-detection by SEM-EDX. It is thus not surprising that no Ag was detectable by TEM-EELS inside the tissues due to the improbability of detecting a low number of isolated particles distributed over a very large sample area. Additionally, the sample preparation necessary for TEM involves a multitude of steps where insufficiently immobile particles might have been leached from the specimen, creating a high potential for false negative findings.

The detected superficial deposits were co-localized with elevated levels of sulfur, possibly presenting insoluble precipitates of Ag_2S or Ag associated with sulfur-rich organic material (Liau et al., 1997). A similar Ag-S association has been found for Ag-NPs internalized in the chloroplasts of *Ottelia alismoides* at exposures of 0.1 mg/L (W. Wang et al., 2023). Due to the low concentrations and lack of suitable sample material, the speciation of these precipitates was not investigated further.

Additionally, only the leaves were subjected to the analysis, with no analysis of the stems carried out. It seems unlikely that Ag was only taken up by the stems, but due to the lack of analyses, this possibility cannot be completely ruled out.

5 Conclusions

The present mesocosm experiment showed that the aquatic macrophyte *Myriophyllum spicatum* accumulates silver in both ionic as well as nanoparticulate form. Neither the particle size distribution nor the applied form of the stabilizing agent PVP had an effect on the concentrations of silver recovered in the plants. Ionic silver accumulated to higher concentrations, but due to the low number of replicates and an outlying value, statistically significant differences were not detected. Investigation of the localization of the accumulated silver by scanning and transmission electron microscopy did not result in the detection of nanoparticles on either the surface or within the leaves. Silver was only detected in conjunction with elevated levels of sulfur on the surface of the leaves treated with ionic silver. Further experiments at higher nominal exposures will be needed to elucidate the mechanism of accumulation and localization of silver in *M. spicatum*.

At 30 µg/L nominal silver concentration, only ionic silver appeared to have any visibly toxic effects on the plants. A statistically insignificant reduction in growth was observed for both ionic silver and the PVP-coated Nanospheres, while the exposure to silver Nanopowder led to minimally higher growth than the reference plants.

The use of PVP as a dispersant resulted in larger, more irregularly shaped particles and a wider size distribution due to pronounced aggregation. This led to a quicker decline of the water concentrations, resulting in higher silver concentrations in the sediment after 35 days of exposure. While up to 50 % of the added silver was not recovered, the sediments were found to be the main sink of both nanoparticulate and ionic silver. This highlights the need for more research on the chronic effects of silver nanoparticles on benthic species and microbial communities present in natural sediments.

In conclusion, the feasibility of studying the chronic environmental behavior of silver nanoparticles at environmentally relevant concentrations was demonstrated in small freshwater mesocosms. The aquatic plant *M. spicatum* accumulated silver irrespective of the applied form and did only show signs of toxicity when exposed to ionic silver. At the chosen exposure, neither superficial nor intracellular localization of the accumulated silver was feasible and higher concentrations might be necessary to elucidate potential uptake and its mechanisms.

References

Aiken, S. G., Newroth, P. R., & Wile, I. (1979). The biology of Canadian weeds.: 34. *Myriophyllum spicatum* l. *Canadian Journal of Plant Science*, *59*(1), 201–215.

Akaighe, N., Maccuspie, R. I., Navarro, D. A., Aga, D. S., Banerjee, S., Sohn, M., & Sharma, V. K. (2011). Humic acid-induced silver nanoparticle formation under environmentally relevant conditions. *Environmental Science & Technology*, *45*(9), 3895–3901.

Alexander, J. W. (2009). History of the medical use of silver. *Surgical Infections*, *10*(3), 289–292.

Alidaee, M. R., Taheri, A., Mansoori, P., & Ghodsi, S. Z. (2005). Silver nitrate cautery in aphthous stomatitis: A randomized controlled trial. *British Journal of Dermatology*, *153*(3), 521–525.

Andrés-Colás, N., Perea-García, A., Puig, S., & Peñarrubia, L. (2010). Deregulated copper transport affects *Arabidopsis* development especially in the absence of environmental cycles. *Plant Physiology*, *153*(1), 170–184.

Arber, A. (2010a). The anatomy of submerged leaves. In *Water plants: A study of aquatic angiosperms* (pp. 163–171). Cambridge University Press.

Arber, A. (2010b). The roots of water plants. In *Water plants: A study of aquatic angiosperms* (pp. 204–209). Cambridge University Press.

Astruc, D., Lu, F., & Aranzaes, J. R. (2005). Nanoparticles as recyclable catalysts: The frontier between homogeneous and heterogeneous catalysis. *Angewandte Chemie - International Edition*, *44*(48), 7852–7872.

Azimzada, A., Jreije, I., Hadioui, M., Shaw, P., Farner, J. M., & Wilkinson, K. J. (2021). Quantification and characterization of Ti-, Ce-, and Ag-nanoparticles in global surface waters and precipitation. *Environmental Science & Technology*, *55*(14), 9836–9844.

Baalousha, M., & Lead, J. R. (2007). Size fractionation and characterization of natural aquatic colloids and nanoparticles. *Science of The Total Environment*, *386*(1), 93–102.

Bard, C. C., Murphy, J. J., Stone, D. L., & Terhaar, C. J. (1976). Silver in photoprocessing effluents. *Journal (Water Pollution Control Federation)*, *48*(2), 389–394.

Bertinato, J., Cheung, L., Hoque, R., & Plouffe, L. J. (2010). Ctr1 transports silver into mammalian cells. *Journal of Trace Elements in Medicine and Biology*, *24*(3), 178–184.

Blaser, S. A., Scheringer, M., MacLeod, M., & Hungerbühler, K. (2008). Estimation of cumulative aquatic exposure and risk due to silver: Contribution of nano-functionalized plastics and textiles. *Science of The Total Environment*, *390*(2), 396–409.

Bour, A., Mouchet, F., Silvestre, J., Gauthier, L., & Pinelli, E. (2015). Environmentally relevant approaches to assess nanoparticles ecotoxicity: A review. *Journal of Hazardous Materials*, *283*,

764–777.

Bundschuh, M., Filser, J., Lüderwald, S., McKee, M. S., Metreveli, G., Schaumann, G. E., Schulz, R., & Wagner, S. (2018). Nanoparticles in the environment: Where do we come from, where do we go to? *Environmental Sciences Europe*, *30*(1).

Burda, C., Chen, X., Narayanan, R., & El-Sayed, M. A. (2005). Chemistry and properties of nanocrystals of different shapes. *Chemical Reviews*, *105*(4), 1025–1102.

Carboni, A., Slomberg, D. L., Nassar, M., Santaella, C., Masion, A., Rose, J., & Auffan, M. (2021). Aquatic mesocosm strategies for the environmental fate and risk assessment of engineered nanomaterials. *Environmental Science & Technology*, *55*(24), 16270–16282.

Cardwell, A. J., Hawker, D. W., & Greenway, M. (2002). Metal accumulation in aquatic macrophytes from southeast Queensland, Australia. *Chemosphere*, *48*(7), 653–663.

Carignan, R., & Kalff, J. (1980). Phosphorus sources for aquatic weeds: Water or sediments? *Science*, *207*(4434), 987–989.

Carpita, N., Sabularse, D., Montezinos, D., & Delmer, D. P. (1979). Determination of the pore size of cell walls of living plant cells. *Science*, *205*(4411), 1144–1147.

CCME. (2015). *Canadian water quality guidelines for the protection of aquatic life: silver*. Canadian Council of Ministers of the Environment.

Chen, Z., Campbell, P. G. C., & Fortin, C. (2012). Silver binding by humic acid as determined by equilibrium ion-exchange and dialysis. *The Journal of Physical Chemistry A*, *116*(25), 6532–6539.

Chhipa, H. (2017). Nanofertilizers and nanopesticides for agriculture. *Environmental Chemistry Letters*, *15*(1), 15–22.

Colman, B. P., Baker, L. F., King, R. S., Matson, C. W., Unrine, J. M., Marinakos, S. M., Gorka, D. E., & Bernhardt, E. S. (2018). Dosing, not the dose: Comparing chronic and pulsed silver nanoparticle exposures. *Environmental Science & Technology*, *52*(17), 10048–10056.

Colman, B. P., Espinasse, B., Richardson, C. J., Matson, C. W., Lowry, G. V., Hunt, D. E., Wiesner, M. R., & Bernhardt, E. S. (2014). Emerging contaminant or an old toxin in disguise? Silver nanoparticle impacts on ecosystems. *Environmental Science & Technology*, *48*(9), 5229–5236.

Cook, C. D. K. (1985). Worldwide distribution and taxonomy of *Myriophyllum* species. *Proceedings of the First International Symposium on Watermilfoil (*Myriophyllum spicatum*) and Related* Haloragaceae *Species*, 1–7.

Couch, R., & Nelson, E. (1985). *Myriophyllum spicatum* in north america. *Proceedings of the First International Symposium on Watermilfoil (*Myriophyllum spicatum*) and Related* Haloragaceae *Species*, 8–18.

Craddock, P. (2014). Production of silver across the ancient world. *ISIJ International*, *54*(5), 1085–1092.

Dang, F., Huang, Y., Wang, Y., Zhou, D., & Xing, B. (2021). Transfer and toxicity of silver nanoparticles in the food chain. *Environmental Science: Nano*, *8*(6), 1519–1535.

Danielsson, L. G. (1982). On the use of filters for distinguishing between dissolved and particulate fractions in natural waters. *Water Research*, *16*(2), 179–182.

Deb, N. (2016). *Plant nutrient coated nanoparticles and methods for their preparation and use* (US Patent 9,359,265 B2). United States Patent and Trademark Office.

Ding, R., Li, L., Yang, P., Luo, L., Li, L., & Wang, Q. (2019). Assessing the environmental occurrence and risk of nano-silver in Hunan, China using probabilistic material flow modeling. *Science of The Total Environment*, *658*, 1249–1255.

Ding, Y., Bai, X., Ye, Z., Gong, D., Cao, J., & Hua, Z. (2019). Humic acid regulation of the environmental behavior and phytotoxicity of silver nanoparticles to *Lemna minor*. *Environmental Science: Nano*, *6*(12), 3712–3722.

Docter, D., Westmeier, D., Markiewicz, M., Stolte, S., Knauer, S. K., & Stauber, R. H. (2015). The nanoparticle biomolecule corona: Lessons learned – challenge accepted? *Chemical Society Reviews*, *44*(17), 6094–6121.

Dong, B., Liu, G., Zhou, J., Wang, J., & Jin, R. (2020). Transformation of silver ions to silver nanoparticles mediated by humic acid under dark conditions at ambient temperature. *Journal of Hazardous Materials*, *383*, 121190.

Dumville, J. C., Gray, T. A., Walter, C. J., Sharp, C. A., Page, T., Macefield, R., Blencowe, N., Milne, T. K., Reeves, B. C., & Blazeby, J. (2016). Dressings for the prevention of surgical site infection. *Cochrane Database of Systematic Reviews*, *12*(12), Cd003091.

Dunn, O. J. (1964). Multiple comparisons using rank sums. *Technometrics*, *6*(3), 241–252.

EC. (2011). Commission recommendation of 18 October 2011 on the definition of nanomaterial. *Official Journal of the European Union*, *L 275*, 38–40.

Fedorenko, G. M., Fedorenko, A. G., Minkina, T. M., Mandzhieva, S. S., Rajput, V. D., Usatov, A. V., & Sushkova, S. N. (2018). Method for hydrophytic plant sample preparation for light and electron microscopy (studies on *Phragmites australis* Cav.). *MethodsX*, *5*, 1213–1220.

Fischer, M. A., & Gottschlich, G. (2005). *Exkursionsflora für Österreich, Liechtenstein und Südtirol: Bestimmungsbuch für alle in der Republik Österreich, in der Autonomen Provinz Bozen, Südtirol (Italien) und im Fürstentum Liechtenstein wildwachsenden sowie die wichtigsten kultivierten Gefäßpflanzen (Farnpflanzen und Samenpflanzen) mit Angaben über ihre Ökologie und Verbreitung* (2., verb. u. erw. Aufl.). Land Oberösterreich, OÖ Landesmuseen.

Fleischer, A., O'Neill, M. A., & Ehwald, R. (1999). The pore size of non-graminaceous plant cell walls is rapidly decreased by borate ester cross-linking of the pectic polysaccharide rhamnogalacturonan II. *Plant Physiology*, *121*(3), 829–838.

Fleming, A. (1929). On the antibacterial action of cultures of a *Penicillium*, with special reference

to their use in the isolation of *B. influenzæ*. *British Journal of Experimental Pathology*, *10*(3), 226–236.

Gao, J., Powers, K., Wang, Y., Zhou, H., Roberts, S. M., Moudgil, B. M., Koopman, B., & Barber, D. S. (2012). Influence of Suwannee River humic acid on particle properties and toxicity of silver nanoparticles. *Chemosphere*, *89*(1), 96–101.

Gatan Ametek. (2022). *EELS atlas: Ag thin film (0-910 eV)*. https://eels.info/atlas/silver

Geranio, L., Heuberger, M., & Nowack, B. (2009). The behavior of silver nanotextiles during washing. *Environmental Science & Technology*, *43*(21), 8113–8118.

Giese, B., Klaessig, F., Park, B., Kaegi, R., Steinfeldt, M., Wigger, H., Arnim von, G., & Gottschalk, F. (2018). Risks, release and concentrations of engineered nanomaterial in the environment. *Scientific Reports*, *8*, 1–18.

Glenn, J. B., White, S. A., & Klaine, S. J. (2012). Interactions of gold nanoparticles with freshwater aquatic macrophytes are size and species dependent. *Environmental Toxicology and Chemistry*, *31*(1), 194–201.

Gottschalk, F., Sonderer, T., Scholz, R. W., & Nowack, B. (2009). Modeled environmental concentrations of engineered nanomaterials (TiO_2, ZnO, Ag, CNT, fullerenes) for different regions. *Environmental Science and Technology*, *43*(24), 9216–9222.

Grudnik, Z. M., & Germ, M. (2010). *Myriophyllum spicatum* and *Najas marina* as bioindicators of trace element contamination in lakes. *Journal of Freshwater Ecology*, *25*(3), 421–426.

Hamilton, J. F. (1988). The silver halide photographic process. *Advances in Physics*, *37*(4), 359–441.

Hanks, N. A., Caruso, J. A., & Zhang, P. (2015). Assessing *Pistia stratiotes* for phytoremediation of silver nanoparticles and Ag(I) contaminated waters. *Journal of Environmental Management*, *164*, 41–45.

Hauser, M., & Nowack, B. (2021). Probabilistic modelling of nanobiomaterial release from medical applications into the environment. *Environment International*, *146*, 106184.

Hedberg, J., Blomberg, E., & Odnevall Wallinder, I. (2019). In the search for nanospecific effects of dissolution of metallic nanoparticles at freshwater-like conditions: A critical review. *Environmental Science & Technology*, *53*(8), 4030–4044.

Heinisch, M., & Buder, E. (2019). *Aqueous fertilizer containing metal nanoparticles* (European Patent 3 205 637 B1). European Patent Office.

Hellmeier, P. (2022). *Wichtige Wasserinhaltsstoffe*. Stadt Wien, Magistratsabteilung 31 - Wiener Wasser.

Hendriks, C., Obernosterer, R., Müller, D., Kytzia, S., Baccini, P., & Brunner, P. H. (2000). Material flow analysis: A tool to support environmental policy decision making. Case-studies on the city of Vienna and the Swiss lowlands. *Local Environment*, *5*(3), 311–328.

Hicks, A. L., & Temizel-Sekeryan, S. (2019). Understanding the potential environmental benefits of nanosilver enabled consumer products. *NanoImpact*, *16*, 100183.

Holden, P. A., Gardea-Torresdey, J. L., Klaessig, F., Turco, R. F., Mortimer, M., Hund-Rinke, K., Cohen Hubal, E. A., Avery, D., Barceló, D., Behra, R., Cohen, Y., Deydier-Stephan, L., Ferguson, P. L., Fernandes, T. F., Herr Harthorn, B., Henderson, W. M., Hoke, R. A., Hristozov, D., Johnston, J. M., ... Nel, A. E. (2016). Considerations of environmentally relevant test conditions for improved evaluation of ecological hazards of engineered nanomaterials. *Environmental Science & Technology*, *50*(12), 6124–6145.

Hong, H., Adam, V., & Nowack, B. (2021). Form-specific and probabilistic environmental risk assessment of 3 engineered nanomaterials (nano-Ag, nano-TiO_2, and nano-ZnO) in European freshwaters. *Environmental Toxicology and Chemistry*, *40*(9), 2629–2639.

Huynh, K. A., & Chen, K. L. (2011). Aggregation kinetics of citrate and polyvinylpyrrolidone coated silver nanoparticles in monovalent and divalent electrolyte solutions. *Environmental Science & Technology*, *45*(13), 5564–5571.

Jiang, H. S., Li, M., Chang, F. Y., Li, W., & Yin, L. Y. (2012). Physiological analysis of silver nanoparticles and $AgNO_3$ toxicity to *Spirodela polyrhiza*. *Environmental Toxicology and Chemistry*, *31*(8), 1880–1886.

Jiang, H. S., Yin, L., Ren, N. N., Xian, L., Zhao, S., Li, W., & Gontero, B. (2017). The effect of chronic silver nanoparticles on aquatic system in microcosms. *Environmental Pollution*, *223*, 395–402.

Kaegi, R., Sinnet, B., Zuleeg, S., Hagendorfer, H., Mueller, E., Vonbank, R., Boller, M., & Burkhardt, M. (2010). Release of silver nanoparticles from outdoor facades. *Environmental Pollution*, *158*(9), 2900–2905.

Kaegi, R., Voegelin, A., Sinnet, B., Zuleeg, S., Hagendorfer, H., Burkhardt, M., & Siegrist, H. (2011). Behavior of metallic silver nanoparticles in a pilot wastewater treatment plant. *Environmental Science & Technology*, *45*(9), 3902–3908.

Kah, M., Tufenkji, N., & White, J. C. (2019). Nano-enabled strategies to enhance crop nutrition and protection. *Nature Nanotechnology*, *14*(6), 532–540.

Kalantari, K., Mostafavi, E., Afifi, A. M., Izadiyan, Z., Jahangirian, H., Rafiee-Moghaddam, R., & Webster, T. J. (2020). Wound dressings functionalized with silver nanoparticles: Promises and pitfalls. *Nanoscale*, *12*(4), 2268–2291.

Kalantzi, I., Mylona, K., Toncelli, C., Bucheli, T. D., Knauer, K., Pergantis, S. A., Pitta, P., Tsiola, A., & Tsapakis, M. (2019). Ecotoxicity of silver nanoparticles on plankton organisms: A review. *Journal of Nanoparticle Research*, *21*(3).

Kausch, W. (1912). Ueber Kollargol bei Sepsis und bei Karzinom. *Deutsche Medizinische Wochenschrift*, *35*, 1635–1637.

Kittler, S., Greulich, C., Diendorf, J., Köller, M., & Epple, M. (2010). Toxicity of silver nanoparticles increases during storage because of slow dissolution under release of silver ions. *Chemistry of Materials*, *22*(16), 4548–4554.

Lalau, C. M., Simioni, C., Vicentini, D. S., Ouriques, L. C., Mohedano, R. A., Puerari, R. C., & Matias, W. G. (2020). Toxicological effects of AgNPs on duckweed (*Landoltia punctata*). *Science of The Total Environment*, *710*, 136318.

Lee, D. Y., Fortin, C., & Campbell, P. G. C. (2004). Influence of chloride on silver uptake by two green algae, *Pseudokirchneriella subcapitata* and *Chlorella pyrenoidosa*. *Environmental Toxicology and Chemistry*, *23*(4), 1012.

Levard, C., Hotze, E. M., Colman, B. P., Dale, A. L., Truong, L., Yang, X. Y., Bone, A. J., Brown, Jr., G. E., Tanguay, R. L., Di Giulio, R. T., Bernhardt, E. S., Meyer, J. N., Wiesner, M. R., & Lowry, G. V. (2013). Sulfidation of silver nanoparticles: Natural antidote to their toxicity. *Environmental Science & Technology*, *47*(23), 13440–13448.

Levard, C., Mitra, S., Yang, T., Jew, A. D., Badireddy, A. R., Lowry, G. V., & Brown, G. E. (2013). Effect of chloride on the dissolution rate of silver nanoparticles and toxicity to *E. coli*. *Environmental Science & Technology*, *47*(11), 5738–5745.

Levard, C., Reinsch, B. C., Michel, F. M., Oumahi, C., Lowry, G. V., & Brown, G. E. (2011). Sulfidation processes of PVP-coated silver nanoparticles in aqueous solution: Impact on dissolution rate. *Environmental Science & Technology*, *45*(12), 5260–5266.

Li, Q., Mahendra, S., Lyon, D. Y., Brunet, L., Liga, M. V., Li, D., & Alvarez, P. J. J. (2008). Antimicrobial nanomaterials for water disinfection and microbial control: Potential applications and implications. *Water Research*, *42*(18), 4591–4602.

Li, S., Chen, S., Zhang, Z., Huang, Y., Li, G. B., Li, Y., Deng, X., & Li, J. (2022). Short-term exposure to silver nano-particles alters the physiology and induces stress-related gene expression in *Nelumbo nucifera*. *Plant Physiology and Biochemistry*, *177*, 38–45.

Li, X., Lenhart, J. J., & Walker, H. W. (2010). Dissolution-accompanied aggregation kinetics of silver nanoparticles. *Langmuir*, *26*(22), 16690–16698.

Liau, S. Y., Read, D. C., Pugh, W. J., Furr, J. R., & Russell, A. D. (1997). Interaction of silver nitrate with readily identifiable groups: Relationship to the antibacterial action of silver ions. *Letters in Applied Microbiology*, *25*(4), 279–283.

Lim, P. O., Kim, H. J., & Gil Nam, H. (2007). Leaf senescence. *Annual Review of Plant Biology*, *58*, 115–136.

Liu, J., & Hurt, R. H. (2010). Ion release kinetics and particle persistence in aqueous nano-silver colloids. *Environmental Science & Technology*, *44*(6), 2169–2175.

Liu, J., Hwang, Y. S., & Lenhart, J. J. (2015). Heteroaggregation of bare silver nanoparticles with clay minerals. *Environmental Science: Nano*, *2*(5), 528–540.

Liu, J., Pennell, K. G., & Hurt, R. H. (2011). Kinetics and mechanisms of nanosilver oxysulfidation. *Environmental Science & Technology*, *45*(17), 7345–7353.

Lodge, D. M. (1991). Herbivory on freshwater macrophytes. *Aquatic Botany*, *41*(1), 195–224.

López-Herrera, A., Avalos-Borja, M., García-Nava, J. R., Trejo-Téllez, L. I., Alarcón, A., Patrón-Soberano, A., Conde-Martinez, V., & Zavaleta-Mancera, H. A. (2021). Interaction of silver nanoparticles with the aquatic fern *Azolla filiculoides*: Root structure, particle distribution, and silver accumulation. *Journal of Nanoparticle Research*, *23*(1), 13.

Lowry, G. V., Espinasse, B. P., Badireddy, A. R., Richardson, C. J., Reinsch, B. C., Bryant, L. D., Bone, A. J., Deonarine, A., Chae, S., Therezien, M., Colman, B. P., Hsu-Kim, H., Bernhardt, E. S., Matson, C. W., & Wiesner, M. R. (2012). Long-term transformation and fate of manufactured Ag nanoparticles in a simulated large scale freshwater emergent wetland. *Environmental Science & Technology*, *46*(13), 7027–7036.

Maksymiec, W. (2007). Signaling responses in plants to heavy metal stress. *Acta Physiologiae Plantarum*, *29*(3), 177–187.

Massarsky, A., Trudeau, V. L., & Moon, T. W. (2014). Predicting the environmental impact of nanosilver. *Environmental Toxicology and Pharmacology*, *38*(3), 861–873.

Metreveli, G., Kurtz, S., Rosenfeldt, R. R., Seitz, F., Kumahor, S. K., Grün, A., Klitzke, S., Vogel, H., Bundschuh, M., Baumann, T., Schulz, R., Manz, W., Lang, F., & Schaumann, G. E. (2021). Distribution of engineered Ag nanoparticles in the aquatic-terrestrial transition zone: A long-term indoor floodplain mesocosm study. *Environmental Science: Nano*, *8*(6), 1771–1785.

Milne, C. J., Lapworth, D. J., Gooddy, D. C., Elgy, C. N., & Valsami-Jones, É. (2017). Role of humic acid in the stability of Ag nanoparticles in suboxic conditions. *Environmental Science & Technology*, *51*(11), 6063–6070.

Minogiannis, P., Valenti, M., Kati, V., Kalantzi, O. I., & Biskos, G. (2019). Toxicity of pure silver nanoparticles produced by spark ablation on the aquatic plant *Lemna minor*. *Journal of Aerosol Science*, *128*, 17–21.

Mitrano, D. M., Lesher, E. K., Bednar, A., Monserud, J., Higgins, C. P., & Ranville, J. F. (2012). Detecting nanoparticulate silver using single-particle inductively coupled plasma-mass spectrometry. *Environmental Toxicology and Chemistry*, *31*(1), 115–121.

Mitrano, D. M., Rimmele, E., Wichser, A., Erni, R., Height, M., & Nowack, B. (2014). Presence of nanoparticles in wash water from conventional silver and nano-silver textiles. *ACS Nano*, *8*(7), 7208–7219.

Mogensen, K. B., & Kneipp, K. (2014). Size-dependent shifts of plasmon resonance in silver nanoparticle films using controlled dissolution: Monitoring the onset of surface screening effects. *The Journal of Physical Chemistry C*, *118*(48), 28075–28083.

Molleman, B., & Hiemstra, T. (2017). Time, pH, and size dependency of silver nanoparticle

dissolution: The road to equilibrium. *Environmental Science: Nano*, *4*(6), 1314–1327.

Moore, M. N. (2006). Do nanoparticles present ecotoxicological risks for the health of the aquatic environment? *Environment International*, *32*(8), 967–976.

Mulenos, M. R., Liu, J., Lujan, H., Guo, B., Lichtfouse, E., Sharma, V. K., & Sayes, C. M. (2020). Copper, silver, and titania nanoparticles do not release ions under anoxic conditions and release only minute ion levels under oxic conditions in water: Evidence for the low toxicity of nanoparticles. *Environmental Chemistry Letters*, *18*(4), 1319–1328.

Nabi, M. M., Wang, J., Meyer, M., Croteau, M.-N., Ismail, N., & Baalousha, M. (2021). Concentrations and size distribution of TiO_2 and Ag engineered particles in five wastewater treatment plants in the united states. *Science of The Total Environment*, *753*, 142017.

Nowack, B., Baalousha, M., Bornhöft, N., Chaudhry, Q., Cornelis, G., Cotterill, J., Gondikas, A., Hassellöv, M., Lead, J., Mitrano, D. M., Von Der Kammer, F., & Wontner-Smith, T. (2015). Progress towards the validation of modeled environmental concentrations of engineered nanomaterials by analytical measurements. *Environmental Science: Nano*, *2*(5), 421–428.

OECD. (2014a). *Test no. 238: Sediment-free* Myriophyllum spicatum *toxicity test*.

OECD. (2014b). *Test no. 239: Water-sediment* Myriophyllum spicatum *toxicity test*.

Oukarroum, A., Barhoumi, L., Pirastru, L., & Dewez, D. (2013). Silver nanoparticle toxicity effect on growth and cellular viability of the aquatic plant *Lemna gibba*. *Environmental Toxicology and Chemistry*, *32*(4), 902–907.

Palácio, S. M., Nogueira, D. A., Espinoza-Quiñones, F. R., De Campos, É. A., & Veit, M. T. (2020). Silver nanoparticles bioaccumulation by aquatic macrophyte *Salvinia auriculata*. *Water, Air, & Soil Pollution*, *231*(2).

Pereira, S. P. P., Jesus, F., Aguiar, S., Oliveira, R. de, Fernandes, M., Ranville, J., & Nogueira, A. J. A. (2018). Phytotoxicity of silver nanoparticles to *Lemna minor*: Surface coating and exposure period-related effects. *Science of The Total Environment*, *618*, 1389–1399.

Peretyazhko, T. S., Zhang, Q., & Colvin, V. L. (2014). Size-controlled dissolution of silver nanoparticles at neutral and acidic pH conditions: Kinetics and size changes. *Environmental Science & Technology*, *48*(20), 11954–11961.

Peters, R. J. B., Bemmel, G. van, Milani, N. B. L., Hertog, G. C. T. den, Undas, A. K., Lee, M. van der, & Bouwmeester, H. (2018). Detection of nanoparticles in Dutch surface waters. *Science of The Total Environment*, *621*, 210–218.

Plessl, C., Jandrisits, P., Krachler, R., Keppler, B. K., & Jirsa, F. (2017). Heavy metals in the mallard *Anas platyrhynchos* from eastern Austria. *Science of The Total Environment*, *580*, 670–676.

Prasad, A., Lead, J. R., & Baalousha, M. (2015). An electron microscopy based method for the detection and quantification of nanomaterial number concentration in environmentally relevant

media. *Science of The Total Environment*, *537*, 479–486.

Pulit-Prociak, J., & Banach, M. (2016). Silver nanoparticles – a material of the future…? *Open Chemistry*, *14*(1), 76–91.

Purcell, T. W., & Peters, J. J. (1998). Sources of silver in the environment. *Environmental Toxicology and Chemistry*, *17*(4), 539–546.

R Core Team. (2022). *R: A language and environment for statistical computing*. R Foundation for Statistical Computing. https://www.R-project.org/

Rahman, M. A., & Hasegawa, H. (2011). Aquatic arsenic: Phytoremediation using floating macrophytes. *Chemosphere*, *83*(5), 633–646.

Rascio, N., & Navari-Izzo, F. (2011). Heavy metal hyperaccumulating plants: How and why do they do it? And what makes them so interesting? *Plant Science*, *180*(2), 169–181.

Ratte, H. T. (1999). Bioaccumulation and toxicity of silver compounds: A review. *Environmental Toxicology and Chemistry*, *18*(1), 89–108.

Robinson, B., Kim, N., Marchetti, M., Moni, C., Schroeter, L., Dijssel, C. van den, Milne, G., & Clothier, B. (2006). Arsenic hyperaccumulation by aquatic macrophytes in the Taupo Volcanic Zone, New Zealand. *Environmental and Experimental Botany*, *58*(1), 206–215.

Römer, I., Wang, Z. W., Merrifield, R. C., Palmer, R. E., & Lead, J. R. (2016). High resolution STEM-EELS study of silver nanoparticles exposed to light and humic substances. *Environmental Science & Technology*, *50*(5), 2183–2190.

Rotter, D., & Schratt-Ehrendorfer, L. (1999). *Geobotanik und Ökologie der Donaualtwässer bei Wien: (Wasser- und Verlandungsvegetation)*. Biologiezentrum d. OÖ. Landesmuseums.

Roubeau Dumont, E., Elger, A., Azéma, C., Castillo Michel, H., Surble, S., & Larue, C. (2022). Cutting-edge spectroscopy techniques highlight toxicity mechanisms of copper oxide nanoparticles in the aquatic plant *Myriophyllum spicatum*. *Science of The Total Environment*, *803*, 150001.

Schindelin, J., Arganda-Carreras, I., Frise, E., Kaynig, V., Longair, M., Pietzsch, T., Preibisch, S., Rueden, C., Saalfeld, S., Schmid, B., Tinevez, J., White, D. J., Hartenstein, V., Eliceiri, K., Tomancak, P., & Cardona, A. (2012). Fiji: An open-source platform for biological-image analysis. *Nature Methods*, *9*(7), 676–682.

Schorn, H. (1919). Zur Anwendung des Kollargol (Heyden) in der Augenheilkunde. *Deutsche Medizinische Wochenschrift*, *30*, 826–827.

Scow, K., Goyer, M., Nelken, L., Payne, E., K., S., Walker, P., Wood, M., Cruse, P., & Moss, K. (1981). *An exposure and risk assessment for silver* (Technical Report (EPA-440/4-81-017)). Office of Water Regulations; Standards, U.S. Environmental Protection Agency.

Smith, E. J., Davison, W., & Hamilton-Taylor, J. (2002). Methods for preparing synthetic freshwaters. *Water Research*, *36*(5), 1286–1296.

Souza, L. R. R., Corrêa, T. Z., Bruni, A. T., & Da Veiga, M. A. M. S. (2021). The effects of solubility of silver nanoparticles, accumulation, and toxicity to the aquatic plant *Lemna minor*. *Environmental Science and Pollution Research*, *28*(13), 16720–16733.

Stegemeier, J. P., Avellan, A., & Lowry, G. V. (2017). Effect of initial speciation of copper- and silver-based nanoparticles on their long-term fate and phytoavailability in freshwater wetland mesocosms. *Environmental Science & Technology*, *51*(21), 12114–12122.

Stegemeier, J. P., Colman, B. P., Schwab, F., Wiesner, M. R., & Lowry, G. V. (2017). Uptake and distribution of silver in the aquatic plant *Landoltia punctata* (duckweed) exposed to silver and silver sulfide nanoparticles. *Environmental Science & Technology*, *51*(9), 4936–4943.

Stetefeld, J., McKenna, S. A., & Patel, T. R. (2016). Dynamic light scattering: A practical guide and applications in biomedical sciences. *Biophysical Reviews*, *8*(4), 409–427.

Strasburger, E., Noll, F., Schenck, H., Schimper, A. F. W., Sitte, P., Ziegler, H., Ehrendorfer, F., & Bresinsky, A. (1991a). Die Gewebe der Sproßpflanze - II.B.: Abschlussgewebe. In *Lehrbuch der Botanik für Hochschulen* (33rd ed., pp. 137–146). Gustav Fischer Verlag.

Strasburger, E., Noll, F., Schenck, H., Schimper, A. F. W., Sitte, P., Ziegler, H., Ehrendorfer, F., & Bresinsky, A. (1991b). Physiologie des Formwechsels - IV.D.: Altern und Tod. In *Lehrbuch der Botanik für Hochschulen* (33rd ed., pp. 429–431). Gustav Fischer Verlag.

Sun, T. Y., Bornhoft, N. A., Hungerbuhler, K., & Nowack, B. (2016). Dynamic probabilistic modeling of environmental emissions of engineered nanomaterials. *Environmental Science and Technology*, *50*(9), 4701–4711.

Temizel-Sekeryan, S., & Hicks, A. L. (2020). Global environmental impacts of silver nanoparticle production methods supported by life cycle assessment. *Resources, Conservation and Recycling*, *156*, 104676.

The Silver Institute. (2000). *World silver survey 2000*.

The Silver Institute. (2020). *World silver survey 2020*.

Thwala, M., Klaine, S. J., & Musee, N. (2016). Interactions of metal-based engineered nanoparticles with aquatic higher plants: A review of the state of current knowledge. *Environmental Toxicology and Chemistry*, *35*(7), 1677–1694.

Thwala, M., Klaine, S. J., & Musee, N. (2021). Exposure media and nanoparticle size influence on the fate, bioaccumulation, and toxicity of silver nanoparticles to higher plant *Salvinia minima*. *Molecules*, *26*(8), 2305.

Topuz, E., Traber, J., Sigg, L., & Talinli, I. (2015). Agglomeration of Ag and TiO_2 nanoparticles in surface and wastewater: Role of calcium ions and of organic carbon fractions. *Environmental Pollution*, *204*, 313–323.

U.S. EPA. (1980). *Ambient water quality criteria for silver* (EPA 440/5-80-071). Office of Water Regulations; Standards, U.S. Environmental Protection Agency.

USGS. (2022). *Mineral commodity summaries 2022*. U.S. Geological Survey.

Ustaoğlu, F., Kükrer, S., Taş, B., & Topaldemir, H. (2022). Evaluation of metal accumulation in Terme river sediments using ecological indices and a bioindicator species. *Environmental Science and Pollution Research*, *29*(31), 47399–47415.

Vance, M. E., Kuiken, T., Vejerano, E. P., McGinnis, S. P., Hochella, M. F., Rejeski, D., & Hull, M. S. (2015). Nanotechnology in the real world: Redeveloping the nanomaterial consumer products inventory. *Beilstein Journal of Nanotechnology*, *6*, 1769–1780.

Voelker, D., Schlich, K., Hohndorf, L., Koch, W., Kuehnen, U., Polleichtner, C., Kussatz, C., & Hund-Rinke, K. (2015). Approach on environmental risk assessment of nanosilver released from textiles. *Environmental Research*, *140*, 661–672.

von der Heyden, B., Roychoudhury, A., & Myneni, S. (2019). Iron-rich nanoparticles in natural aquatic environments. *Minerals*, *9*(5), 287.

von der Kammer, F., Legros, S., Hofmann, T., Larsen, E. H., & Loeschner, K. (2011). Separation and characterization of nanoparticles in complex food and environmental samples by field-flow fractionation. *TrAC Trends in Analytical Chemistry*, *30*(3), 425–436.

Wang, H., Adeleye, A. S., Huang, Y., Li, F., & Keller, A. A. (2015). Heteroaggregation of nanoparticles with biocolloids and geocolloids. *Advances in Colloid and Interface Science*, *226*, 24–36.

Wang, H., Dong, Y., Zhu, M., Li, X., Keller, A. A., Wang, T., & Li, F. (2015). Heteroaggregation of engineered nanoparticles and kaolin clays in aqueous environments. *Water Research*, *80*, 130–138.

Wang, T., & Liu, W. (2022). Emerging investigator series: Metal nanoparticles in freshwater: Transformation, bioavailability and effects on invertebrates. *Environmental Science: Nano*, *9*(7), 2237–2263.

Wang, W., Yuan, L., Zhou, Ji., Zhu, X., Liao, Z., Yin, L., Li, W., & Jiang, H. S. (2023). Inorganic carbon utilization: A target of silver nanoparticle toxicity on a submerged macrophyte. *Environmental Pollution*, *318*, 120906.

Warrington, P. D. (1988). *The pH tolerance of the aquatic plants of British Columbia: Part 1. Literature survey of the pH limits of aquatic plants of the world.* British Columbia. Water Management Branch.

Welch, B. L. (1951). On the comparison of several mean values: An alternative approach. *Biometrika*, *38*(3/4), 330–336.

WHO. (2021). *Silver in drinking-water. Background document for development of WHO guidelines for drinking-water quality.* World Health Organization.

Wiberg, N. (2008a). Das Element Silber. In *Holleman-Wiberg: Lehrbuch der Anorganischen Chemie* (pp. 1452–1457). De Gruyter.

Wiberg, N. (2008b). Heterogene Gleichgewichte. In *Holleman-Wiberg: Lehrbuch der Anorganis-*

chen Chemie (pp. 212–217). De Gruyter.

Wickham, H. (2016). *ggplot2: Elegant graphics for data analysis*. Springer-Verlag New York.

Wigger, H., Hackmann, S., Zimmermann, T., Köser, J., Thöming, J., & Gleich, A. von. (2015). Influences of use activities and waste management on environmental releases of engineered nanomaterials. *Science of The Total Environment*, *535*, 160–171.

Wimmer, A., Markus, A. A., & Schuster, M. (2019). Silver nanoparticle levels in river water: Real environmental measurements and modeling approaches—a comparative study. *Environmental Science & Technology Letters*, *6*(6), 353–358.

Yeshchenko, O. A., Dmitruk, I. M., Alexeenko, A. A., Kotko, A. V., Verdal, J., & Pinchuk, A. O. (2012). Size and temperature effects on the surface plasmon resonance in silver nanoparticles. *Plasmonics*, *7*(4), 685–694.

Yuan, L., Richardson, C. J., Ho, M., Willis, C. W., Colman, B. P., & Wiesner, M. R. (2018). Stress responses of aquatic plants to silver nanoparticles. *Environmental Science & Technology*, *52*(5), 2558–2565.

Zhang, W., Xiao, B., & Fang, T. (2018). Chemical transformation of silver nanoparticles in aquatic environments: Mechanism, morphology and toxicity. *Chemosphere*, *191*, 324–334.

Zhou, D., Abdel-Fattah, A. I., & Keller, A. A. (2012). Clay particles destabilize engineered nanoparticles in aqueous environments. *Environmental Science & Technology*, *46*(14), 7520–7526.

Appendix

Table A.1: Summary of physico-chemical parameters measured during the course of the experiment.

Parameter	Group	Day 0	Day 35	Range	Change [%]
Conductivity [µS/cm]	Reference	422.6 ± 8.0	323.2 ± 28.3	296.3 - 431.7	-23.4 ± 8.0
	Nanopowder	421.3 ± 2.0	325.5 ± 7.2	317.2 - 432.9	-22.8 ± 1.4
	Nanospheres	424.8 ± 2.5	354.1 ± 5.9	350.2 - 427.6	-16.6 ± 0.9
	Ionic Silver	423.1 ± 1.0	349.3 ± 5.9	342.6 - 423.9	-17.4 ± 1.2
Temperature [°C]	Reference	22.7 ± 0.6	21.3 ± 0.1	21.3 - 24.4	-5.8 ± 2.4
	Nanopowder	22.3 ± 0.1	21.4 ± 0.1	21.3 - 23.9	-4.0 ± 0.4
	Nanospheres	23.4 ± 0.4	21.5 ± 0.1	20.4 - 24.1	-8.1 ± 1.2
	Ionic Silver	22.9 ± 0.1	21.5 ± 0.1	20.3 - 23.3	-6.1 ± 0.7
Dissolved Oxygen [mg/l]	Reference	7.8 ± 0.0	7.8 ± 0.0	7.8 - 8.4	+0.0 ± 0.0
	Nanopowder	7.7 ± 0.1	7.7 ± 0.1	7.6 - 8.3	+0.9 ± 0.8
	Nanospheres	8.1 ± 0.1	7.6 ± 0.1	7.4 - 9.3	-7.0 ± 0.7
	Ionic Silver	8.1 ± 0.0	7.6 ± 0.3	7.4 - 9.3	-5.8 ± 4.0
pH	Reference	8.64 ± 0.02	8.62 ± 0.01	8.59 - 8.73	-0.24 ± 0.23
	Nanopowder	8.64 ± 0.01	8.57 ± 0.01	8.56 - 8.69	-0.84 ± 0.13
	Nanospheres	8.70 ± 0.00	8.59 ± 0.02	8.57 - 8.76	-1.26 ± 0.26
	Ionic Silver	8.70 ± 0.01	8.57 ± 0.05	8.53 - 8.72	-1.44 ± 0.66
Chloride [mg/l]	Reference	13.05 ± 0.05	12.80 ± 0.17	12.61 - 13.24	-1.93 ± 1.55
	Nanopowder	13.08 ± 0.01	12.94 ± 0.11	13.80 - 13.21	-1.11 ± 0.84
	Nanospheres	13.44 ± 0.05	13.23 ± 0.02	13.20 - 13.71	-1.57 ± 0.33
	Ionic Silver	13.49 ± 0.07	13.35 ± 0.02	13.20 - 13.92	-1.04 ± 0.45
Sulfate [mg/l]	Reference	31.31 ± 0.21	31.01 ± 0.09	30.91 - 31.66	-0.97 ± 0.69
	Nanopowder	31.39 ± 0.07	31.13 ± 0.20	30.67 - 31.88	-0.82 ± 0.53
	Nanospheres	32.41 ± 0.06	31.83 ± 0.05	31.78 - 32.94	-1.79 ± 0.29
	Ionic Silver	32.47 ± 0.09	31.98 ± 0.08	31.86 - 32.97	-1.50 ± 0.51
Nitrate [mg/l]	Reference	0.8 ± 0.0	<LOD	<LOD - 0.9	-100
	Nanopowder	0.9 ± 0.0	<LOD	<LOD - 0.9	-100
	Nanospheres	0.5 ± 0.0	<LOD	<LOD - 0.5	-100
	Ionic Silver	0.4 ± 0.1	<LOD	<LOD - 1.0	-100
TOC [mg/l]	Reference	1.50 ± 0.03	1.40 ± 0.15	0.78 - 1.87	-6.7 ± 10.9
	Nanopowder	1.53 ± 0.03	1.50 ± 0.25	0.89 - 1.79	-2.4 ± 14.5
	Nanospheres	2.20 ± 0.03	1.58 ± 0.08	1.44 - 2.42	-28.4 ± 3.2
	Ionic Silver	2.12 ± 0.07	1.61 ± 0.04	1.57 - 2.53	-24.0 ± 2.4
DOC [mg/l]	Reference	1.56 ± 0.44	1.38 ± 0.13	0.87 - 2.07	-7.0 ± 25.1
	Nanopowder	1.37 ± 0.04	1.36 ± 0.04	0.85 - 1.92	-0.7 ± 3.8
	Nanospheres	1.72 ± 0.16	1.52 ± 0.05	1.39 - 2.18	-10.9 ± 7.2
	Ionic Silver	1.65 ± 0.04	1.59 ± 0.05	1.50 - 2.18	-3.7 ± 1.4

Abstract

Due to its high toxicity, the environmental release of silver from anthropogenic activities such as the photographic industry, has aroused the interest of both researchers and the public in the past. While these discharges have continuously decreased in the past decades, with the advent of nanotechnology, new applications of silver have emerged. This has stimulated new research on the possible environmental effects of silver nanoparticles, especially in aquatic ecosystems. Even though they are essential inhabitants of these ecosystems, the interaction of nanoparticles with aquatic macropyhtes has however remained a niche topic. Thus, in the present study, *Myriophyllum spicatum*, a common submerged macrophyte and established species for ecotoxicity tests was exposed to either two types of polyvinylpyrrolidone-stabilized silver nanoparticles or $AgNO_3$ over a period of five weeks in a laboratory mesocosm experiment. A nominal exposure of 30 µg/L added over three weeks was chosen to provide a compromise between current predicted environmental concentrations and analytical sensitivity. The goal of the study was to to assess the distribution of silver between the plants, sediments and aquatic phase, as well as effects on the growth of the plants. Furthermore, the potential localization of accumulated silver in the plant leaves was studied using scanning and transmission electron microscopy with element-selective detection.

The sediments were found to act as the main sink of both silver nanoparticles as well as $AgNO_3$, while only a minor percentage was taken up by the plants and remained suspended in the aquatic phase. As evidenced by the tissue concentrations, silver was accumulated by *M. spicatum* from all applied forms, with $AgNO_3$ having the highest bioavailability and bioconcentration factor. $AgNO_3$ was furthermore the only form of silver to show any noticeable toxicity to the plants. Electron microscopy only allowed the detection of silver on the surface of plants exposed to $AgNO_3$, with no evidence of internalization into the leaves. No silver was detected on or in the leaves of plants exposed to the nanoparticles, most likely due to a combination of insufficient sensitivity and low tissue concentrations.

The present study showed, that the aquatic macrophyte *M. spicatum* bioaccumulates silver from PVP-stabilized nanoparticles without obvious toxic effects at concentrations similar to predicted environmental concentrations. Further research is needed to assess the mechanisms of nanoparticle bioaccumulation and the long-term effects of low environmental nanoparticle exposure to both aquatic plants and species depending on their ecosystem services.

Zusammenfassung

Aufgrund der hohen Toxizität von Silber auf aquatische Organismen, haben Silberemissionen in der Vergangenheit akademisches als auch öffentliches Interesse erregt. Während diese Emissionen in den letzten Jahrzehnten kontinuierlich zurückgegangen sind, haben sich mit dem Aufkommen der Nanotechnologie neue Anwendungsmöglichkeiten für Silber ergeben. Dies hat Forschungen zu den möglichen Umweltwirkungen von Silbernanopartikeln, insbesondere in aquatischen Ökosystemen, angeregt. Obwohl sie essentielle Ökosystemdienstleistungen erbringen, ist die Wechselwirkung von Nanopartikeln mit aquatischen höheren Pflanzen, im Gegensatz zu tierischen Organismen, bisher kaum erforscht worden. Daher wurde in der vorliegenden Arbeit die submerse Pflanze *Myriophyllum spicatum* zwei Arten von Polyvinylpyrrolidon-stabilisierten Silbernanopartikeln oder gelöstem Silber (als $AgNO_3$) über einen Zeitraum von fünf Wochen in einem Mesokosmenexperiment ausgesetzt. Eine nominale Exposition von 30 µg/L über drei Wochen wurde gewählt, um einen Kompromiss zwischen den erwarteten Umweltkonzentrationen und ausreichender analytischer Empfindlichkeit zu finden. Ziel der Studie war es, die Akkumulation von Silber in den Pflanzen, den Sedimenten und das Verhalten in der Wassersäule, sowie die Auswirkungen auf das Wachstum der Pflanzen zu bewerten. Darüber hinaus wurde die mögliche Lokalisierung des akkumulierten Silbers in den Blättern mit Hilfe der Raster- und Transmissionselektronenmikroskopie mit elementselektiven Techniken untersucht.

Sowohl Silbernanopartikel als auch $AgNO_3$ akkumulierten hauptsächlich in den Sedimenten, während nur ein geringer Anteil von den Pflanzen aufgenommen wurde oder in der Wassersäule verblieb. Alle angewandten Arten von Silber wurden von *M. spicatum* akkumuliert, wobei $AgNO_3$ die höchste Bioverfügbarkeit aufwies. Darüber hinaus war $AgNO_3$ die einzige Form von Silber, die eine merkliche Toxizität für die Pflanzen aufwies. Silber konnte jedoch nur auf der Oberfläche jener Pflanzen, die $AgNO_3$ ausgesetzt waren, nachgewiesen werden, während keine der eingesetzen Nanopartikel detektiert wurden. Eine intrazelluläre Aufnahme von Silber konnte ebenfalls nicht nachgewiesen werden.

Die Ergebnisse der Arbeit zeigten, dass *M. spicatum*, bei Konzentrationen höher als den erwarteten Umweltkonzentrationen, Silber aus Nanopartikeln ohne signifikante Toxizität bioakkumuliert. Weitere Forschung ist erforderlich, um die Mechanismen der Akkumulation sowie die langfristigen Auswirkungen von geringen Umweltkonzentrationen sowohl auf Pflanzen als auch auf Arten, die von ihren Ökosystemdienstleistungen abhängig sind, zu bewerten.